

## ABSTRACT

Title of Dissertation: INVESTIGATING THE MECHANISM OF PHENOL  
PHOTOOXIDATION BY CHROMOPHORIC  
DISSOLVED ORGANIC MATTER

Kelli Ann Sikorski, Doctor of Philosophy, 2014

Dissertation directed by: Professor Neil V. Blough  
Department of Chemistry and Biochemistry

It is well established that organic pollutants such as phenols are degraded in the presence of chromophoric dissolved organic matter (CDOM) and sunlight in natural waters. Early work attributed the photochemical loss of phenols to the involvement of photoproducted reactive oxygen species (ROS) such as singlet oxygen ( $^1\text{O}_2$ ), hydroxyl radical ( $\bullet\text{OH}$ ) or peroxy radicals ( $\text{RO}_2\bullet$ ). However, evidence for the involvement of triplet excited states of aromatic ketones/aldehydes within CDOM has accumulated in the literature. To probe the mechanism of the photosensitized loss of phenols by humic substances (HS), the dependence of the initial rate of 2,4,6-trimethylphenol (TMP) loss ( $R_{\text{TMP}}$ ) on dioxygen concentration and irradiation wavelength was examined both for a variety of untreated as well as borohydride-reduced HS and  $\text{C}_{18}$  extracts from the Delaware Bay and

Mid-Atlantic Bight. The effect of  $[O_2]$  and borohydride-reduction of SRFA was also examined for a series of substituted phenols of varying one-electron reduction potentials. We find that  $R_{TMP}$  was inversely proportional to dioxygen concentration at  $[O_2] > 50 \mu M$ , a dependence consistent with reaction with triplet excited states, but not with  $^1O_2$  or  $RO_2$ . Modeling the dependence of  $R_{TMP}$  on  $[O_2]$  provided rate constants for TMP reaction,  $O_2$  quenching and lifetimes compatible with a triplet intermediate. Borohydride reduction significantly reduced TMP loss, supporting the role of aromatic ketone triplets in this process. However, for most samples, the incomplete loss of sensitization following borohydride reduction, as well as the inverse dependence of  $R_{TMP}$  on  $[O_2]$  for these reduced samples, suggests that there remains another class of oxidizing triplet sensitizer, perhaps quinones. However, the results of the wavelength dependence reveal that the sensitization is driven primarily by shorter wavelength UV-B and UV-A absorbing moieties, consistent with the involvement of aromatic ketones and aldehydes but appearing to exclude the longer wavelength (visible) absorbing quinones as sensitizers. An inverse dependence of  $\Phi$  on one-electron reduction potential was observed where  $DMOP \approx TMP > 4-MOP > 4-MP > phenol$ . Similar dependencies were observed for TMP and 4-MOP in the dependence of  $R_{probe}$  on  $[O_2]$  whereas DMOP did not exhibit a substantially lower  $R_{probe}$  at high  $[O_2]$  as would be expected for a triplet sensitization mechanism. Moreover, that a significant amount of sensitization is observed following borohydride reduction of SRFA for DMOP under high  $[O_2]$ , as well as the very low sensitization observed at low  $[O_2]$  indicates that a separate pathway, unrelated to triplets, may be important for the mechanism of DMOP photooxidation by chromophoric dissolved organic matter.

INVESTIGATING THE MECHANISM OF PHENOL PHOTOOXIDATION  
BY CHROMOPHORIC DISSOLVED ORGANIC MATTER

by

Kelli Ann Sikorski

Dissertation submitted to the Faculty of the Graduate School of the  
University of Maryland, College Park in partial fulfillment  
of the requirements for the degree of  
Doctor of Philosophy  
2014

Advisory Committee:

Professor Neil V. Blough, Chair/advisor  
Professor Daniel Falvey  
Professor Cheng Lee  
Professor Amy Mullin  
Professor Alba Torrents

© Copyright by  
Kelli Ann Sikorski  
2014



## ACKNOWLEDGEMENTS

I sincerely thank my advisor, Dr. Neil Blough for his guidance and support. When I arrived to the University of Maryland in the Fall of 2008, I knew nothing of natural water photochemistry and certainly had a lot to learn about being a proficient scientific researcher and writer. Your patience along this journey is much appreciated.

I also wish to thank Andrea Andrew and Yi Zhang for their friendship which has expanded both my scientific and worldly knowledge. Through our time together, I have learned so much about being a better colleague. Much gratitude is also owed to the past and present members of the Blough research group (Min Jia, Lynne Heighton, Dan Baluha) as well as the undergraduate students whom have assisted me in the lab (Erin Norcross, Shuo (Mike) Fang and Kelsey Melloy). I have enjoyed your mentorship and company immensely.

My journey to the completion of this dissertation began over two decades ago and is almost entirely attributed to my grandparents, Marian and S. Larry Sikorski and my father, Larry Sikorski. As a child they encouraged me to explore my surroundings and supported creative thinking and artistic pursuits. As an adolescent they reinforced the importance of education and faith. Endless “fireside chats” and un-enumerable hours of phone calls have kept me afloat and motivated to achieve my goal. Thank you for all that you have taught me; it is finally time for me to collect my second marshmallow.

My friends Elizabeth Ricketts, Melissa Halpern and Jackie Bakunas have been steadfast pillars of strength during my most difficult times and great sources of joy and happiness in my life. What would I do without you ladies?

Last but certainly not least, I wish to express my gratitude to Mr. Paul Simon, my best friend and love of my life. You have changed my life in ways that I cannot describe. Your unconditional support during the last year-and-a-half will never be forgotten. I love you, forever. I hereby dedicate this dissertation to my future children, so that when I tell them they should never doubt themselves in whatever pursuits they undertake, there shall be a physical reference for them.

## TABLE OF CONTENTS

Acknowledgements.....	i
Table of Contents.....	iii
List of Tables.....	iv
List of Figures.....	v
List of Schemes.....	vii
List of Abbreviations.....	viii
CHAPTER I: Introduction.....	1
Background.....	1
Optical Properties and Sodium Borohydride (NaBH <sub>4</sub> ) Reduction .....	5
Reactive Oxygen Species (ROS).....	8
Triplet Excited States.....	11
CHAPTER II: Dependence of the Initial Rate of 2,4,6-trimethylphenol (TMP) on TMP Concentration, Dioxygen Concentration and Sodium Borohydride Reduced Humic Substances.....	16
Abstract.....	16
Introduction.....	16
Materials and Methods.....	19
Materials.....	19
Apparatus.....	19
Photochemical Experiments.....	21
Sodium Borohydride (NaBH <sub>4</sub> ) Reduction.....	23
Results and Discussion.....	24
Effects of NaBH <sub>4</sub> Reduction .....	24
Effects of Dioxygen Concentration.....	34
Modeling.....	36
CHAPTER III: Wavelength Dependence of the Photosensitized Oxidation of 2,4,6-trimethylphenol (TMP) by HS and CDOM: Effects of NaBH <sub>4</sub> Reduction and [O <sub>2</sub> ].....	44
Abstract.....	44
Introduction.....	44
Materials and Methods.....	48
Materials.....	48
Apparatus.....	48
Sodium Borohydride (NaBH <sub>4</sub> ) Reduction.....	52
Photochemical Experiments.....	53

Results and Discussion.....	54
Effect of Borohydride Mass Excess Ratio.....	54
Wavelength Dependence of $R_{\text{TMP}}$ .....	58
Wavelength Dependence of $R(\lambda)$ .....	63
Apparent Polychromatic Quantum Efficiencies.....	69
 CHAPTER IV: Effects of Borohydride Reduction and $[\text{O}_2]$ on the Sensitized Loss of a Series of Phenols by Suwannee River Fulvic Acid (SRFA).....	74
Abstract.....	74
Introduction.....	74
Materials and Methods.....	77
Materials.....	77
Apparatus.....	77
Photochemical Experiments.....	79
Sodium Borohydride ( $\text{NaBH}_4$ ) Reduction.....	81
Results and Discussion.....	81
Effect of [probe] and $\text{NaBH}_4$ Reduction .....	81
Effect of $[\text{O}_2]$ .....	87
Apparent (polychromatic) quantum efficiencies.....	90
 CHAPTER V: Summary and Future Work.....	93
Summary.....	93
Future Work.....	94
 Appendix I: Scheme of Triplet Chromophore Formation and Derivation of Equation II.12	
 Appendix II: Dependence of the Optical Properties of SRFA, SRHA and LAC on Mass Excess of Sodium Borohydride	

## LIST OF TABLES

Table I.1 Carbon and oxygen content, distribution of oxygen in reactive functional groups and ketone and quinone carbonyl moiety contents of humic and fulvic acids.

Table I.2: Rate constants for quenching of aromatic ketone triplet states by phenols

Table II.1 Values of  $a^*(350)$ ,  $S$  and  $R_{\text{TMP}}$  for untreated and borohydride-reduced SRFA, SRHA, LAC and  $C_{18}$  extracts of the Delaware Bay

Table II.2: Apparent (polychromatic) quantum efficiencies ( $\Phi$ ) for TMP loss by untreated and borohydride-reduced SRFA, SRHA, LAC and  $C_{18}$  extracts of the Delaware Bay

Table II.3: Calculations and sensitivity analyses for  $\hat{k}_t$ ,  $\hat{k}_{\text{TMP}}$  and  $\hat{k}_Q$  for untreated and borohydride-reduced SRFA and SRHA.

Table II.4: Results from curve fitting the dependence of  $R_{\text{TMP}}$  on  $[O_2]$  to Eqn. II.12 for untreated and borohydride-reduced SRFA, SRHA, LAC and  $C_{18}$  extracts of the Delaware Bay

Table III.1: Mass excess of  $\text{NaBH}_4$  added to 500 mg  $\text{L}^{-1}$  SRFA, SRHA or LAC

Table III.2: Values of  $a^*(350)$ ,  $S$  and  $R_{\text{TMP}}$  for untreated and borohydride-reduced SRFA, SRHA and LAC using 5X-100X  $\text{NaBH}_4$  mass excess ratios

Table III.3: Values of slope (normalized to SRFA) and coefficients of determination for wavelength dependence of untreated and borohydride-reduced SRFA, SRHA, LAC, UBS, LBS and SS.

Table III.4: Values of  $R_{\text{TMP}}$  and  $R_{\text{EX}}$  for SRFA, SRHA and LAC at all wavelength cutoff filters employed.

Table III.5: Values of  $R_{\text{TMP}}$  and  $R_{\text{EX}}$  for UBS, LBS and SS at all wavelength cutoff filters employed.

Table III.6: Values of  $\Phi$  and  $\Phi_{\text{diff}}$  for SRFA, SRHA, LAC and  $C_{18}$  extracts of the Delaware Bay as determined by Eqns. III.5-6.

Table IV.1: Structures, values of acid dissociation constants, detector wavelengths and mobile phase compositions and one-electron reduction potentials employed in this study

Table IV.2: Values of  $R_{\text{probe}}$  for untreated and borohydride-reduced SRFA for  $[\text{probe}] = 10 - 250 \mu\text{M}$  under aerated conditions.

Table IV.3: Values of half-saturation concentration of  $R_{\text{TMP}}$  (a) and maximal rate of  $R_{\text{TMP}}$  (b) from data in Figure IV.4.

Table IV.4: Values of  $R_{\text{probe}}$ ,  $R_{\text{EX}}$  and  $\Phi$  for  $[\text{probe}] = 100$  and  $250 \mu\text{M}$  and untreated or borohydride-reduced SRFA under aerated conditions.

## LIST OF FIGURES

Figure I.1: Map of Sample Stations in Delaware Bay and Mid-Atlantic Bight (MAB)

Figure I.2: Absorbance spectra of Suwanee River Fulvic Acid (SRFA), Humic Acid (SRHA) and Lignin, Alkali treated, Carboxylated (LAC) at  $10 \text{ mg L}^{-1}$  at  $\text{pH}=7$

Figure I.3: General mechanism of sodium borohydride reduction of a carbonyl moiety.

Figure I.4: Proposed reaction model of excited triplet states of aromatic ketones with phenols

Figure II.1 Wavelength dependence of the absolute irradiance of the xenon arc lamp employing a 325 nm wavelength cutoff filter

Figure II.2: Wavelength dependence of  $R(\lambda)$  for untreated and borohydride-reduced SRFA, SRHA, LAC and  $\text{C}_{18}$  extracts of the Delaware Bay

Figure II.3: Absorbance spectra of untreated and borohydride-reduced SRFA, SRHA, LAC and  $\text{C}_{18}$  extracts of the Delaware Bay

Figure II.4 Absorbance difference spectra of untreated and borohydride-reduced SRFA, SRHA, LAC and  $\text{C}_{18}$  extracts of the Delaware Bay

Figure II.5 Dependence of  $R_{\text{TMP}}$  on  $[\text{TMP}]$  for untreated and borohydride-reduced SRFA, SRHA, LAC and  $\text{C}_{18}$  extracts of the Delaware Bay under aerated ( $250 \mu\text{M O}_2$ ) conditions

Figure II.6: Dependence of  $R_{\text{TMP}}$  on  $[\text{TMP}]$  for untreated and borohydride-reduced SRFA, SRHA, LAC and  $\text{C}_{18}$  extracts of the Delaware Bay at aerated ( $250 \mu\text{M}$ ) and low ( $22 \mu\text{M}$ )  $[\text{O}_2]$

Figure II.7: Dependence of  $R_{\text{TMP}}$  on  $[\text{O}_2]$  at fixed  $[\text{TMP}] = 100 \mu\text{M}$  for untreated and borohydride-reduced SRFA, SRHA, LAC and  $\text{C}_{18}$  extracts of the Delaware Bay

Figure II.8: Comparison of results from curve fitting the dependence of  $R_{\text{TMP}}$  on  $[\text{O}_2]$  to Eqn. II.12 for Reduced SRFA, SRFA and LAC using values of  $\bar{k}_t$  and  $\bar{k}_{\text{TMP}}$  for SRFA or unique values of Reduced SRFA, SRHA and LAC.

Figure III.1: Average absolute irradiance of the high pressure xenon arc lamp with various wavelength cutoff filters employed in this study.

Figure III.2: Absorbance spectra of untreated and borohydride-reduced SRFA, SRHA and LAC at 10 mg L<sup>-1</sup>. Overlaid are the absolute irradiance profiles of the xenon arc lamp with each long pass wavelength filter employed in this study .

Figure III.3: Absorbance spectra of untreated and borohydride-reduced UBS, LBS, SS at 10 mg L<sup>-1</sup>. Overlaid are the absolute irradiance profiles of the xenon arc lamp with each long pass wavelength filter employed in this study

Figure III.4: Absorbance spectra and R<sub>TMP</sub> for untreated and borohydride-reduced SRFA, SRHA and LAC treated using 0X to 100X NaBH<sub>4</sub> mass excess ratios

Figure III.5: Difference in absorbance and fractional absorbance spectra of SRFA, SRHA and LAC treated using 0X to 100X NaBH<sub>4</sub> mass excess ratios

Figure III.6: Dependence of R<sub>TMP</sub> on wavelength for untreated and borohydride-reduced SRFA, SRHA and LAC under 5% and 20% [O<sub>2</sub>] conditions

Figure III.7: Dependence of R<sub>TMP</sub> on wavelength for untreated and borohydride-reduced SRFA, SRHA, LAC and C18 extracts of the Delaware Bay at 5% [O<sub>2</sub>]

Figure III.8: Log-transformed values of RTMP for untreated and borohydride-reduced SRFA, SRHA, LAC, UBS, LBS and SS.

Figure III.9: Wavelength dependence of R(λ) for untreated and borohydride-reduced SRFA, SRHA and LAC for various wavelength cutoff filters

Figure III.10: Wavelength dependence of R(λ) for untreated and borohydride-reduced UBS, LBS and SS for various wavelength cutoff filters

Figure III.11: Wavelength dependence of R<sub>TMP</sub> for 10 mg L<sup>-1</sup> and 17 mg L<sup>-1</sup> LAC

Figure III.12: Dependence of Φ for TMP loss on wavelength for untreated and borohydride-reduced SRFA, SRHA, LAC, UBS, LBS and SS under 5% [O<sub>2</sub>] conditions

Figure IV.1: Absorbance spectra of untreated and borohydride-reduced SRFA at 10 mg L<sup>-1</sup> at pH=7.0 and absolute irradiance profile of the xenon arc lamp with a 325 nm filter.

Figure IV.2: Wavelength dependence of the rate of light excitation (R<sub>EX</sub>) for untreated and borohydride-reduced SRFA.

Figure IV.3: Dependence of R<sub>probe</sub> on [probe] for untreated and borohydride-reduced SRFA under aerated conditions.

Figure IV.4: Dependence of R<sub>probe</sub> on [probe] for untreated and borohydride-reduced SRFA at high (250 μM) and low (22 μM) [O<sub>2</sub>] conditions

Figure IV.5: Dependence of  $R_{\text{probe}}$  on  $[O_2]$  at 100  $\mu\text{M}$  DMOP and TMP and = 50  $\mu\text{M}$  4-MOP.

Figure IV.6: Dependence of  $R_{\text{probe}}$  on  $[O_2]$  for 100  $\mu\text{M}$  and 50  $\mu\text{M}$  4-MOP employing data from 15 minute and 10 minute irradiations

Figure IV.7: Values of  $\Phi$  for 100 and 250  $\mu\text{M}$  DMOP, TMP, 4-MOP, 4-MP and phenol with untreated and borohydride-reduced SRFA.

## LIST OF SCHEMES

Scheme II.1: Scheme of Triplet Chromophore Formation, Fate and Reactions with TMP



## LIST OF ABBREVIATIONS

a	maximal rate of phenol probe loss
$a(\lambda)$	absorbance coefficient
$A(\lambda)$	absorbance at a given wavelength
$a^*(\lambda)$	specific absorbance coefficient
$a^*(\lambda_{\text{Ref}})$	specific absorbance coefficient at a reference wavelength
2-AN	2-acetonaphthone
B	half-saturation of the initial rate
b	pathlength
BQ	benzoquinone
$\text{Br}^-$	bromide ion
CDOM	chromophoric dissolved organic matter
$^1\text{CDOM}$	ground state chromophoric dissolved organic matter
$^3\text{CDOM}^*$	triplet excited state of chromophoric dissolved organic matter
$\text{CO}_3^-$	carbonate radical
$\text{CO}_3^{2-}$	carbonate
CT	charge transfer
3,4-DMOP	3,4-dimethoxyphenol
DMSO	dimethyl sulfoxide
DOM	dissolved organic matter
$\text{H}_2$	hydrogen
$\text{H}_2\text{O}_2$	hydrogen peroxide
HPLC	high performance liquid chromatpgraphy

HS	humic substances
$h\nu$	photon
$I(\lambda)$	spectral photon irradiance
IPA	isopropyl alcohol
$k_c$	rate constant for chemical quenching of triplet by external donor
$k_f$	rate constant for triplet formation
$k_{\text{REC}}$	rate constant for recombination of radical species
$k_{\text{RXN}}$	rate constant for reaction to form products
$k_p$	rate constant for physical quenching of triplet with external donor
$k_Q$	rate constant for quenching of triplet by dioxygen (energy transfer)
$k_t$	rate constant for radiationless transition of triplet to ground state
KHP	potassium hydrogen phthalate
$\text{K}_2\text{HPO}_4$	dipotassium hydrogen phosphate
$\text{KH}_2\text{PO}_4$	potassium dihydrogen phosphate
LAC	lignin, alkali-treated, carboxylated
LBS	lower bay sample
LMW	low molecular weight
3'-MAP	3'-methoxyacetophenone
MAB	mid-Atlantic bight
MeOH	methanol
4-MOP	4-methoxyphenol
4-MP	4-methylphenol

NaBH <sub>4</sub>	sodium borohydride
N <sub>2</sub>	nitrogen
NMR	nuclear magnetic resonance
•OH	hydroxyl radical
O <sub>2</sub>	dioxygen
PAR	photosynthetically active radiation
PB	phosphate buffer
PhOH	phenol
R( $\lambda$ )	wavelength dependence of the light excitation rate
R <sub>EX</sub>	rate of light excitation
RO <sub>2</sub>	peroxy radical
ROS	reactive oxygen species
R <sub>TMP</sub>	initial rate of 2,4,6-trimethylphenol loss
S	spectral slope
SS	shelf sample
SRFA	Suwannee River Fulvic Acid
SRHA	Suwannee River Humic Acid
TMP	2,4,6-trimethylphenol
TOC	total organic carbon
UBS	upper bay sample
UHP	ultra-high purity
UV	ultraviolet radiation
$\phi$	branching ratio of chemical and physical quenching of triplet

$\Phi$	apparent polychromatic quantum yield
$\Phi_{\text{diff}}$	apparent quantum efficiency of species eliminated by reduction
$\Phi^{\text{T}}$	apparent polychromatic quantum efficiency of triplet states

## Chapter I: Introduction

### 1.1 Background

Pollution of aquatic environments by natural and anthropogenic compounds remains an ongoing, global issue. A wide variety of pollutants are found in natural waters across the United States, particularly in the Delaware River, where one study alone detected and quantified nearly 100 organic contaminants (Sheldon and Hites, 1978). Phenol and phenolic compounds are ubiquitous within this category due to their use in the production of pharmaceutical and agricultural products as well as the production of synthetic fibers and the epoxy resin precursor bisphenol-A (Barron, *et. al.*, 2002). Despite their utility in these processes, phenolic compounds at low concentrations can be toxic to organisms and upon chlorination can form objectionable taste and odor in drinking water (Barron, *et. al.*, 2002; DeZuane, 1997).

Common fates of organic pollutants include dilution, biodegradation, volatilization and photochemical processes. For transformation of poorly biodegradable or non-volatile organic chemicals such as phenols, direct or indirect photolysis can be a dominant sink (Zepp and Cline, 1977). Direct photolysis (light absorption followed by chemical reaction) of phenols in natural waters is considered to be a minor degradation pathway as phenols absorb little in the wavelength regime provided by sunlight ( $\geq 290$  nm) (Canonica *et. al.*, 1995). Therefore, indirect or “sensitized” photolysis (chemical reaction initiated following light absorption by another chromophore) could be important. Initial investigations reported enhanced rates of chemical decomposition in the presence of sunlight in natural waters, but not in pure water (Ross and Crosby, 1973 and 1975; Zepp, 1980; Draper and Crosby, 1976; Zepp *et. al.*, 1975 and 1977; Mill *et. al.*, 1980).

The primary light-absorbing constituent of natural waters is chromophoric dissolved organic matter (CDOM) and is operationally defined as the fraction of dissolved organic matter (DOM) which passes through a 0.2 micron ( $\mu\text{m}$ ) filter and can absorb UV and visible light. Light absorption by CDOM plays many important roles in aquatic environments. At higher concentrations found in some inland waterways, the absorption of sunlight by CDOM can both positively and negatively impact the aquatic photic zone. Light-sensitive organisms are protected from harmful UV rays (Blough and Del Vecchio, 2002; Blough *et. al.*, 1993; de Mora *et. al.*, 2000) however absorption by CDOM of photosynthetically active radiation (PAR) can limit primary productivity (Aiken *et. al.*, 1985; Blough and Del Vecchio 2002). Light absorption by CDOM also initiates a suite of photochemical reactions including the production of biologically labile low molecular weight compounds and atmospherically importance trace gases ( $\text{CO}_2$ , CO, COS) (Mopper and Kieber, 2002; Stubbins *et. al.*, 2011; White *et. al.*, 2010) and initiates photochemical degradation of a wide variety of pollutants (Gerecke *et. al.*, 2001; Burns *et. al.*, 1996; Latch *et. al.*, 2003; Chin *et. al.*, 2004; Guerard *et. al.*, 2009; Grannas *et. al.*, 2012; Packer *et. al.*, 2003; Boreen *et. al.*, 2003).

Sources of CDOM are generally grouped into two categories based on its location. Terrestrial CDOM arises from the decomposition of vascular plant matter and lignin precursor materials and is imparted to rivers, streams and lakes via rainfall. Marine CDOM is found in off-shore environments and in open oceans and results from dilution of Terrestrial CDOM inputs or is produced *in-situ* from microbial action on phytoplankton - although both mechanisms are possible and remain an active area of research (Coble, 2007, Andrew *et. al.*, 2013). Degradation pathways for CDOM include

weathering during downstream transport, microbial action and photobleaching as a result of light absorption, the latter of which is proposed to dominate (Vodacek *et. al.*, 1997; Nelson *et. al.*, 1998).

In order to study the properties of CDOM in a laboratory setting, research cruises are conducted to collect natural water samples or standard reference materials are procured through the International Humic Substance Society (IHSS). The IHSS provides humic substances extracted from a singular body of water such as the Suwannee River in Georgia, which allows for comparison of results among research laboratories. It is important to note that CDOM which has been extracted from natural waters is referred to as humic substances as it may no longer be truly representative of the original material due to the chemical extraction process employed (Green and Blough, 1994; Thomas-Smith and Blough, 2001).

Humic substances are further discriminated by their solubility characteristics in acidic solution conditions. For example, fulvic acids are soluble at all pH whereas humic acids are insoluble in very acidic conditions ( $\text{pH} < 2$ ). Fulvic acids generally have lower average molecular weight and carbon (40-50%) content but higher oxygen (40-50%) content compared to humic acid (54-59% C; 33-38% O) (Stevenson, 1994). Lignin, regarded as terrestrial CDOM starting material is treated by alkali and then carboxylated for use in the laboratory and is termed LAC and is employed along with Suwannee River Fulvic (SRFA) and Humic (SRHA) Acid in this research.

Researchers wishing to characterize CDOM from bodies of water such as the Delaware Bay and Mid-Atlantic Bight (MAB) collect natural water samples along a transect of water during different seasons and at various depths (Fig. I.1).

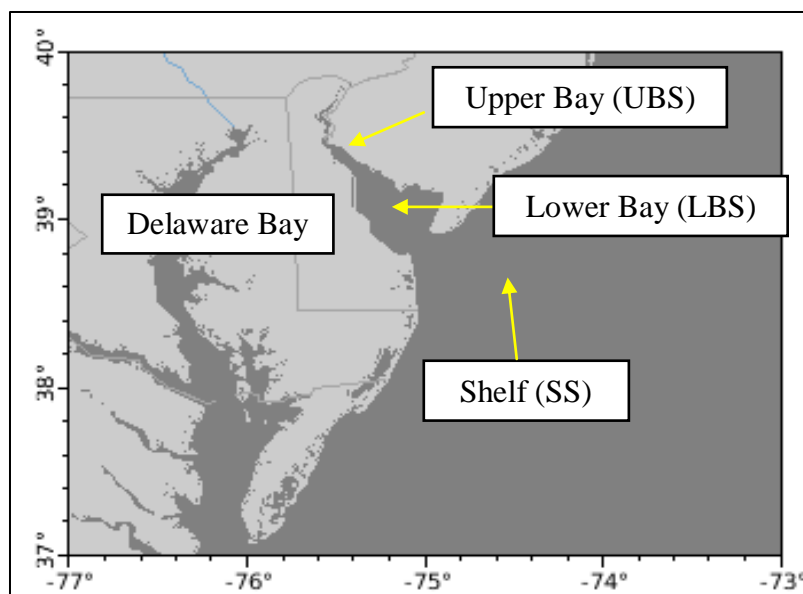


Figure I.1: Map of Sample Stations in Delaware Bay and Mid-Atlantic Bight (MAB)

Analyses such as ultraviolet/visible absorption, fluorescence and total organic carbon (TOC) are often performed on-board the research vessel, but photochemical tests performed in the laboratory require higher concentrations of CDOM and thus CDOM is extracted from the natural water and prepared for long-term storage. Briefly, samples (20 L) are collected onboard a research vessel at each of various locations and depths, filtered (Gelman, 0.2  $\mu\text{m}$ ), acidified and pumped through a pre-treated  $\text{C}_{18}$  solvent phase extraction cartridge then rinsed with Milli-Q water to remove salts.

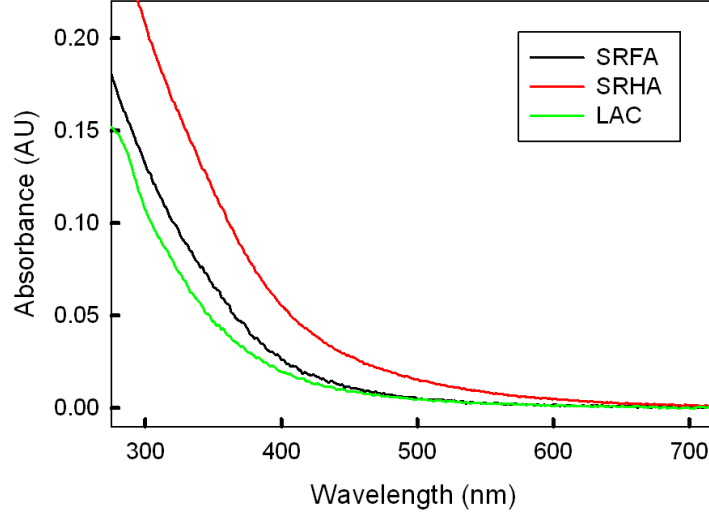
The extracted material is eluted from the  $\text{C}_{18}$  cartridge using methanol, evaporated to dryness, re-constituted with a few milliliters (mL) of Milli-Q water, adjusted to neutral pH then stored frozen until further analysis (Ma *et. al.*, 2010). These are then referred to as  $\text{C}_{18}$  or MAB extracts where samples collected at the Upper Bay Station (UBS), Lower Bay Station (LBS) and Shelf Station (SS) and are employed in this research.



## 1.2 Optical Properties and Sodium Borohydride Reduction

Assignment of a singular molecular structure to CDOM is impractical due to the spatial variation in CDOM source material and temporal variation due to seasonal impacts such as photobleaching in summer months. CDOM is known to contain saturated and unsaturated hydrocarbons, aromatic structures, carboxyl-rich alicyclic molecules, substituted phenols, ketones, aldehydes, quinones and carbohydrates which have been identified through electron spin resonance (Lakatos *et. al.*, 1977; Paul *et. al.*, 2006),  $^{13}\text{C}$  nuclear magnetic resonance spectroscopy (Herkton *et. al.*, 2006; Thorn *et. al.*, 1989; McKnight *et. al.*, 1994), electrochemistry (Aeschbacher *et. al.*, 2010 and 2011), pyrolysis (Schulten *et. al.*, 1999; de Haan 1983b; MacCarthy *et. al.*, 1985) and ultra-high mass resolution (Mopper *et. al.*, 2007; Remucal *et. al.*, 2012; Stenson *et. al.*, 2003; Kujawinski *et. al.*, 2004)) mass spectrometry and other techniques. Although significant advancements in the knowledge of CDOM structural components have been made, the exact assembly of these units is yet unknown.

The ultraviolet-visible (UV) absorption spectrum of CDOM has no distinct absorption bands, featuring elevated absorbance at short wavelengths that decreases in an approximately exponential fashion with increasing wavelength. UV-Vis spectra of SRFA, SRHA, LAC are shown in Figure I.2.



**Figure I.2** Absorbance spectra of Suwanee River Fulvic Acid (SRFA), Humic Acid (SRHA) and Lignin, Alkali treated, Carboxylated (LAC) at  $10 \text{ mg L}^{-1}$  at  $\text{pH}=7$

UV-Vis spectra are described quantitatively using the specific absorption coefficient ( $a^*(\lambda)$ ) and spectral slope parameter (S). Specific absorption coefficients are determined by Equation I.1:

$$a^*(\lambda) = 2.303 \cdot A(\lambda) / (b \cdot C) = a(\lambda) / C \quad (\text{I.1})$$

where 2.303 is the conversion factor between  $\log_{10}$  and  $\ln$ ,  $A(\lambda)$  is the absorbance at a given wavelength,  $b$  is the path length in meters and  $C$  is the concentration of total organic carbon in  $\text{mg C L}^{-1}$ . The absorption spectrum of CDOM is fitted using a non-linear least squares fitting routine over a specific wavelength interval (usually 290-820 nm) to Equation I.2:

$$a(\lambda) = a(\lambda_0) e^{-S(\lambda-\lambda_0)} \quad (\text{I.2})$$

where  $a(\lambda)$  is the absorption coefficient at any wavelength,  $a(\lambda_0)$  is the absorption coefficient measured at any reference wavelength, typically 350 nm and  $S$  represents how

rapidly the absorption decreases with increasing wavelength (Blough and Del Vecchio, 2002).

The characteristics of the absorption spectrum at short wavelengths has been attributed to direct absorption and emission from donor and acceptor moieties within CDOM whereas the long wavelength tail is proposed to arise from charge-transfer interactions between donors (*e.g.* polyhydroxylated aromatics, phenols or indoles) and acceptors (*e.g.* quinones) in close proximity (short-range) and not from a simple superposition of the absorption characteristics of individual chromophores (Del Vecchio and Blough, 2002 and 2004; Blough and Green, 1995; Goldstone *et. al.*, 2004; Power and Langford, 1988; Ariese *et. al.* 2004).

Evidence supporting this electronic interaction model was provided by the results of treating CDOM with sodium borohydride ( $\text{NaBH}_4$ ), a mild and selective reductant of carbonyl-containing moieties such as ketones, aldehydes and quinones to their respective alcohols and hydroquinones. Reduction of these acceptor moieties within CDOM is predicted to decrease long-wavelength absorption by removing electron acceptors as well as decrease short wavelength absorption via the direct loss of absorption from the acceptors. Sodium borohydride reduction of carbonyl-containing moieties is described using the following reaction (Fig. I.3):

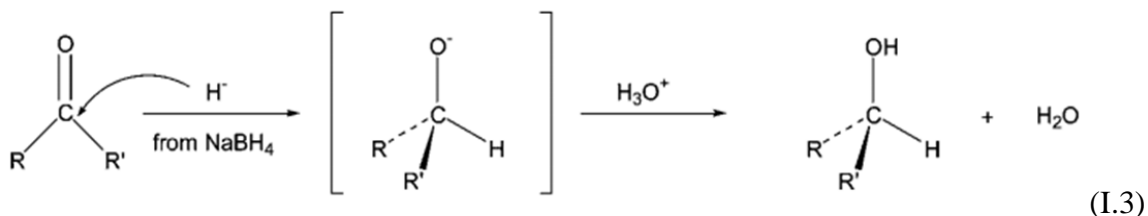


Figure I.3: General mechanism of sodium borohydride reduction of a carbonyl moiety.

This figure was adapted from Tinnacher and Honeyman, 2008.

where during the first step sodium borohydride donates a hydride ion by nucleophilic addition followed by protonation of the tetrahedral alkoxide intermediate by water to form the alcohol (Tinnacher and Honeyman, 2008). The borohydride reduction of humic substances efficiently reduced aliphatic and aromatic ketones and quinones to secondary alcohols and hydroquinones, respectively, however hydroquinones are generally re-oxidize relatively rapidly in the presence of molecular oxygen and are not irreversibly reduced using this process (Thorn *et. al.*, 1996; Weber *et. al.*, 1996). Thus, sodium borohydride reduction performed under aerobic conditions is a selective reductant of ketone/aldehyde moieties within CDOM.

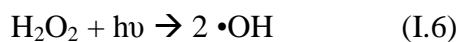
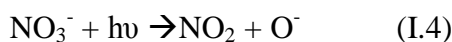
Ma *et. al.* (2010), Golanoski *et. al.* (2012), Yi *et. al.* (2012), Baluha *et. al.* (2013), Sharpless (2013) and others have reported significant loss of absorption across the visible and ultraviolet wavelengths upon borohydride reduction of HS, LAC and C<sub>18</sub> extracts of the MAB. The largest absolute and largest fractional losses of absorption were observed in the UV and visible regimes, respectively, where the original absorption was decreased by  $\geq 50\%$  following reduction.

### **1.3 Photochemical Properties**

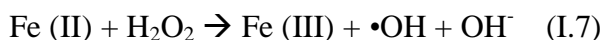
#### **1.3.1 Reactive Oxygen Species (ROS) Photoproduced by CDOM**

In surface waters, reactive intermediates are produced upon absorption of sunlight by CDOM and in the presence of dissolved oxygen. Initial investigations on the mechanism of phenol photooxidation by CDOM implicated photoproduced reactive oxygen species (ROS) such as hydroxyl radical ( $\bullet\text{OH}$ ), singlet oxygen ( $^1\text{O}_2$ ), and peroxy radicals ( $\text{RO}_2$ ) as the intermediates initiating phenol degradation.

The hydroxyl radical is relatively short-lived but is one of the most potent, non-selective oxidizing transient among ROS present in natural waters. In the absence of oxygen, •OH is produced from inorganic sources such as the photolysis of nitrite (NO<sub>2</sub><sup>-</sup>) (Zafiriou and True, 1979; Zarifriou and Bonneau, 1987), nitrate (NO<sub>3</sub><sup>-</sup>) (Zepp *et. al.*, 1987; Zellner *et. al.*, 1990; Zafiriou and True, 1979) or H<sub>2</sub>O<sub>2</sub> (Zellner *et. al.*, 1990). These reactions are summarized below in Equations I.3 - I.6:

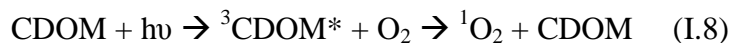


Although significant levels of •OH can be produced by the photolysis of nitrate and nitrite, production by photolysis of H<sub>2</sub>O<sub>2</sub> is limited due to the narrow window of spectral overlap of H<sub>2</sub>O<sub>2</sub> absorption with the solar spectrum. Hydrogen peroxide, the formation of which may require O<sub>2</sub>, acts with iron (II) to form •OH via the Fenton reaction (Zepp *et. al.*, 1992) as described in Equation I.7.



The mechanism of the direct photoproduction of •OH by CDOM has yet to be conclusively addressed (Takeda *et. al.*, 2004, Mopper and Zhou, 1990; Zhou and Mopper, 1990; Vaughan and Blough, 1998, Sharpless and Blough, 2014). Sinks of •OH include reaction with carbonate (CO<sub>3</sub><sup>2-</sup>), bicarbonate (HCO<sub>3</sub><sup>-</sup>) and to a lesser extent CDOM. Rate constants for reaction of •OH with undissociated phenols are reasonably large ( $k = 9 \times 10^9 \text{ M}^{-1} \text{ s}^{-1}$ ) (Bonin *et. al.*, 2007) however the low steady state concentration ( $10^{-17} - 10^{-15} \text{ M}$ ) precludes it as a dominant reaction pathway (Vione *et. al.*, 2006).

Singlet oxygen ( $^1\text{O}_2$ ) is produced by CDOM via energy transfer from triplet excited states of CDOM ( $^3\text{CDOM}^*$ ) to ground-state oxygen (Haag and Hoigné, 1986; Zepp et. al., 1977) as described by Equation I.8:



Approximately 1% of sunlight absorbed by CDOM in natural waters results in the production of  $^1\text{O}_2$ . Of the two lowest electronically excited states of  $\text{O}_2$  collectively referred to as  $^1\text{O}_2$ , only  $^1\Delta_g$  is considered herein due to the rapid decay of  $^1\Sigma_g^+$  to the  $^1\Delta_g$  state (Schweitzer and Schmidt, 2003). Singlet oxygen rapidly relaxes in by water and thus has a relatively short lifetime (4  $\mu\text{s}$ ) (Scully and Hoigné, 1987), with steady-state concentrations ranging from  $1 \times 10^{-14} \text{ M}$  to  $1 \times 10^{-12} \text{ M}$  (Scully and Hoigné, 1987; Zepp et. al., 1977). Rate constants for reaction of phenolic compounds with  $^1\text{O}_2$  were found to be greater than  $\bar{k} = 1 \times 10^8 \text{ M}^{-1} \text{ s}^{-1}$  at higher pH values where these compounds are deprotonated (Tratnyek and Hoigné, 1994). However, under the environmentally relevant conditions employed in this research, phenols are expected to remain protonated where the rate constants for reaction of undissociated phenols with  $^1\text{O}_2$  are small ( $\bar{k} = 1 \times 10^6 - 1 \times 10^8 \text{ M}^{-1} \text{ s}^{-1}$ ) depending on ring substituents, where the smallest value was observed for phenol and increased for methyl -and chloro-substituted phenols (Scully and Hoigné, 1987). Thus, it can be concluded that  $^1\text{O}_2$  does not play a major role in the photooxidation of undissociated phenols.

Alkylperoxy radicals ( $\text{RO}_2^\bullet$ ) are thought to be produced by photolysis of CDOM (Mill et. al., 1980; Mill et. al., 1978) however radical trapping experiments showed no major photochemical source of  $\text{RO}_2^\bullet$  (Kieber and Blough, 1990; Johnson et. al., 1996; Blough 1997). In general, phenols are known to react with organic peroxy radicals,

however rate constants for reaction of undissociated phenols is small ( $k = 1 \times 10^3 - 1 \times 10^6 \text{ M}^{-1} \text{ s}^{-1}$ ) (Neta et. al., 1990). Alkylperoxy radicals are probably not controlling the photooxidized sensitization of phenols in the presence of CDOM in natural waters.

### 1.3.2 Triplet Excited States of Carbonyl-Containing Moieties within CDOM

The observation that the rates of phenol degradation measured in natural waters were much larger than could be accounted for by ROS was a major challenge to the assumption that ROS were acting as the intermediates initiating photooxidation of phenols. Zepp et. al. (1978) first proposed that excited triplet states could react with organic contaminants in natural waters, specifically the photoisomerization of cis-1,3-pentadiene through energy transfer from triplets. During this time, the photophysical properties of triplet excited states were characterized, and the estimated lifetime of humic triplets was determined to be  $\sim 2 \mu\text{s}$  in air-saturated solution (up to  $\sim 50 \mu\text{s}$  in deoxygenated water) and the reactive triplet state concentration was estimated at  $\sim 1 \times 10^{-14} \text{ M}$  in surface, sunlit natural waters (Zepp et. al., 1985; Canonica et. al., 1995a).

Canonica et. al. (1995a) demonstrated similar photochemical behavior for humic substances and the model aromatic ketones, benzophenone (BP), 3'-methoxyacetophenone (3'-MAP) and 2-acetonaphthone (2-AN), in the photosensitized oxidation of a variety of methoxy- and methyl- substituted phenols. These model sensitizers were chosen because these aromatic ketones can absorb sunlight and a significant fraction of carbon atoms in fulvic and humic acids are present as carbonyl moieties (Table I.1) (Stevenson, 1994).

	C (%)	O (%)	C=O (as % of total O)
Humic Acids	53 - 58	33 - 38	15-30
Fulvic Acids	40 - 50	40 - 50	4 - 17

	Ketone (cmole kg <sup>-1</sup> )	Quinone (cmole kg <sup>-1</sup> )	Total (cmole kg <sup>-1</sup> )
Humic Acids	70 - 170	105 - 230	175 - 400
Fulvic Acids	50 - 200	120 - 225	220 - 400

**Table I.1:** (top panel) Carbon and oxygen content (mole %) of humic and fulvic acids and distribution of oxygen in reactive functional groups of humic and fulvic acids (as a percentage of oxygen) (bottom panel) Ketone and quinone carbonyl moiety contents of humic and fulvic acids (mole C kg<sup>-1</sup>).

It was established by Aguer *et. al.* (2005) that a small amount of humic substances could transform a large amount of 2,4,6-trimethylphenol (TMP), suggestive of a catalytic reaction and regeneration of the chromophore. Thus, the photochemical properties of the chromophores acting to degrade TMP, rather than their concentration, might be important.

Canonica *et. al.* (1995a) proposed a mechanism for the reaction of triplet excited state carbonyl moieties with substituted phenols (Figure I.4) which describes the reduction of the triplet excited state ketone to its ketyl radical (through electron or hydrogen atom transfer) and subsequently formation of the phenoxyl radical.



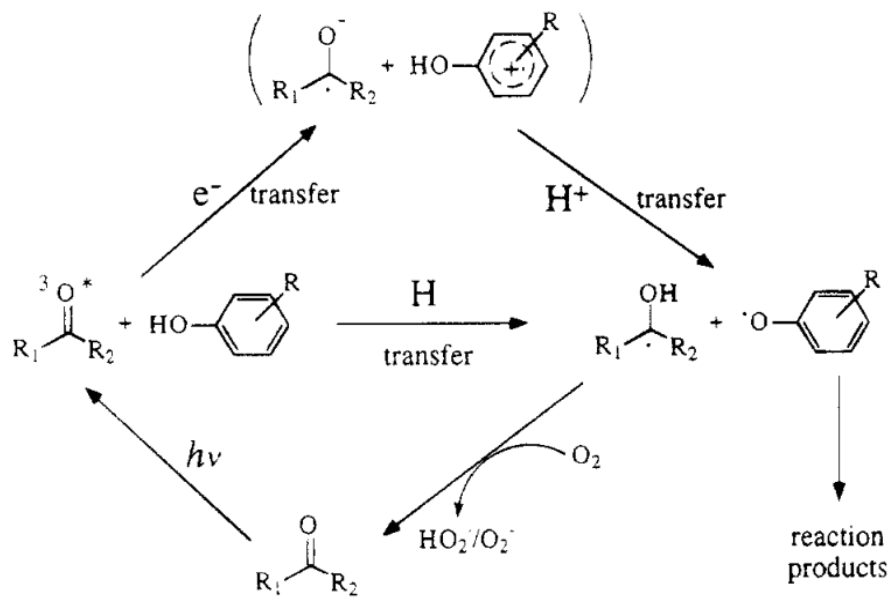


Figure I.4: Proposed reaction model of excited triplet aromatic ketones with phenols.

This figure is adapted from Canonica et. al., 1995a.

Rate constants for quenching of triplet BP by a series of substituted phenols ranged from  $\bar{k} = 2.6 - 5.6 \times 10^9 \text{ M}^{-1} \text{ s}^{-1}$  (see Table I.2) whereas rate constants for 3'-MAP and 2-AN were slightly lower and varied over two orders of magnitude ( $\bar{k}_{q,P} = 10^7 - 10^9 \text{ M}^{-1} \text{ s}^{-1}$ ).

**TABLE 2: Rate Constants for Quenching of Aromatic Ketone Triplet States by Phenols<sup>a</sup>**

quencher	$k_{q,P}(\text{BP})$ ( $\text{M}^{-1} \text{s}^{-1}$ )	$k_{q,P}(3'\text{-MAP})$ ( $\text{M}^{-1} \text{s}^{-1}$ )	$k_{q,P}(2\text{-AN})$ ( $\text{M}^{-1} \text{s}^{-1}$ )
trolox	$(4.1 \pm 0.2) \times 10^9$	$(2.2 \pm 0.2) \times 10^9$	$(2.7 \pm 0.2) \times 10^9$
DMOP	$(5.6 \pm 0.2) \times 10^9$	$(2.4 \pm 0.3) \times 10^9$	$(3.1 \pm 0.1) \times 10^9$
TMP	$(5.1 \pm 0.9) \times 10^9$	$(2.6 \pm 0.3) \times 10^9$	$(7.2 \pm 0.1) \times 10^8$
4-MOP	$(4.2 \pm 0.6) \times 10^9$	$(2.7 \pm 0.3) \times 10^9$	$(1.8 \pm 0.1) \times 10^9$
4-MP	$(4.2 \pm 0.2) \times 10^9$	$(3.0 \pm 0.2) \times 10^9$	$(8.4 \pm 0.3) \times 10^7$
tyrosine	$(2.6 \pm 0.2) \times 10^9$	$(6.6 \pm 0.8) \times 10^8$	$(3.7 \pm 1.3) \times 10^7$
phenol	$(3.9 \pm 0.7) \times 10^9$	$(5.1 \pm 0.4) \times 10^8$	$(3.3 \pm 1.3) \times 10^7$
4-CBP	$(2.9 \pm 0.3) \times 10^9$	$(4.6 \pm 0.6) \times 10^8$	$(2.6 \pm 1.3) \times 10^7$
4-CNP	$(3.0 \pm 0.3) \times 10^9$	$(1.2 \pm 0.5) \times 10^8$	$(1.3 \pm 1.3) \times 10^7$

<sup>a</sup> Errors given as 95% confidence intervals estimated from data fits by the Levenberg–Marquardt method.

**Table I.2:** Rate constants for quenching of aromatic ketone triplets by phenols. Table adapted from Canonica et. al. (2000).

BP was found to react unselectively with all substituted phenols employed in the study with rate constants close to the diffusion limit with water as the solvent. The impact of solvent selection is highlighted by comparison of results obtained by Das and Bhattacharyya (1981) whom reported for BP an increase in rate constant with increasing electron-donating character of the phenol para-substituent from  $\bar{k}_{q,P} = 4.0 \times 10^7 \text{ M}^{-1} \text{ s}^{-1}$  (for *p*-cyano and 4-CNP) to  $\bar{k}_{q,P} = 4.9 \times 10^9 \text{ M}^{-1} \text{ s}^{-1}$  (for *p*-methoxy and 4-MOP) using 1:4 acetonitrile/water as the solvent. Few other studies have examined the triplet state quenching of triplet excited states by phenols using water as the solvent.

The mechanism next describes the oxidation of the ketyl radical by dioxygen where the ground state ketone is regenerated and peroxide (or superoxide) is produced

(Canonica *et. al.*, 1995a). The rate constant for quenching of the triplet by dioxygen was determined to be  $k_{q,O_2} = 2.3 \times 10^9 \text{ M}^{-1} \text{ s}^{-1}$  under aerated conditions. Based on calculations using this rate constant and triplet lifetimes, it was estimated that the triplet population is decreased by ~90% via quenching by dioxygen (Canonica *et.al.*, 2000). Fates of the phenoxyl radical include dimerization (or polymerization) as well as reaction with other reactive species to form products. Jonsson *et. al.* (1993) reported from pulse radiolysis experiments rate constants for reaction of phenoxyl radicals and the superoxide anion radical ( $O_2^{\cdot -}$ ) to range from  $k = 2.0 \times 10^8 \text{ M}^{-1} \text{ s}^{-1}$  to  $3.0 \times 10^9 \text{ M}^{-1} \text{ s}^{-1}$  for a variety of substituted phenols and thus represent a reasonable sink of this radical species.

The mechanism presented in Figure I.4 suggests that the reaction proceeds via electron transfer or hydrogen atom abstraction. Determination of triplet energies by luminescence spectroscopy of the phenols employed in this study (Canonica, *et. al.*, 1995a) were 321 – 346  $\text{kJ mol}^{-1}$ , much larger than the triplet energies determined for the model sensitizers (250 – 300  $\text{kJ mol}^{-1}$ ) eliminating triplet-triplet energy transfer as a viable reaction mechanism. Instead, an electron transfer mechanism was suggested based on the results of deuterium isotope effects of different phenols for fulvic and humic acids. This work provided strong evidence that triplet excited states of CDOM ( $^3\text{CDOM}^*$ ), in particular triplet excited states arising from ketones, aldehydes or quinones, were important to this mechanism but did not preclude the involvement of long-lived photooxidants such as peroxy radicals ( $\text{RO}_2^{\cdot}$ ). Importantly, Canonica *et. al.* (1995b) suggested the use of the methyl-substituted phenol 2,4,6-trimethylphenol (TMP) as the best probes for triplet excited states of CDOM whereas methoxy-substituted phenols were recommended for reaction with long-lived photooxidants such as  $\text{RO}_2^{\cdot}$ .

Triplet excited states of CDOM and HS were strongly implicated in the sunlight-mediated transformation of other organic pollutants such as monuron (Vialaton *et. al.*, 1997), Mirex (Lambrych and Hassett, 2006), bisphenol-A (Zhan *et. al.* 2006; Chin *et. al.*, 2004) and sulfa drugs (Boreen *et. al.*, 2005). For these samples, the rate of phototransformation was enhanced upon deoxygenation and decreased upon addition of oxygen or isoprene as triplet quenchers, providing further evidence for the role of triplets for these chemicals.

These and other studies have presented strong lines of circumstantial evidence that triplet excited states of aromatic ketones and aldehydes play a major role in the photooxidation of phenols (and some other compounds) in natural waters, however none have performed direct experimental tests of this hypothesis.

In Chapter II, the dependence of the initial rate of 2,4,6-trimethylphenol (TMP) loss ( $R_{\text{TMP}}$ ) on dioxygen concentration for both untreated and borohydride-reduced HS and C18 extracts of the MAB are determined. In Chapter III, the effect of increasing borohydride-to-HS mass ratios on the optical and photochemical properties of HS are explored along with the wavelength dependence of  $R_{\text{TMP}}$  under low (62  $\mu\text{M}$ ) and aerated (250  $\mu\text{M}$ ) dioxygen concentrations for untreated and borohydride-reduced HS and C<sub>18</sub> extracts of the MAB.

We find that  $R_{\text{TMP}}$  was inversely proportional to dioxygen concentration at  $[\text{O}_2] > 50 \mu\text{M}$ , a dependence consistent with reaction with triplet excited states, but not with  $^1\text{O}_2$  or  $\text{RO}_2$ . Modeling the dependence of  $R_{\text{TMP}}$  on  $[\text{O}_2]$  provided rate constants for TMP reaction,  $\text{O}_2$  quenching and lifetimes compatible with a triplet intermediate. Borohydride reduction significantly reduced TMP loss, supporting the role of aromatic ketone triplets

in this process. However, for most samples, the incomplete loss of sensitization following borohydride reduction, as well as the inverse dependence of  $R_{\text{TMP}}$  on  $[\text{O}_2]$  for these reduced samples, suggests that there remains another class of oxidizing triplet sensitizer, perhaps quinones. However, the results of the wavelength dependence reveal that the sensitization is driven primarily by shorter wavelength UV-B and UV-A absorbing moieties, consistent with the involvement of aromatic ketones and aldehydes but appearing to exclude the longer wavelength (visible) absorbing quinones as sensitizers. An inverse dependence of  $\Phi$  on one-electron reduction potential was observed where  $\text{DMOP} \approx \text{TMP} > 4\text{-MOP} > 4\text{-MP} > \text{phenol}$ . Similar dependencies were observed for TMP and 4-MOP in the dependence of  $R_{\text{probe}}$  on  $[\text{O}_2]$  whereas DMOP did not exhibit a substantially lower  $R_{\text{probe}}$  at high  $[\text{O}_2]$  as would be expected for a triplet sensitization mechanism. Moreover, that a significant amount of sensitization is observed following borohydride reduction of SRFA for DMOP under high  $[\text{O}_2]$ , as well as the very low sensitization observed at low  $[\text{O}_2]$  indicates that a separate pathway, unrelated to triplets, may be important for the mechanism of DMOP photooxidation by chromophoric dissolved organic matter.

## **Chapter II: Dependence of the Initial Rate of 2,4,6-trimethylphenol (TMP) on [TMP], [Dioxygen] and Sodium Borohydride Reduced Humic Substances**

### **Abstract**

To probe the mechanism of the photosensitized loss of phenols by humic substances (HS), the dependence of the initial rate of 2,4,6-trimethylphenol (TMP) loss ( $R_{\text{TMP}}$ ) on dioxygen concentration was examined both for a variety of untreated as well as borohydride-reduced HS and  $C_{18}$  extracts from the Delaware Bay and Mid-Atlantic Bight.  $R_{\text{TMP}}$  was inversely proportional to dioxygen concentration at  $[O_2] > 50 \mu\text{M}$ , a dependence consistent with reaction with triplet excited states, but not with  $^1O_2$  or  $RO_2$ . Modeling the dependence of  $R_{\text{TMP}}$  on  $[O_2]$  provided rate constants for TMP reaction,  $O_2$  quenching and lifetimes compatible with a triplet intermediate. Borohydride reduction significantly reduced TMP loss, supporting the role of aromatic ketone triplets in this process. However, for most samples, the incomplete loss of sensitization following borohydride reduction, as well as the inverse dependence of  $R_{\text{TMP}}$  on  $[O_2]$  for these samples, suggests that there remains another class of oxidizing triplet sensitizer, perhaps quinones.

### **2.1 Introduction**

The photosensitized oxidation of phenols in natural waters by the chromophore-containing constituents of dissolved organic matter (CDOM) and humic substances (HS) has been the focus of numerous studies over the last twenty years (see footnote). In early work, attention was centered on photoproducted reactive oxygen species (ROS) (Blough and Zepp, 1995), namely peroxy radicals ( $RO_2$ ) (Mill *et. al.*, 1980), the hydroxyl radical ( $\bullet\text{OH}$ ) (Zepp *et. al.*, 1987; Vaughan and Blough, 1998) and singlet dioxygen ( $^1O_2$ ) (Zepp *et. al.*, 1977 and 1981; Haag *et. al.*, 1984), as the intermediates initiating oxidation.

However, radical trapping experiments showed little evidence of a major photochemical source of RO<sub>2</sub> (Kieber and Blough, 1990; Johnson, et. al., 1996; Blough 1997). Further, both RO<sub>2</sub> and <sup>1</sup>O<sub>2</sub> have rate constants for reaction with undissociated phenols that are relatively small, of the order 10<sup>3</sup> to 10<sup>6</sup> M<sup>-1</sup>s<sup>-1</sup> for RO<sub>2</sub> (Neta et. al., 1990) and 10<sup>6</sup> to 10<sup>8</sup> M<sup>-1</sup>s<sup>-1</sup> for <sup>1</sup>O<sub>2</sub> (Scully and Hoigné, 1987; Tratnyek and Hoigné, 1991 and 1994), depending on the phenol ring substituent(s). Although the rate constants for the reaction of •OH with phenols are much larger (Lundqvist and Eriksson, 2000), the very low steady state concentrations of this intermediate found in most natural waters appeared to preclude this species as a dominant sink as well (Faust and Hoigné, 1987; Haag and Hoigné, 1985). Based on estimates of the steady-state concentrations of these ROS produced photochemically from CDOM in natural waters (Blough and Zepp, 1995), the measured loss rates of many phenols at environmentally relevant concentrations appeared significantly larger than could be produced by these ROS (Faust and Hoigné, 1987).

Canonica *et. al.*, (1995) first provided evidence that excited triplet states of CDOM, in particular oxidizing triplet states arising from aromatic ketones, could be important in phenol oxidation. Later studies by Canonica *et. al.* (2000, 2007, 2008) and co-workers (Wenk et. al., 2011), as well as by other investigators (Aguer *et. al.*, 1997; Halladja *et. al.*, 2007; Guerard *et. al.*, 2009; Cawley *et. al.*, 2009), provided additional support for the involvement of triplet states not only in the CDOM-sensitized oxidation of phenols, but in the oxidation of other compounds as well (Guerard *et. al.*, 2009; Boreen, *et. al.*, 2005; Werner *et. al.*, 2005; Canonica *et. al.*, 2006).

However, relatively few of these studies performed direct experimental tests of the triplet photosensitization hypothesis, and none, to our knowledge, have directly probed the possible role of ketone triplets in this sensitization. Here, we examine the dependence of the rates of the photosensitized loss of 2,4,6-trimethylphenol (TMP) on  $[O_2]$ , both for a variety of untreated HS samples as well as those reduced with sodium borohydride. Sodium borohydride is known to reduce selectively carbonyl-containing compounds such as ketones and aldehydes within HS (Johnson and Rickborn, 1970; Leenheer *et. al.*, 1995; Tinnacher and Honeyman, 2007). Moreover, prior work has shown that borohydride reduction of HS substantially alters the optical properties of these materials and that these changes are largely irreversible following re-oxidation under aerated conditions, consistent with the reduction of ketones/aldehydes to alcohols (Tinnacher and Honeyman, 2007; Ma *et. al.*, 2010).

We find that borohydride reduction significantly reduces TMP loss, supporting the role of aromatic ketone triplets in this process. Further, above  $\sim 50 \mu M O_2$ , the initial rate of TMP loss ( $R_{TMP}$ ) is inversely proportional to  $[O_2]$ ; a dependence that is consistent with reaction with triplets, but not with  $^1O_2$  or  $RO_2$ . Together, these results provide strong evidence that the triplet states of aromatic ketones/aldehydes play a significant role in the photosensitized loss of TMP by CDOM as originally proposed by Canonica and co-workers (1995 a,b). However, the incomplete loss of sensitization for most samples following borohydride reduction, as well as the inverse dependence of  $R_{TMP}$  on  $[O_2]$  for these samples, suggests that there remains another class of oxidizing triplet sensitizers, perhaps quinones.



## **2.2 Materials and Methods**

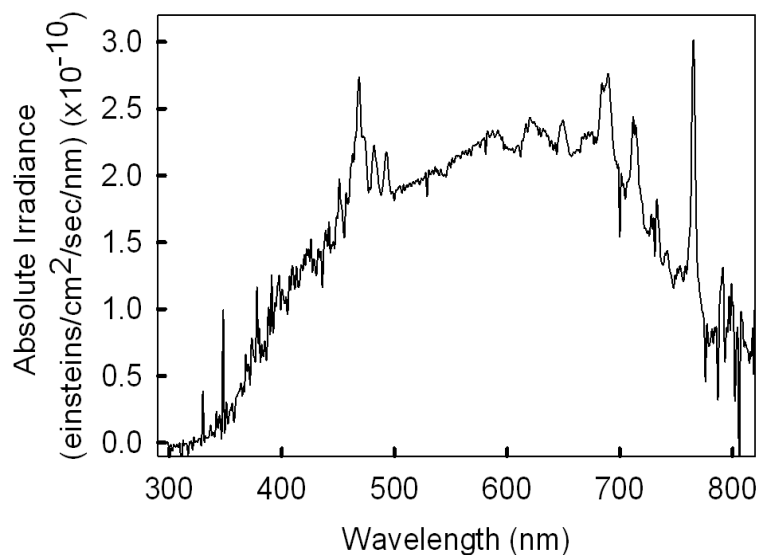
### **2.2.1 Materials**

All chemicals were used as received. Analytical grade 2,4,6-trimethylphenol (TMP) was obtained from Fluka. Lignin, alkali extracted and carboxylated (LAC), was obtained from Sigma Aldrich (Lot #19714DS). Suwanee River humic acid (SRHA) and Suwanee River fulvic acid (SRFA) were obtained from the International Humic Substances Society. Solid-phase C<sub>18</sub> extracts from a Delaware Bay upper bay station (UBS; 39.633N, -75.574W), lower bay station (LBS; 38.882N, -75.094W) and shelf station (SS; 38.6763 N, -74.8873 W) within the Middle Atlantic Bight (MAB) were collected in December 2006 and processed as previously reported (Ma *et. al.*, 2010). Water was obtained from a Millipore Milli-Q purification system. Dipotassium hydrogen phosphate (K<sub>2</sub>HPO<sub>4</sub>) and dimethyl sulfoxide (DMSO) were obtained from Sigma Aldrich whereas potassium dihydrogen phosphate (KH<sub>2</sub>PO<sub>4</sub>), sodium borohydride (NaBH<sub>4</sub>) and 2-propanol (IPA) were obtained from Fischer Scientific. Ultra-high purity compressed gases were obtained from Airgas. Potassium hydrogen phthalate (KHP) was obtained from Nacalai Tesque, Inc.

### **2.2.2 Apparatus**

TMP analyses were performed in triplicate using RP-HPLC system consisting of a Shimadzu LC-10AS pump, 50 µL loop and a Waters RCM 8x10 cartridge which supported a Waters Nova-Pak C<sub>18</sub> column (5x100mm, 4µm pore size). Analyses were performed under isocratic conditions using a mobile phase composition of 60% methanol, 30% water and 10% dilute acetic acid (1%) at a flow rate of 1 mL min.<sup>-1</sup> TMP detection was performed using a Dionex AD25 absorbance detector set to 280 nm.

Samples were irradiated in a 1 cm quartz cuvette using a 300 W high pressure xenon arc lamp following passage through 8 cm of water to remove infrared radiation and a longpass wavelength filter (50% transmission at 325 nm) to simulate the solar spectrum. The spectral output of the lamp was measured using an Ocean Optics USB2000 spectroradiometer and is provided in Fig. II.1. The integrated intensity was approximately 57 mW/cm<sup>2</sup> and did not change significantly throughout the study period.



**Figure II.1:** Absolute irradiance of the high pressure xenon arc lamp employed in this study. The spectral output of the lamp was recorded using an Ocean Optics USB2000 spectroradiometer where the integrated intensity is ~57 mW/cm<sup>2</sup>.

Ultraviolet/visible absorption measurements employed a Shimadzu 2401-PC dual beam spectrophotometer. Spectra were collected versus air over the range 190-820 nm and corrected by subtraction of a Milli-Q water spectrum. Total organic carbon (TOC) was determined using high temperature oxidation (680°C) on a Shimadzu 5000A TOC

analyzer calibrated using KHP. Specific absorption coefficients,  $a^*(\lambda)$ , were obtained using equation II.1

$$a^*(\lambda) = 2.303 \cdot A(\lambda) / (b \cdot C) \quad (\text{II.1})$$

where  $A(\lambda)$  is the absorbance at a given wavelength,  $b$  is the pathlength in meters and  $C$  is the concentration of total organic carbon in mg carbon  $\text{L}^{-1}$ . The spectral slope parameter ( $S$ ) was obtained by a non-linear least squares fitting of the spectra over the range from 290 to 820 nm to equation II.2

$$a^*(\lambda) = a^*(\lambda_{\text{Ref}}) e^{-S(\lambda - \lambda_{\text{Ref}})} \quad (\text{II.2})$$

where  $a^*(\lambda_{\text{Ref}})$  is the specific absorption coefficient at the reference wavelength of 350 nm.

### 2.2.3 Photochemical Experiments.

Stock solutions of 1000  $\text{mg L}^{-1}$  LAC, SRHA and SRFA and 500  $\mu\text{M}$  TMP were prepared in MQ water. The SRHA stock solution was passed through a 0.2  $\mu\text{m}$  filter prior to use. The absorbance of the  $\text{C}_{18}$  extracts were matched at 350 nm to a spectrum of 10  $\text{mg L}^{-1}$  ( $[\text{DOC}] = 4.9 \text{ mg C L}^{-1}$ ) SRFA at  $\text{pH}=7.0$ , the concentration used in the irradiations. All stock solutions and samples were stored in the dark at  $4^\circ\text{C}$  when not in use. Just prior to irradiation, final solutions containing SRFA, SRHA, LAC ( $10 \text{ mg L}^{-1}$ ) or the  $\text{C}_{18}$  extracts and TMP (5-100  $\mu\text{M}$ ) were prepared in 50 mM phosphate buffer at  $\text{pH}=7.0$  (PB). Control samples contained TMP alone in PB. IPA and DMSO, at 100 mM, were used in independent experiments as hydroxyl radical scavengers. Samples were transferred to a 1 cm quartz cuvette and were irradiated for 15 minutes under differing  $[\text{O}_2]$  achieved through mixing ultra-high purity (UHP) nitrogen, dioxygen or air in a dual flow rotameter. Samples reduced with sodium borohydride (see below) were treated in a

similar manner. Aerated solutions were kept open to the atmosphere, whereas analyses performed under controlled dioxygen conditions were sparged for 5 minutes prior to irradiation followed by flushing of the headspace of a closed vial during irradiation.

Quantification of TMP was performed using RP-HPLC at 5 minute intervals during the 15 minute irradiation time in which [TMP] decreased linearly. The direct photochemical loss of TMP was negligible (<5%) over this time period.

Estimated (polychromatic) apparent quantum efficiencies ( $\Phi$ ) of TMP loss for both untreated and borohydride-reduced samples were calculated using equation II.3,

$$\Phi = R_{\text{TMP}} / R_{\text{EX}} \quad (\text{II.3})$$

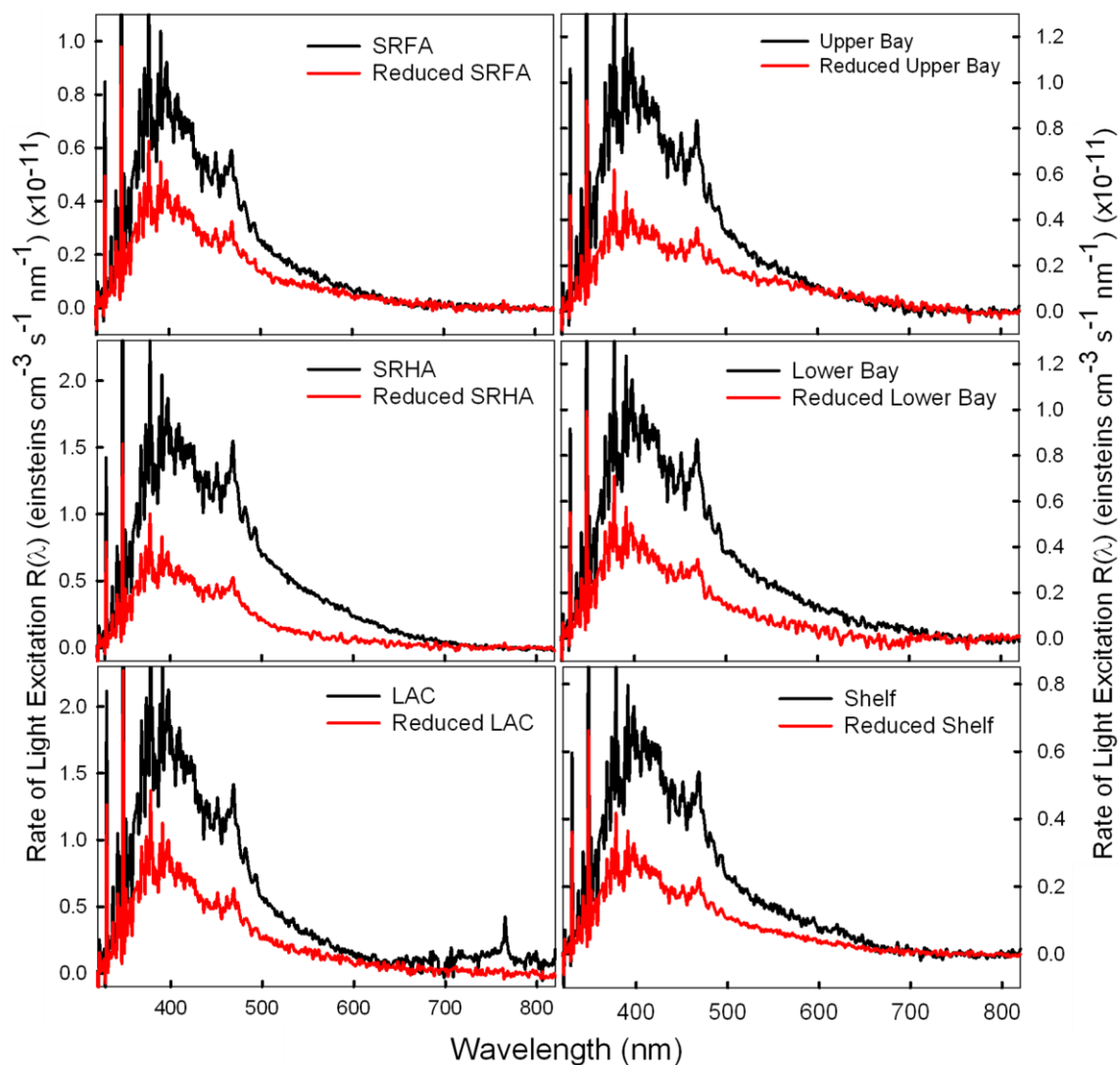
where  $R_{\text{TMP}}$  is the initial rate of TMP loss at 100  $\mu\text{M}$  TMP and 250  $\mu\text{M}$   $\text{O}_2$  (air-saturated), and  $R_{\text{EX}}$  is the rate of light excitation given by equation II.4,

$$R_{\text{EX}} = I(\lambda) \cdot a(\lambda) = \int_{190}^{820} R(\lambda) d\lambda \quad (\text{II.4})$$

where  $a(\lambda)$  is the absorption coefficient of the sample,  $I(\lambda)$  is the spectral photon irradiance at the front face of the cuvette as measured with the Ocean Optics spectroradiometer and  $R(\lambda)$  provides the wavelength dependence of the light excitation rate (see Fig. II.2). To obtain an estimate of the apparent quantum efficiency of the species eliminated by borohydride reduction, equation 2.5 was employed,

$$\Phi_{\text{diff}} = (R_{\text{TMP}}^{\text{U}} - R_{\text{TMP}}^{\text{R}}) / (R_{\text{EX}}^{\text{U}} - R_{\text{EX}}^{\text{R}}) \quad (\text{II.5})$$

where the superscripts U and R denote untreated and borohydride-reduced samples, respectively.



**Figure II.2:** Wavelength dependence of  $R(\lambda) = (a(\lambda) \cdot I(\lambda))$  for untreated (black trace) and borohydride-reduced (red trace) SRFA, SRHA, LAC and  $C_{18}$  extracts of the Delaware Bay and Mid-Atlantic Bight.

#### 2.2.4 NaBH<sub>4</sub> Reduction.

Sodium borohydride (NaBH<sub>4</sub>) was employed to reduce LAC, SRHA, SRFA and  $C_{18}$  extracts as previously reported (Tinnacher and Honeyman, 2007, Ma *et. al.*, 2010). Briefly, concentrated solutions of humic substances (HS) or the  $C_{18}$  extracts were transferred to a 1 cm quartz cuvette and purged with UHP nitrogen for 15 minutes to

exclude dioxygen. A five-fold excess by weight of  $\text{NaBH}_4$  was added and the sample was immediately placed under nitrogen purge. The reduction was considered to be complete when no further changes in the optical properties were observed, usually after 24 hours. Borohydride-reduced samples (4 mL) were passed over a 2.5 cm x 8 cm Sephadex G-10 (40 – 120  $\mu\text{m}$ ) column equilibrated with Milli-Q water to remove excess borate and borohydride and adjust the pH to neutral. Note that upon re-introduction of dioxygen, any quinones previously reduced to hydroquinones by borohydride under anaerobic conditions are expected to be re-oxidized to quinones within 24 hr (Tinnacher and Honeyman, 2007, Ma *et. al.*, 2010; Aeschbacher *et. al.*, 2010) and thus would not be removed by this procedure.

## **2.3 Results and Discussion**

### **2.3.1. Effects of $\text{NaBH}_4$ Reduction on Absorption Spectra and TMP Sensitization**

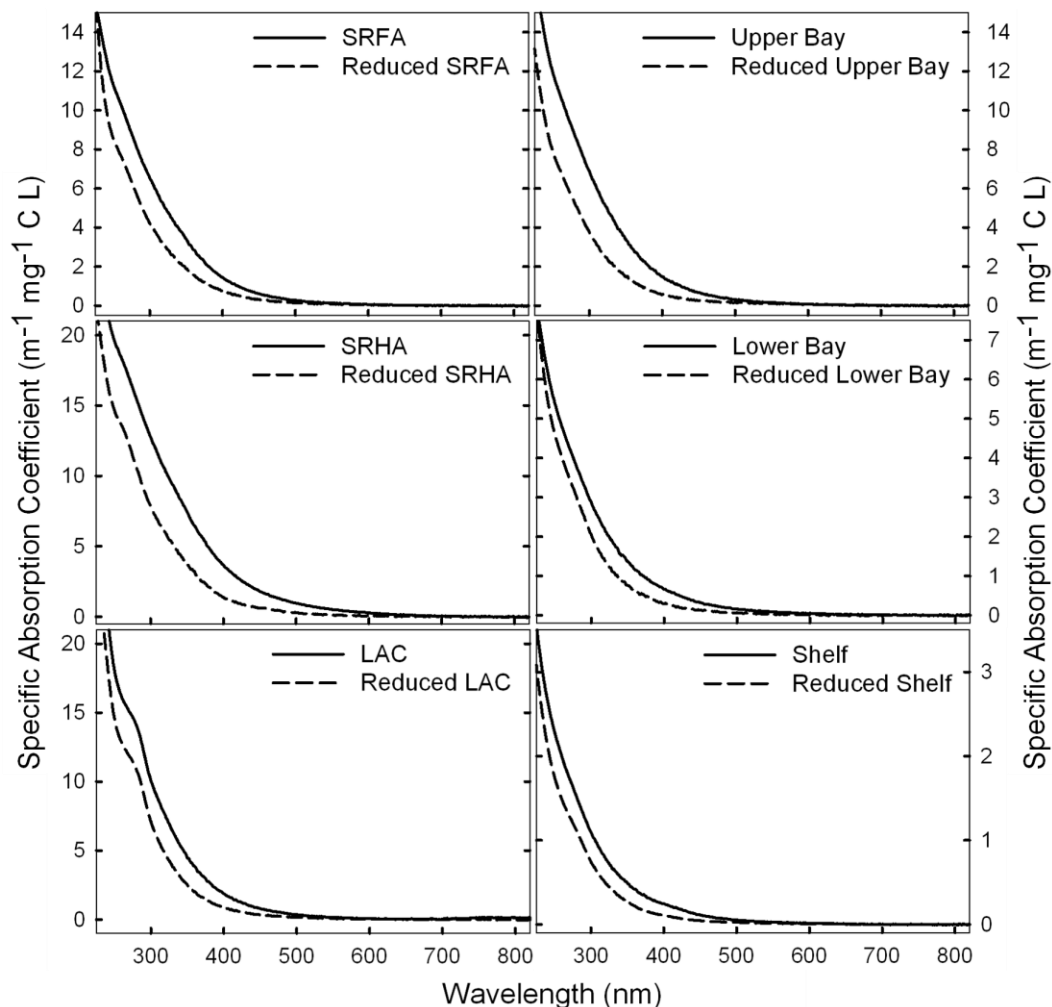
The specific absorption coefficients ( $a^*(350)$ ) of the untreated samples decreased in the order  $\text{SRHA} > \text{LAC} > \text{SRFA} \sim \text{UBS} > \text{LBS} > \text{SS}$  (Table II.1).

	$a^*(350)$ ( $\text{m}^{-1} \text{mg}^{-1} \text{C L}^{-1}$ )	$S$ ( $\text{nm}^{-1}$ )	$R_{\text{TMP}}$ ( $\text{M s}^{-1}$ ) ( $\times 10^{-8}$ )
SRFA	3.42	0.014	$2.1 \pm 0.5$
Reduced SRFA	1.90	0.016	$0.80 \pm 0.10$
SRHA	7.46	0.012	$1.3 \pm 0.1$
Reduced SRHA	3.74	0.015	$0.51 \pm 0.08$
LAC	4.48	0.016	$0.69 \pm 0.12$
Reduced LAC	2.52	0.019	$0.00 \pm 0.08$
UBS	3.39	0.015	$1.7 \pm 0.2$
Reduced UBS	1.48	0.017	$0.62 \pm 0.16$
LBS	1.37	0.014	$2.2 \pm 0.1$
Reduced LBS	0.76	0.017	$0.92 \pm 0.11$
SS	0.49	0.015	$2.3 \pm 0.3$
Reduced SS	0.27	0.020	$0.97 \pm 0.17$

**Table II.1:** Values of specific absorbance coefficient at 350 nm ( $a^*(350)$ ), spectral slope ( $S$ ) and initial rate of TMP loss ( $R_{\text{TMP}}$ ) for unaltered and borohydride-reduced SRFA, SRHA, LAC and C18 extracts from upper bay station (UBS), lower bay station (LBS) and shelf station (SS) from the Delaware Bay and Mid-Atlantic Bight.  $R_{\text{TMP}}$  was determined at  $[\text{TMP}] = 100 \mu\text{M}$  and  $[\text{O}_2] = 250 \mu\text{M}$  and the uncertainty for  $S = 0.001 \text{ nm}^{-1}$  and  $a^*(350) = 0.01 \text{ m}^{-1} \text{mg}^{-1} \text{C L}$ .

A similar trend was observed in the loss of specific absorption at 350 nm ( $\Delta a^*(350)$ ) following borohydride reduction, where SRHA exhibited the largest  $\Delta a^*(350)$  ( $3.7 \text{ m}^{-1} \text{mg}^{-1} \text{L}^{-1}$ ), while  $\Delta a^*(350)$  for LAC was similar to the upper bay sample (UBS) and SRFA (2.0, 1.9 and  $1.5 \text{ m}^{-1} \text{mg}^{-1} \text{L}^{-1}$ , respectively) and the lowest values were

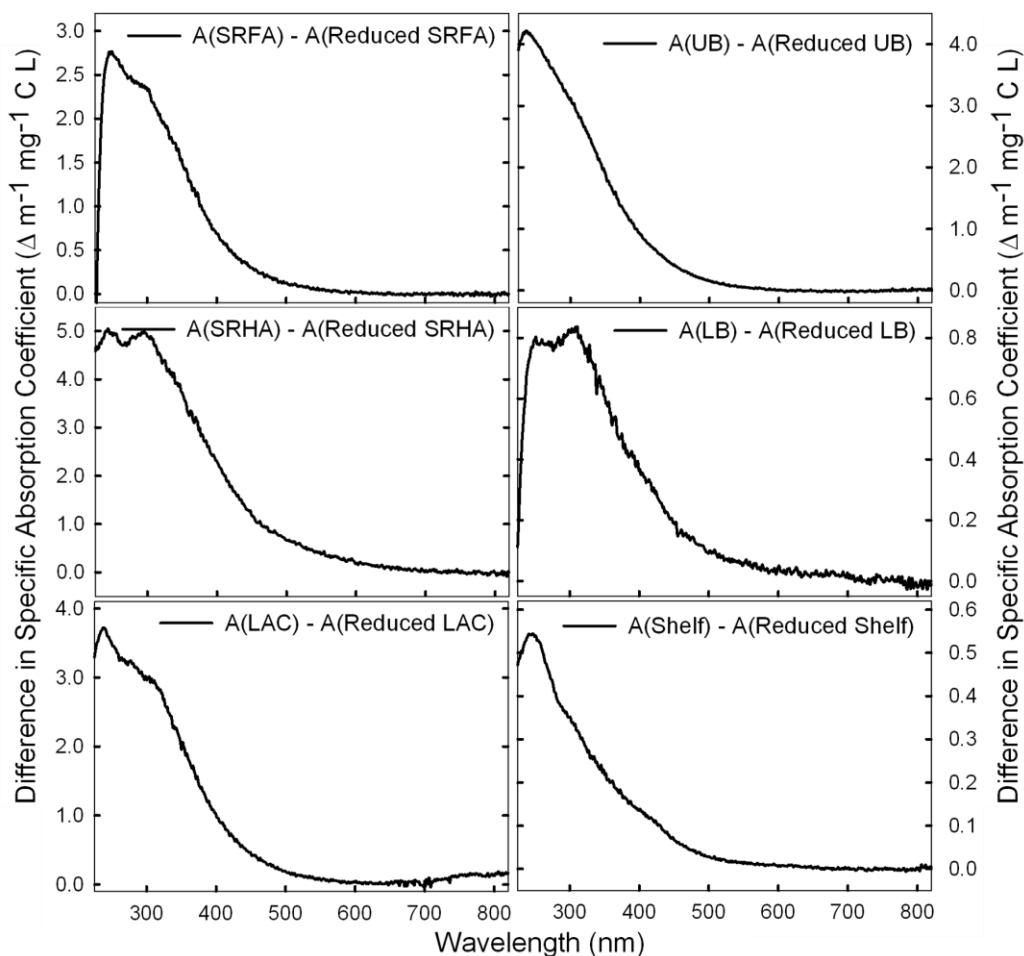
observed for lower bay sample (LBS) and shelf sample (SS) ( $0.61$  and  $0.22 \text{ m}^{-1} \text{ mg}^{-1} \text{ L}^{-1}$ , respectively). As previously reported (Tinnacher and Honeyman, 2007, Ma *et. al.*, 2010), borohydride reduction produced the largest absolute absorption losses in the ultraviolet (Fig. II.3-4), but the greatest fractional losses in the visible.



**Figure II.3:** Absorption spectra of untreated and borohydride-reduced SRFA, SRHA, LAC and  $C_{18}$  extracts of an upper bay station (UBS), lower bay station (LBS) and shelf station (SS) obtained from the Delaware Bay and Mid-Atlantic Bight. Samples are in water at  $pH=7$ . SRFA, SRHA and LAC concentrations were  $10 \text{ mg L}^{-1}$ , whereas carbon concentrations were  $4.93$ ,  $3.95$  and  $1.97 \text{ mg C L}^{-1}$ , respectively. The absorbance of UBS,



*LBS and SS were matched at 350 nm to that of SRFA at 10 mg L<sup>-1</sup>, whereas carbon concentrations were 6.49, 12.2 and 22.1 mg C L<sup>-1</sup>, respectively.*

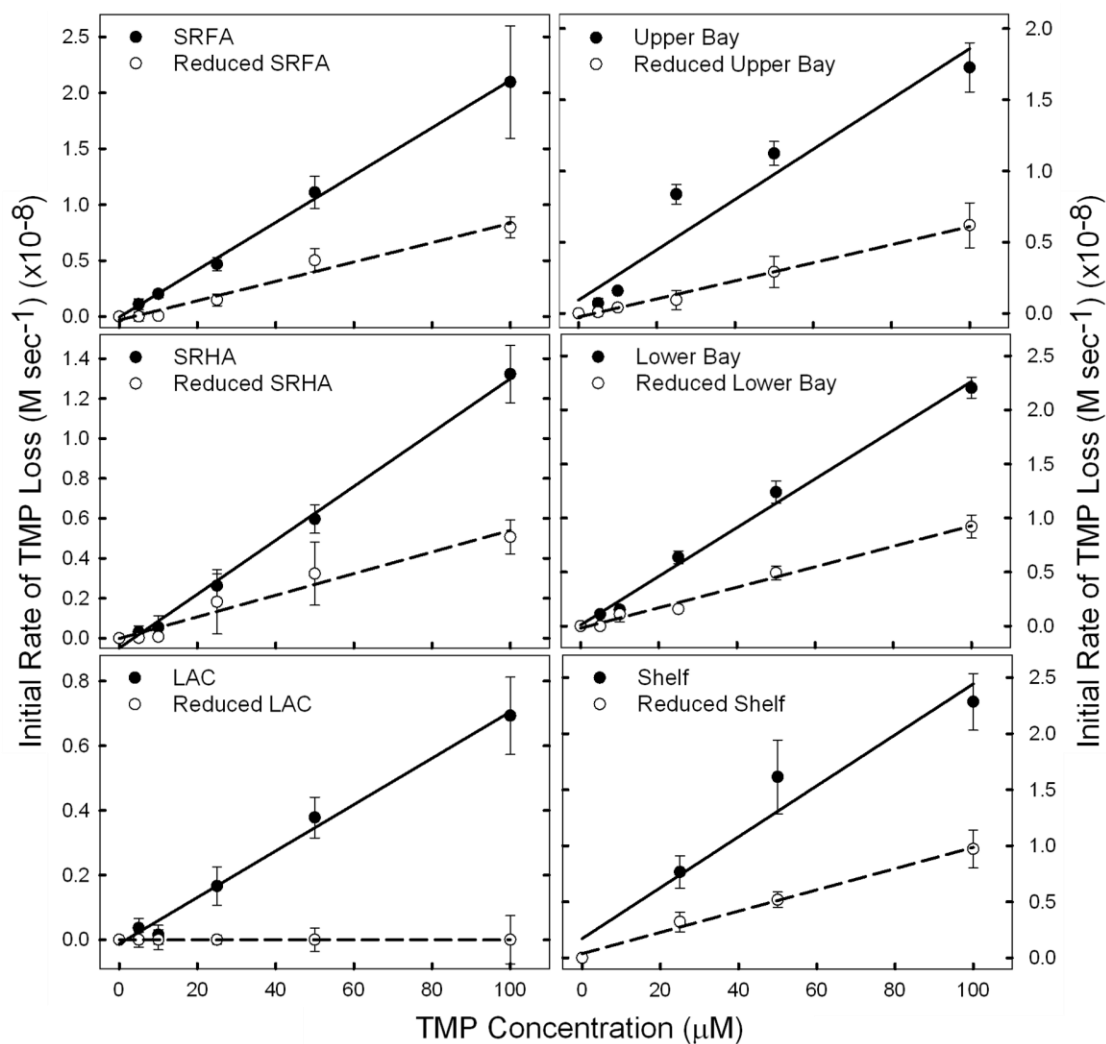


**Figure II.4:** Absorbance difference spectra for SRFA, SRHA, LAC, upper bay sample (UBS), lower bay sample (LBS) and shelf sample (SS). The difference in absorbance was calculated using  $\Delta a^* = a^*(t) - a^*(0)$  where  $a^*(t)$  and  $a^*(0)$  are the specific absorption coefficients of the borohydride-reduced and untreated samples, respectively.

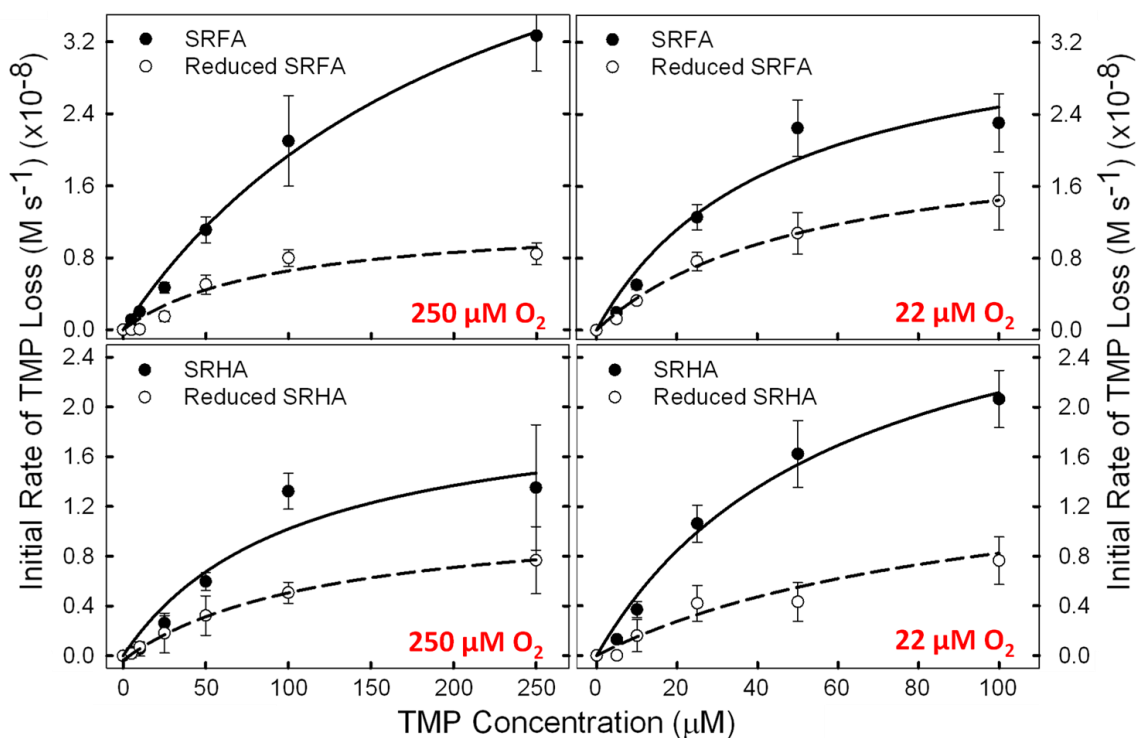
Consequently, the values of S, the spectral slope parameter, increased for all samples following borohydride reduction (Table II.1). The preferential loss of long-wavelength visible absorption has been previously attributed to the loss of charge-transfer

(CT) transitions owing to the removal of carbonyl-containing electron acceptors (Ma *et. al.*, 2010; Del Vecchio and Blough, 2004; Boyle, *et. al.*, 2009) whereas the loss of absorption in the ultraviolet can be attributed to the direct loss of absorption from ketones/aldehydes resulting from their reduction to aliphatic and aromatic alcohols, as well as from a possible contribution from the loss of charge-transfer transitions in the near UV (Del Vecchio and Blough, 2004). Prior NMR and IR measurements (Leenheer *et. al.*, 1995; Tinnacher and Honeyman, 2007) have shown that aquatic humic substances contain significant levels of aromatic ketones/aldehydes that are removed by borohydride reduction, producing a concomitant loss of absorption at wavelengths in the UV-A where these species are expected to absorb.

To determine how the removal of ketone/aldehyde moieties by chemical reduction affects the photosensitized oxidation of TMP, the dependence of the initial rate of TMP loss ( $R_{\text{TMP}}$ ) on [TMP] was first examined for both untreated and borohydride-reduced samples under equal mass concentrations. Under aerated conditions (250  $\mu\text{M}$   $\text{O}_2$ ), the  $R_{\text{TMP}}$  of the untreated samples appeared to increase linearly with increasing [TMP] over the range from 5 to 100  $\mu\text{M}$  (Fig. II.5); only at [TMP]  $\geq$  100  $\mu\text{M}$  was curvature observed, suggestive of saturation in the initial rate (Fig. II.6, left panels).



**Figure II.5:** Dependence of the initial rate of TMP loss ( $R_{TMP}$ ) on [TMP] for both untreated and borohydride-reduced SRFA, SRHA, LAC, UBS, LBS and SS under aerated conditions ( $250 \mu\text{M O}_2$ ). Other conditions as in Figure II.3. Error bars represent  $\pm 1$  standard deviation of at least three independent determinations.



**Figure II.6:** Dependence of  $R_{\text{TMP}}$  on  $[\text{TMP}]$  for both untreated and borohydride-reduced SRFA and SRHA at high (250  $\mu\text{M}$ ) and low (22  $\mu\text{M}$ )  $[\text{O}_2]$ . The data were fit to the equation  $R_{\text{TMP}} = a \cdot [\text{TMP}] / (b + [\text{TMP}])$  using a non-linear least squares fitting routine.

In contrast, the borohydride-reduced samples exhibited an ~50-100% reduction in  $R_{\text{TMP}}$ , while the  $R_{\text{TMP}}$  of samples exhibiting residual TMP loss also appeared to increase linearly with increasing  $[\text{TMP}]$  (Fig. II.5;  $[\text{TMP}] \leq 100 \mu\text{M}$ ).

At  $[\text{O}_2] = 250 \mu\text{M}$ , complete loss of sensitization was observed for LAC following borohydride reduction, suggesting that ketone/aldehyde moieties and their associated triplet excited states are principally responsible for the loss of TMP in this sample (Fig. II.5). For the remaining samples, the incomplete loss of sensitization could be attributed to a number of factors: 1) incomplete reduction of ketone/aldehyde moieties in these samples; 2) reaction with ROS such as  $^1\text{O}_2$ ,  $\text{RO}_2$  or  $\bullet\text{OH}$ ; or 3) reaction with

triplet excited states of other remaining species such as quinones (Bisby and Parker, 1995; Amada *et. al.*, 1995; Garg *et. al.*, 2007).

Based on prior studies that investigated the effect of borohydride concentration on the kinetics and extent of the absorption losses following reduction (Tinnacher and Honeyman, 2007; Ma *et. al.*, 2010), the incomplete removal of ketone/aldehyde moieties, although possible, appears unlikely. Further, addition of  $\bullet\text{OH}$  scavengers, DMSO and IPA, had no effect on  $R_{\text{TMP}}$ , thus precluding a significant contribution from  $\bullet\text{OH}$  in these samples (data not shown). As shown below, the inverse dependence of  $R_{\text{TMP}}$  on  $[\text{O}_2]$  also precludes a significant sink due to reaction with  $\text{RO}_2$  and  $^1\text{O}_2$ . Because quinones are not irreversibly reduced by borohydride (Tinnacher and Honeyman, 2007; Ma *et. al.*, 2010) or electrochemically (Aeschbacher *et. al.*, 2010), following aeration, reaction of TMP with the excited triplet states of quinones remains a possible pathway (Bisby and Parker, 1995; Amada *et. al.*, 1995).

To allow for a comparison among the untreated samples, as well as to examine further the effects of borohydride reduction on TMP loss, estimated (polychromatic) apparent quantum efficiencies ( $\Phi$ ), obtained at  $[\text{TMP}] = 100 \mu\text{M}$  under aerated conditions ( $250 \mu\text{M O}_2$ ), were calculated as described in Materials and Methods (Table II.2).

	$R_{TMP}$ ( $M s^{-1}$ ) ( $\times 10^{-8}$ )	$R_{EX}$ ( $M s^{-1}$ ) ( $\times 10^{-6}$ )	$\Phi$ (%)	$\Phi_{diff}$ (%)
SRFA	$2.1 \pm 0.5$	1.1	$2.0 \pm 0.5$	$2.7 \pm 0.5$
Reduced SRFA	$0.80 \pm 0.10$	0.57	$1.4 \pm 0.2$	
SRHA	$1.3 \pm 0.1$	2.5	$0.53 \pm 0.04$	$0.49 \pm 0.11$
Reduced SRHA	$0.51 \pm 0.08$	0.86	$0.60 \pm 0.09$	
LAC	$0.69 \pm 0.12$	2.6	$0.27 \pm 0.05$	$0.49 \pm 0.09$
Reduced LAC	$0.00 \pm 0.08$	1.2	$0.00 \pm 0.00$	
Upper Bay	$1.7 \pm 0.2$	1.4	$1.2 \pm 0.1$	$1.5 \pm 0.3$
Reduced Upper Bay	$0.62 \pm 0.16$	0.65	$0.95 \pm 0.24$	
Lower Bay	$2.2 \pm 0.1$	1.4	$1.5 \pm 0.1$	$1.5 \pm 0.1$
Reduced Lower Bay	$0.92 \pm 0.11$	0.57	$1.6 \pm 0.2$	
Shelf	$2.3 \pm 0.3$	0.90	$2.6 \pm 0.3$	$2.7 \pm 0.5$
Reduced Shelf	$0.97 \pm 0.17$	0.40	$2.4 \pm 0.4$	

**Table II.2:** Apparent (polychromatic) quantum efficiencies ( $\Phi$ ) for TMP loss by untreated and borohydride-reduced SRFA, SRHA, LAC and  $C_{18}$  extracts from an upper bay station (UBS), lower bay station (UBS) and shelf station (SS) from the Delaware Bay and Mid-Atlantic Bight.  $R_{TMP}$  as determined at  $[TMP] = 100 \mu M$  and  $[O_2] = 250 \mu M$ .  $R_{EX}$  is the rate of light absorption calculated as determined in Materials and Methods. Note that higher  $\Phi_{diff}$  indicates that the loss of absorption (difference in the rate of light absorption) following borohydride reduction is smaller proportionally than the decrease of  $R_{TMP}$ . Uncertainties for  $\Phi$  were propagated from the determination of  $R_{TMP}$ .

These efficiencies are similar in magnitude to the apparent quantum yields for  $^1O_2$  production previously reported for a variety of humic substances (Aguer and Richard, 1996; Sandvik *et. al.*, 2000; Zepp *et. al.*, 1985; Paul *et. al.*, 2004). It should be noted,

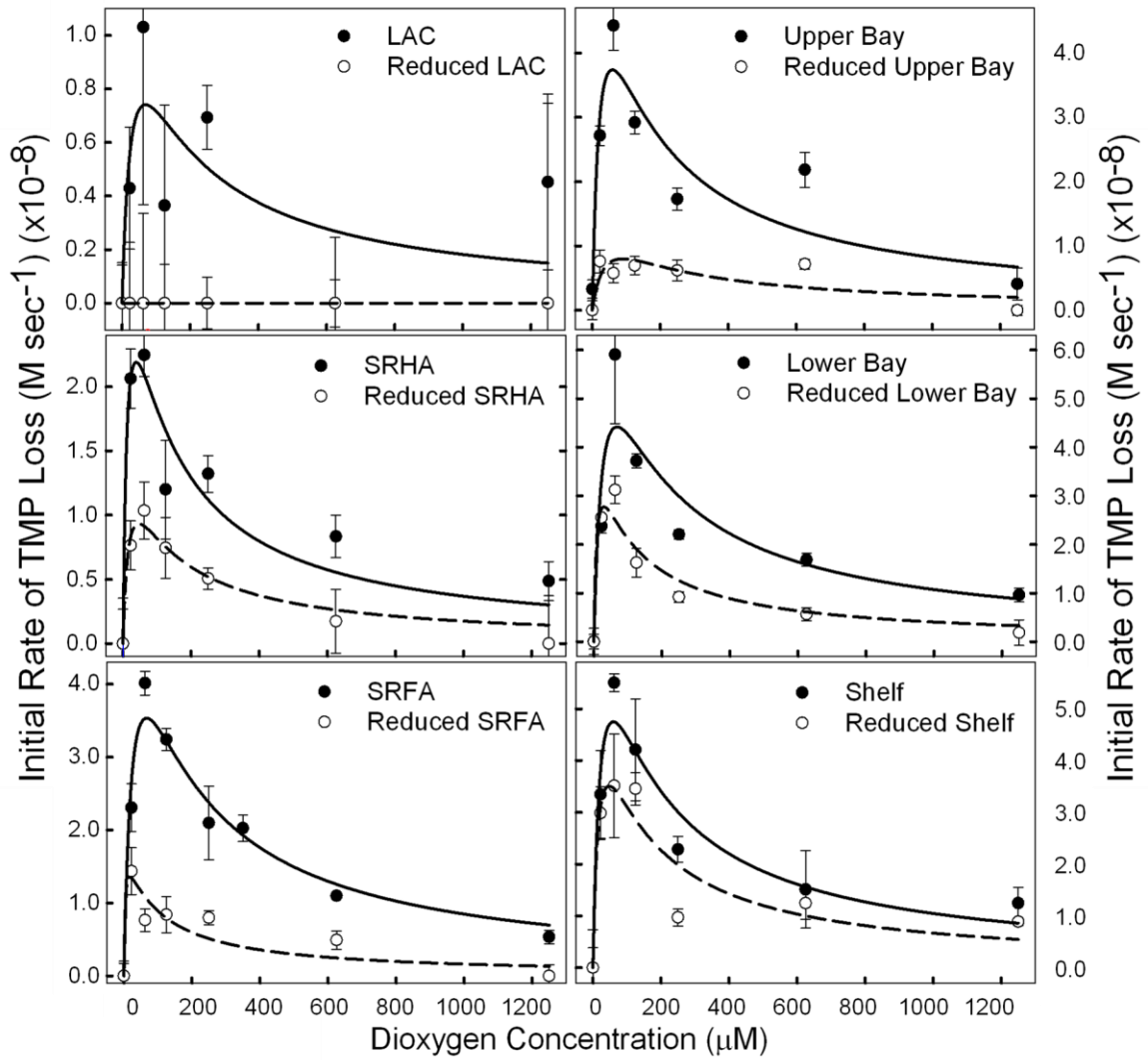
however, that our values represent a lower bound to the maximum efficiencies, because quantitative reaction with the TMP-reactive intermediate was not attained at the employed [TMP] and [O<sub>2</sub>] (Figs. II.5-6; see also Model below). Moreover,  $R(\lambda)$ , the rate of light excitation for these samples, exhibit maxima at ~390 to 400 nm and extend into the visible (Fig. II.2), where CT absorption should dominate and ketones/aldehydes would not absorb as significantly, thus further lowering these yields.

For four of the six samples (SRHA, UBS, LBS and SS), values of  $\Phi$  for borohydride reduced samples and  $\Phi_{\text{diff}}$  remained comparable to those values obtained for the untreated samples. The remaining reduced samples either exhibited values of  $\Phi$  that were either indistinguishable from zero (LAC) or were significantly lower than the untreated samples (SRFA). Thus, only for SRFA and LAC do the results suggest that borohydride reduction eliminates a more highly-efficient sensitizing component from these samples. Because triplet yields for aromatic ketones are generally large (close to unity in many cases), the  $\Phi_{\text{diff}}$  do not increase to the extent one would anticipate if all of the absorption lost under borohydride reduction was due to aromatic ketones/aldehydes. This outcome is likely a result of two factors: 1) the difference in  $R(\lambda)$  between untreated and borohydride-reduced samples peaks at longer wavelengths in the UV-A and extends into the visible where ketones/aldehydes would not contribute (thus lowering  $\Phi_{\text{diff}}$ ) (Fig. II.2); and 2) the possible quenching of a significant fraction of ketone excited states through CT interactions.

### 2.3.2 Effects of [O<sub>2</sub>] on TMP Photosensitization

Further evidence for the involvement of excited triplet states in the loss of TMP was provided by the dependence of  $R_{\text{TMP}}$  on [TMP] at low [O<sub>2</sub>] (22  $\mu\text{M}$ ) (Fig. II.6, right panels). In contrast to the aerated solutions,  $R_{\text{TMP}}$  showed evidence of saturation at  $[\text{TMP}] \leq 100 \mu\text{M}$  for both untreated and borohydride-reduced samples at low [O<sub>2</sub>]. This result is consistent with a competition between O<sub>2</sub> and TMP for reaction with a common intermediate such as a triplet; at low [O<sub>2</sub>], triplet state quenching by O<sub>2</sub> would be significantly reduced, thus allowing for near-quantitative reaction of TMP with the triplet at much lower [TMP]. The competition between O<sub>2</sub> and TMP for a common intermediate was also observed in the dependence of  $R_{\text{TMP}}$  on [O<sub>2</sub>] at a fixed [TMP] (Fig II.7).





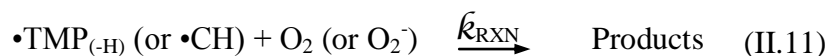
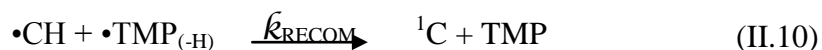
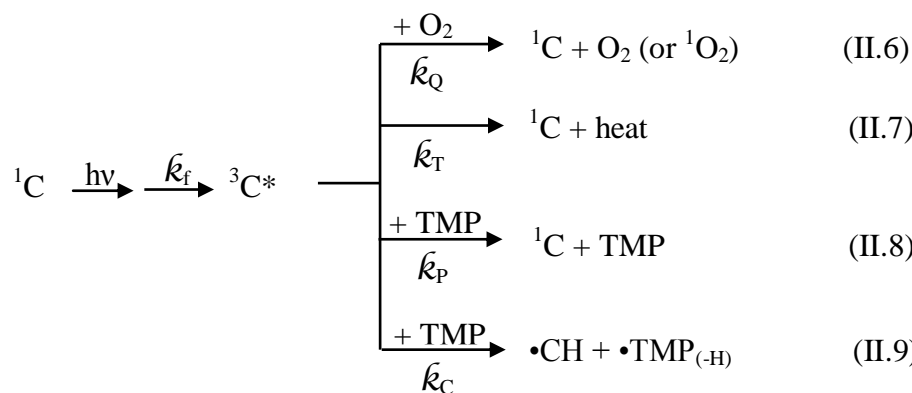
**Figure II.7:** Dependence of  $R_{TMP}$  on  $[O_2]$  at a fixed  $[TMP] = 100 \mu M$  for both untreated and borohydride-reduced SRFA, SRHA, LAC, UBS, LBS and SS. Data were fit to Eqn. II.12 employing a non-linear least squares fitting routine using fixed values of  $\tilde{\kappa}_i = 6.6 \times 10^4 s^{-1}$ ,  $\tilde{\kappa}_{TMP} = 2.5 \times 10^9 M^{-1} s^{-1}$ ,  $[TMP] = 1.0 \times 10^{-4} M$  and  $\tilde{\kappa}_Q = 2.0 \times 10^9 M^{-1} s^{-1}$  (see Model).

For all untreated samples,  $R_{\text{TMP}}$  exhibited an inverse relationship with  $[\text{O}_2]$  over the range from  $\sim 50 \mu\text{M}$  to  $1.2 \text{ mM}$ . Below  $\sim 50 \mu\text{M}$   $\text{O}_2$  however,  $R_{\text{TMP}}$  decreased precipitously, becoming undetectable under anaerobic conditions. As shown below, the inverse relationship between  $R_{\text{TMP}}$  and  $[\text{O}_2]$  can be adequately modeled as a competition between triplet state quenching by  $\text{O}_2$  and triplet reaction with TMP. However, the absence of TMP loss under anaerobic conditions requires that  $\text{O}_2$  plays another critical role in the photosensitized loss of TMP. This role is attributed to reaction of  $\text{O}_2$  (or co-produced  $\text{O}_2^-$ ) with the radical intermediates generated by triplet-TMP reaction, thus leading to products and precluding recombination (see Model below).

For those borohydride-reduced samples that retained measurable TMP loss,  $R_{\text{TMP}}$  exhibited a similar inverse dependence on  $[\text{O}_2]$ , suggesting that the remaining sensitization also arises from triplet states (Fig. II.7).

### 2.3.4 Modeling

The preceding results can be readily interpreted within the following simple model:



Here the chromophore,  $^1\text{C}$ , undergoes excitation ultimately to produce an excited triplet state,  $^3\text{C}^*$ , at rate  $\bar{k}_f$ . Subsequently, this species can undergo quenching by dioxygen (Eqn. II.6), relaxation to the ground state (Eqn. II.7) and physical or chemical reaction with TMP (Eqns. II.8-9). The radical intermediates produced by reaction II.9 can recombine (Eqn. II.10), or undergo further reactions in the presence of dioxygen (Eqn. II.11), leading to stable products and thus precluding recombination.

For simplicity, we have assumed that recombination follows first, instead of second order kinetics, thus leading to the following expression that relates the initial rate of TMP loss to TMP and  $[\text{O}_2]$  (see Appendix I for derivation).

$$R_{\text{TMP}} = - \left( \frac{d[\text{TMP}]}{dt} \right)_0 = \left( \frac{\phi \bar{k}_f \bar{k}_{\text{TMP}} [\text{TMP}]}{\bar{k}_t + \bar{k}_{\text{TMP}} [\text{TMP}] + \bar{k}_Q [\text{O}_2]} \right) \cdot \left( 1 - \frac{1}{1 + (\bar{k}_{\text{RXN}} [\text{O}_2] / \bar{k}_{\text{REC}})} \right) \quad (\text{II.12})$$

where  $\phi = \bar{k}_C / (\bar{k}_C + \bar{k}_P)$  and  $\bar{k}_{\text{TMP}} = \bar{k}_C + \bar{k}_P$ . To estimate the values of  $\bar{k}_t$  and  $\bar{k}_{\text{TMP}}$ , the data in Figure II.6 were fit using a non-linear least squares routine to the equation  $y = a \cdot x / (b+x)$ , where  $y = R_{\text{TMP}}$ ,  $a = \phi \cdot \bar{k}_f$ ,  $x = [\text{TMP}]$  and  $b = (\bar{k}_t + \bar{k}_Q [\text{O}_2]) / \bar{k}_{\text{TMP}}$ . The values of  $b$  obtained at high and low  $[\text{O}_2]$  were utilized along with their respective  $[\text{O}_2]$  and a fixed value of  $\bar{k}_Q = 2.0 \times 10^9 \text{ M}^{-1} \text{ s}^{-1}$  (Zepp *et. al.*, 1985; Paul *et. al.*, 2004; Muvrov *et. al.*, 1993) to calculate  $\bar{k}_t$  and  $\bar{k}_{\text{TMP}}$  for both untreated and borohydride-reduced SRHA and SRFA. Alternatively, the value of  $\bar{k}_{\text{TMP}}$  was fixed at  $2.6 \times 10^9 \text{ M}^{-1} \text{ s}^{-1}$  ( $\bar{k}_{\text{TMP}}$  for reaction with the aromatic ketone, 3'-methoxyacetophenone (3'-MAP)) (Canonica *et. al.*, 2000) and values of  $\bar{k}_t$  and  $\bar{k}_Q$  were calculated (Table II.3).

	$\bar{k}_Q = 2.0 \times 10^9 \text{ M}^{-1} \text{ s}^{-1}$ Calculate $\bar{k}_t$ , $\bar{k}_{TMP}$		$\bar{k}_{TMP}(3'\text{-MAP}) = 2.6 \times 10^9 \text{ M}^{-1} \text{ s}^{-1}$ Calculate $\bar{k}_t$ , $\bar{k}_Q$	
	$\bar{k}_t$ ( $\tau_T$ ) $(\text{s}^{-1})$ ( $\mu\text{s}$ )	$\bar{k}_{TMP}$ $(\text{M}^{-1} \text{ s}^{-1})$	$\bar{k}_t$ ( $\tau_T$ ) $(\text{s}^{-1})$ ( $\mu\text{s}$ )	$\bar{k}_Q$ $(\text{M}^{-1} \text{ s}^{-1})$
SRFA	$6.7 \times 10^4$ (15)	$2.5 \times 10^9$	$6.9 \times 10^4$ (15)	$2.1 \times 10^9$
Reduced SRFA	$5.6 \times 10^5$ (1.8)	$1.2 \times 10^{10}$	$1.3 \times 10^5$ (7.7)	$4.5 \times 10^8$
SRHA	$5.8 \times 10^5$ (1.7)	$1.0 \times 10^{10}$	$1.5 \times 10^5$ (6.7)	$5.0 \times 10^8$
Reduced SRHA	$4.1 \times 10^5$ (2.4)	$7.2 \times 10^9$	$1.5 \times 10^5$ (6.7)	$7.2 \times 10^8$

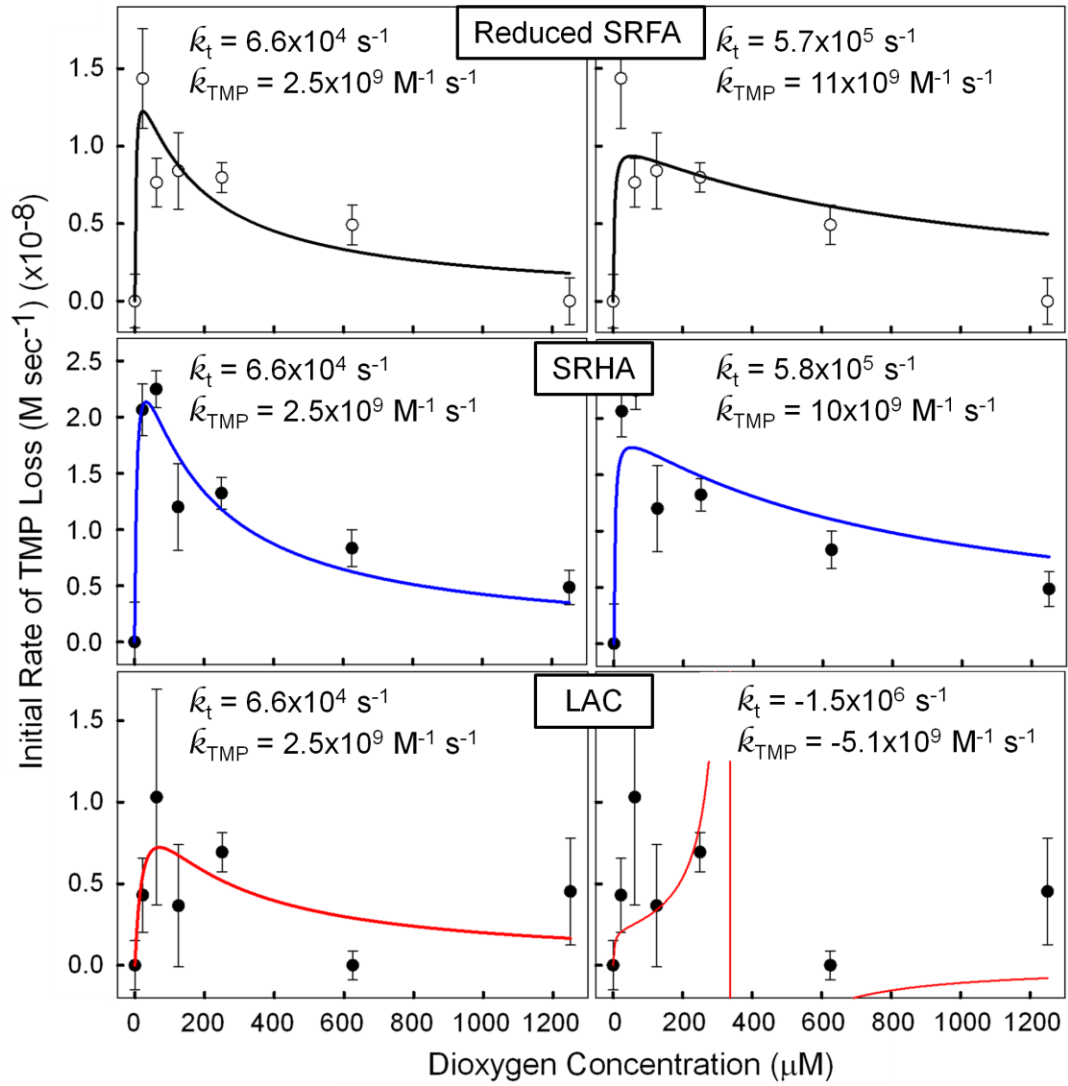
**Table II.3:** Calculations and sensitivity analyses for  $\bar{k}_t$ ,  $\bar{k}_{TMP}$  and  $\bar{k}_Q$ . The dependence of  $R_{TMP}$  on  $[TMP]$  at high (250  $\mu\text{M}$ ) and low (22  $\mu\text{M}$ ) dioxygen concentration were fitted using  $R_{TMP} = a \cdot [TMP] / (b + [TMP])$  where  $b$  represents  $[TMP]_{1/2}$ . These  $b$  values were employed, along with fixed  $[TMP] = 100 \mu\text{M}$  and  $\bar{k}_Q = 2.0 \times 10^9 \text{ M}^{-1} \text{ s}^{-1}$  to calculate values of  $\bar{k}_t$  and  $\bar{k}_{TMP}$  (left panel). Alternatively, the  $b$  values were employed along with fixed  $\bar{k}_{TMP} = 2.6 \times 10^9 \text{ M}^{-1} \text{ s}^{-1}$  ( $\bar{k}_{TMP}$  for reaction with the aromatic ketone 3'-methoxyacetophenone (3'-MAP)) to calculate  $\bar{k}_t$  and  $\bar{k}_Q$  (right panel). SRFA had the lowest relative error in the determinations of  $\bar{k}_t$  and  $\bar{k}_{TMP}$  (45% and 46%, respectively). Reduced SRFA, SRHA and Reduced SRHA had noticeably higher relative errors for  $\bar{k}_t$  and  $\bar{k}_{TMP}$  (55%, 80% and 82%, respectively).

These calculations produced triplet lifetimes ranging from ~2 to 15  $\mu\text{s}$ , values of  $\bar{k}_Q$  ranging from  $0.5 - 2.1 \times 10^9 \text{ M}^{-1} \text{ s}^{-1}$  and  $\bar{k}_{TMP}$  ranging from  $2.5 - 10 \times 10^9 \text{ M}^{-1} \text{ s}^{-1}$ , in reasonable agreement with the expected magnitudes for these rate constants (see footnote).

Canonica *et. al.*, 1995; Canonica and Hoigné, 1995; Canonica *et. al.*, 2000; Halladja *et. al.*, 2007; Halladja *et. al.*, 2009; Al Housari *et. al.*, 2010

Additionally, excellent agreement was observed for SRFA (<5% uncertainty) between literature and calculated values of  $\tilde{k}_Q$  (at fixed  $\tilde{k}_{TMP}$ ) and  $\tilde{k}_{TMP}$  (at fixed  $\tilde{k}_Q$ ); further, very similar values of  $\tilde{k}_t$  were obtained using either the fixed value of  $\tilde{k}_Q$  or  $\tilde{k}_{TMP}$  (Table II.3).

The complete  $[O_2]$  dependence for both untreated and borohydride-reduced SRFA and SRHA were fit to Eqn. II.12 using a non-linear least squares routine employing their unique, fixed values of  $\tilde{k}_t$  and  $\tilde{k}_{TMP}$  (Table II.3),  $\tilde{k}_Q=2 \times 10^9 \text{ M}^{-1} \text{ s}^{-1}$  and  $[TMP]=1 \times 10^{-4} \text{ M}$ . However, using the fixed values of  $\tilde{k}_t$  and  $\tilde{k}_{TMP}$  obtained for SRFA produced improved fits for all data (Fig. II.8) and reduced the uncertainty in the determination of  $\phi \cdot k_f$  and  $\tilde{k}_{RXN}/\tilde{k}_{REC}$  (Table 2). For this reason, we used the values obtained for SRFA, namely  $\tilde{k}_{TMP} = 2.5 \times 10^9 \text{ M}^{-1} \text{ s}^{-1}$ ,  $\tilde{k}_t = 6.6 \times 10^4 \text{ s}^{-1}$  with  $[TMP] = 1 \times 10^{-4} \text{ M}$  and  $\tilde{k}_Q = 2.0 \times 10^9 \text{ M}^{-1} \text{ s}^{-1}$  to fit the entire  $[O_2]$  dependence of all samples (Fig. II.7), while leaving the parameters  $\tilde{k}_{RXN}/\tilde{k}_{REC}$  and  $\phi \cdot k_f$  to vary.



**Figure II.8:** Curve fitting results using values of  $\hat{k}_t$  and  $\hat{k}_{\text{TMP}}$  determined for SRFA (**left panel**) or the unique values determined for Reduced SRFA, SRHA and LAC (**right panel**). Fits obtained using values determined for SRFA of  $\hat{k}_t = 6.6 \times 10^4 \text{ s}^{-1}$  and  $\hat{k}_{\text{TMP}} = 2.5 \times 10^9 \text{ M}^{-1} \text{ s}^{-1}$  (**left panel**) were superior to those obtained using individual values of  $\hat{k}_t$  and  $\hat{k}_{\text{TMP}}$  for Reduced SRFA, SRHA or LAC (**right panel**), namely in the reduced uncertainty in the determination of  $\varphi \cdot k_f$  and  $\hat{k}_{\text{RXN}}/\hat{k}_{\text{REC}}$ .

	$\tilde{k}_{\text{RXN}} / \tilde{k}_{\text{REC}}$ ( $\times 10^4$ )	$\varphi \cdot \tilde{k}_f$ ( $\text{M s}^{-1}$ ) ( $\times 10^{-8}$ )	$\Phi^T(\%)$	$\Phi_{\text{diff}}^T(\%)$
SRFA	$2.1 \pm 0.5$	$7.7 \pm 0.8$	$7.3 \pm 0.8$	$13 \pm 1$
Reduced SRFA	$30 \pm 75$	$1.4 \pm 0.3$	$2.5 \pm 0.5$	
SRHA	$6.1 \pm 3.4$	$3.3 \pm 0.5$	$1.3 \pm 0.2$	$1.1 \pm 0.2$
Reduced SRHA	$4.2 \pm 1.7$	$1.5 \pm 0.2$	$1.8 \pm 0.3$	
LAC	$1.9 \pm 2.3$	$1.7 \pm 0.8$	$0.66 \pm 0.31$	$1.2 \pm 0.6$
Reduced LAC	$0.0 \pm 0.0$	$0.0 \pm 0.0$	$0.0 \pm 0.0$	
UBS	$2.6 \pm 1.5$	$7.4 \pm 1.7$	$5.3 \pm 1.2$	$7.0 \pm 1.6$
Reduced UBS	$1.2 \pm 1.0$	$2.3 \pm 1.0$	$3.5 \pm 1.5$	
LBS	$1.9 \pm 1.2$	$9.8 \pm 2.6$	$6.8 \pm 1.8$	$7.1 \pm 2.7$
Reduced LBS	$10 \pm 8.2$	$3.6 \pm 0.6$	$6.3 \pm 0.3$	
SS	$2.6 \pm 0.9$	$9.5 \pm 1.4$	$11 \pm 2$	$7.2 \pm 1.1$
Reduced SS	$4.0 \pm 2.4$	$5.9 \pm 1.2$	$15 \pm 3$	

*Table II.4: Results from curve-fitting the dependence of  $R_{\text{TMP}}$  on  $[\text{O}_2]$  to Eqn. II.12 (see text) for untreated and borohydride-reduced SRFA, SRHA, LAC, UBS, LBS and SS. For all samples, the fixed values obtained for SRFA of  $\tilde{k}_t = 6.6 \times 10^4 \text{ s}^{-1}$ ,  $\tilde{k}_{\text{TMP}} = 2.5 \times 10^9 \text{ M}^{-1} \text{ s}^{-1}$  and  $\tilde{k}_Q = 2.0 \times 10^9 \text{ M}^{-1} \text{ s}^{-1}$  were utilized in the fitting. Uncertainties for  $\Phi^T$  were propagated from the determination of  $\varphi \cdot \tilde{k}_f$ . Note that higher  $\Phi_{\text{diff}}^T$  indicates that the loss of absorption (difference in the rate of light excitation) under borohydride reduction is smaller proportionally than the decrease of  $R_{\text{TMP}}$ .*

Within the scatter of the data, fits to the dependence of  $R_{\text{TMP}}$  on  $[\text{O}_2]$  for the untreated samples were quite reasonable using this approach (Fig. II.7). The observation that a single set of rate constants could well reproduce these data suggests that there are no major variations in the rate constants among these samples. Independently varying the

magnitude of  $\tilde{k}_t$ ,  $\tilde{k}_{\text{TMP}}$  and  $\tilde{k}_Q$  by a factor of 2 (smaller or larger) gave rise to significantly poorer fits, indicating that these values are reasonably robust (data not shown). Using this approach, the fits for the borohydride reduced samples were also reasonable, although it is not clear that employing the parameters for untreated SRFA are appropriate in these cases. Although there remains an inverse relationship between  $R_{\text{TMP}}$  and  $[\text{O}_2]$  for the borohydride-reduced samples between  $\sim 50$  and  $250 \mu\text{M}$ , we cannot be sure that this dependence is identical to the untreated samples provided the limited number and scatter of the data points. Thus, while we have provided the fitted values of  $\tilde{k}_{\text{RXN}}/\tilde{k}_{\text{REC}}$  and  $\phi \cdot \tilde{k}_t$  for the borohydride-reduced samples in Table II.4 for completeness, we believe these values to be more tenuous.

The parameter  $\tilde{k}_{\text{RXN}}/\tilde{k}_{\text{REC}}$  represents the ratio of the rate constant for product formation ( $\tilde{k}_{\text{RXN}}$ ) to that of recombination ( $\tilde{k}_{\text{REC}}$ ). Fitted values of  $\tilde{k}_{\text{RXN}}/\tilde{k}_{\text{REC}}$  varied by no more than a factor of  $\sim 3$  and were large ( $\sim 10^4$ ), indicating that the reaction to form products occurs far more rapidly than recombination even when low concentrations  $\text{O}_2$  are present (Table II.4).

The product  $\phi \cdot \tilde{k}_t$ , as obtained from the fit, represents the maximal rate of TMP loss under quantitative reaction with the TMP-reactive triplets (Fig. II.7, Table II.4). This rate will be equal to the rate of reactive triplet formation if  $\phi$ , the branching ratio between chemical and physical quenching, is unity. Past work indicates that  $\phi$  is near unity for the reaction of aromatic ketone triplets with phenols (Canonica *et. al.*, 2000; Das *et. al.*, 1981a-b; Encinas *et. al.*, 1985) and thus we have assumed that these results are equivalent to the triplet formation rates for those triplets reactive with TMP. Thus, using the fitted



values of  $\phi \cdot k_f$ , we can estimate triplet yields ( $\Phi^T$ ) using the equations employed previously (Eqns. II.6-8, Table II.4).

The estimated triplet yields vary widely, from 0 to 15%, and exhibit the same trends as observed in Table II.2, with untreated SRHA and LAC exhibiting far lower yields than SRFA and the C<sub>18</sub> extracts (Table II.4). As noted above however, these estimates are based on polychromatic radiation where  $R(\lambda)$  is weighted to longer wavelengths in the UV and near-visible, and thus may underestimate triplet quantum yields associated with ketone/aldehydes moieties. Nevertheless, these yields are similar in overall magnitude to those reported for <sup>1</sup>O<sub>2</sub> quantum yields obtained under aerated conditions and are thus also consistent with a triplet intermediate (Haag *et. al.*, 1984; Dalrymple *et. al.*, 2010; Paul *et. al.*, 2004). The results further imply that the triplet states of aromatic ketones/aldehydes contribute significantly to the production of <sup>1</sup>O<sub>2</sub>, consistent with a prior report (Halladja *et. al.*, 2007).

These results provide strong evidence that excited triplet states of aromatic ketones/aldehydes play a significant role in the photosensitized loss of TMP by HS and CDOM (Canonica, 2007; Canonica and Laubscher, 2008; Wenk *et. al.*, 2011; Canonica *et. al.*, 2000). However, the incomplete loss of sensitization for all samples (except LAC) suggests that there remains another class of triplet sensitizer capable of reaction with phenols. Excellent evidence exists for the presence of quinones within HS and CDOM (Aeschbacher *et. al.*, 2010). Because triplet states of quinones are known to react facilely with phenols (Bisby and Parker, 1995; Amada *et. al.*, 1995), as well as produce singlet dioxygen (Wilkinson *et. al.*, 1993; Gutiérrez *et. al.*, 1997), these species represent reasonable candidates.

### **Chapter III: Wavelength Dependence of the Photosensitized Oxidation of 2,4,6-trimethylphenol (TMP) by HS and CDOM: Effects of Sodium Borohydride Reduction and [O<sub>2</sub>]**

#### **Abstract**

To further probe the mechanism of the CDOM-sensitized oxidation of phenols, we examined the spectral dependence of the initial rate of 2,4,6-trimethylphenol loss ( $R_{\text{TMP}}$ ) for untreated and borohydride-reduced SRFA, SRHA, LAC and C<sub>18</sub> extracts of the Delaware Bay. We find that 1) increasing the mass excess of borohydride leads to additional losses of absorbance and decreases in  $R_{\text{TMP}}$ , but except for LAC,  $R_{\text{TMP}}$  is never completely eliminated; 2) decreasing [O<sub>2</sub>] increases  $R_{\text{TMP}}$  for both untreated and borohydride-reduced samples by ~2 for a four-fold reduction of [O<sub>2</sub>] from 250  $\mu\text{M}$  to 63  $\mu\text{M}$ ; 3)  $R_{\text{TMP}}$  drops off rapidly with increasing  $\lambda$ , far more rapidly than the rate of light excitation ( $R_{\text{EX}}$ ), for both untreated and borohydride-reduced samples indicating that UVB and UVA wavelengths are primarily responsible for the sensitization. Except for SRHA, wavelengths > 400 nm give rise to little or no detectable sensitization which argues against major sensitization by long-wavelength absorbing species.

#### **3.1 Introduction**

Pollutants such as phenols are imparted to aquatic environments in a variety of ways, including accidental or intentional release of agricultural or pharmaceutical products containing these compounds. Phenols have a broad range of toxicities depending on their substituents, and some phenols can impart objectionable odor and

taste to water at the parts per billion (ppb) level (Afghan et. al., 1989). A major sink of phenols in the environment is through sunlight-mediated photodegradation, either through direct light absorption or indirectly in the presence of light-absorbing sensitizers (Boreen et. al., 2003). Measured rates of phenol degradation in natural waters were shown to be much larger than those observed for direct photolysis alone, indicating that an indirect, sensitized mechanism was important (Aguer et. al., 2005). Chromophoric dissolved organic matter (CDOM), as the primary light absorbing component of natural waters, was an obvious candidate for the main sensitizer initiating oxidation. Knowledge of the wavelength dependence of the photooxidation of phenols by HS and CDOM has important implications for environmental remediation efforts and for understanding the underlying molecular basis of the observed optical and photochemical properties of CDOM.

The structural basis of the observed optical and photochemical properties of CDOM remains an active area of research, owing to its complex structure and spatial and temporal variability. Absorption spectra of CDOM from freshwater (Blough and Del Vecchio, 2002; Yacobi *et. al*, 2003) and marine aquatic environments (Blough and Del Vecchio, 2002; Nelson and Siegel, 2002; Coble, 2007) feature no distinct absorption bands and have higher absorption at short wavelengths that decreases in an approximately exponential manner (de Haan, 1983a; Blough and Green, 1995; Twardowski *et.al*, 2004). Del Vecchio and Blough, 2004; Boyle *et. al.*, 2009; Ma *et.al.*, 2010) provided evidence that the long wavelength absorption tail arises through electronic interactions between chromophores (interaction model) and not through a simple summation of independently

absorbing and emitting chromophores within CDOM (superposition model) (Del Vecchio and Blough, 2002; Ma *et. al.*, 2010, Sharpless and Blough, 2014).

The primary mechanism of the sunlight-mediated degradation of phenols by CDOM and HS was initially attributed to reactive oxygen species (ROS) such as organic peroxy radicals (ROO•) (Faust and Hoigné, 1987), singlet dioxygen ( $^1\text{O}_2$ ) (Scully and Hoigné, 1987) and hydroxyl radical (HO•) (Haag and Hoigné 1985). However significant lines of evidence have since been presented that instead implicate triplet excited states of carbonyl-containing moieties within HS and CDOM (Canonica *et. al.*, 1995a; Halladja *et. al.* 2007; Cawley *et. al.*, 2009, Golanoski *et. al.*, 2012).

We recently reported that the initial rate of TMP loss ( $R_{\text{TMP}}$ ) decreased by ~50% for sodium borohydride-reduced SRFA, SRHA and  $\text{C}_{18}$  extracts of the Delaware Bay and by 100% for lignin that has been alkali-treated and carboxylated (LAC) (Golanoski, *et. al.*, 2012). These results were attributed to the complete or partial reduction of aromatic aldehydes/ketones to alcohols and that triplet excited states of these moieties played a major role in TMP sensitization by HS/CDOM (Golanoski *et. al.*, 2012). It was suggested that the remaining  $R_{\text{TMP}}$  was due to either incomplete reduction of HS/CDOM or that there existed another class of triplet oxidants, possibly quinones. Despite its importance, investigating the role of quinones poses significant experimental challenges as quinones are not expected to be irreversibly reduced using  $\text{NaBH}_4$  owing to a relatively rapid re-oxidation upon exposure to air (Ma *et. al.*, 2010). Recently, sorbic acid (2,4-hexadienoic acid) and halides (i.e.  $\text{Cl}^-$ ,  $\text{Br}^-$  or  $\text{I}^-$ ) have been utilized as quenchers of triplet excited states. Researchers have encountered significant difficulties as sorbic acid is not selective for the quenching of quinone triplets (Grebel, *et. al.*, 2011), halides

are prone to complex photochemical reactions in water (Grebel, et. al., 2010; Jammoul, et. al., 2009, Glover, C. and Rosario-Ortiz, F., 2013) and their effect was recently attributed largely to ionic strength effects and not to the halide itself (Grebel et. al., 2012).

To establish first whether the partial loss of phenol sensitization was due to incomplete reduction, the effect of increased mass excess of sodium borohydride ( $\text{NaBH}_4$ ) on the optical and photochemical properties of HS and CDOM was first examined. To further probe the mechanism of the CDOM-sensitized oxidation of phenols, we examined the spectral dependence of  $R_{\text{TMP}}$  for untreated and borohydride-reduced SRFA, SRHA, LAC and  $\text{C}_{18}$  extracts of the Delaware Bay. To the best of our knowledge, no study has examined systematically the wavelength dependence of the sensitized photooxidation of phenols. This work thus provides additional insight on the mechanism of phenol photooxidation by HS and CDOM across the ultraviolet (UV) and visible wavelength regimes.

We find that 1) increasing the mass excess of borohydride does lead to additional losses of absorbance and decreases in  $R_{\text{TMP}}$ , but still does not entirely eliminate TMP sensitization (except for LAC); 2) decreasing  $\text{O}_2$  concentration increases  $R_{\text{TMP}}$  for both untreated and borohydride-reduced samples by  $\sim 2$  for a four-fold reduction of  $[\text{O}_2]$  3)  $R_{\text{TMP}}$  drops off rapidly with increasing  $\lambda$ , far more rapidly than  $R_{\text{EX}}$ , for both untreated and borohydride-reduced samples indicating that UVB and UVA wavelengths are primarily responsible for the sensitization. Except for SRHA, wavelengths  $> 400$  nm produce to little or no sensitization, thus arguing against a major role for long-wavelength absorbing species in this sensitization.

## **3.2 Methods and Materials**

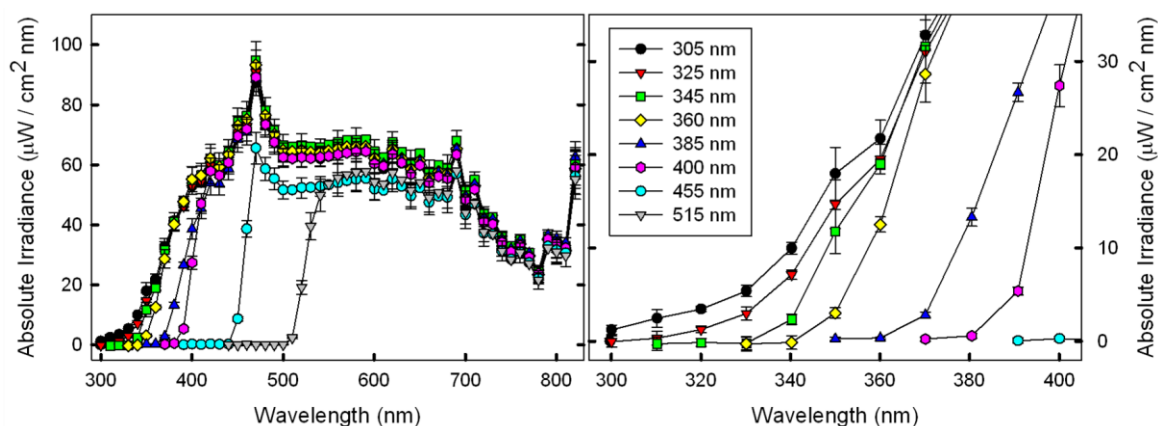
### **3.2.1 Materials**

All chemicals were used as received. Analytical grade 2,4,6-trimethylphenol (TMP) was obtained from Fluka. Lignin, alkali extracted and carboxylated (LAC), was obtained from Sigma Aldrich (Lot #19714DS). Suwanee River humic acid (SRHA) and Suwanee River fulvic acid (SRFA) were obtained from the International Humic Substances Society. Solid-phase C<sub>18</sub> extracts from a Delaware Bay upper bay station (UBS; 39.63N, -75.58W), lower bay station (LBS; 38.99N, -75.13W) and shelf station (SS; 38.68N, -74.89W) within the Middle Atlantic Bight (MAB) were collected in October 2006 and processed as previously reported (Ma et. al., 2010). Water was obtained from a Millipore Milli-Q purification system. Dipotassium hydrogen phosphate (K<sub>2</sub>HPO<sub>4</sub>) was obtained from Sigma Aldrich, whereas potassium dihydrogen phosphate (KH<sub>2</sub>PO<sub>4</sub>) and sodium borohydride (NaBH<sub>4</sub>) were obtained from Fischer Scientific. Ultra-high purity compressed gases were obtained from Airgas. Potassium hydrogen phthalate (KHP) was obtained from Nacalai Tesque, Inc.

### **3.2.2 Apparatus**

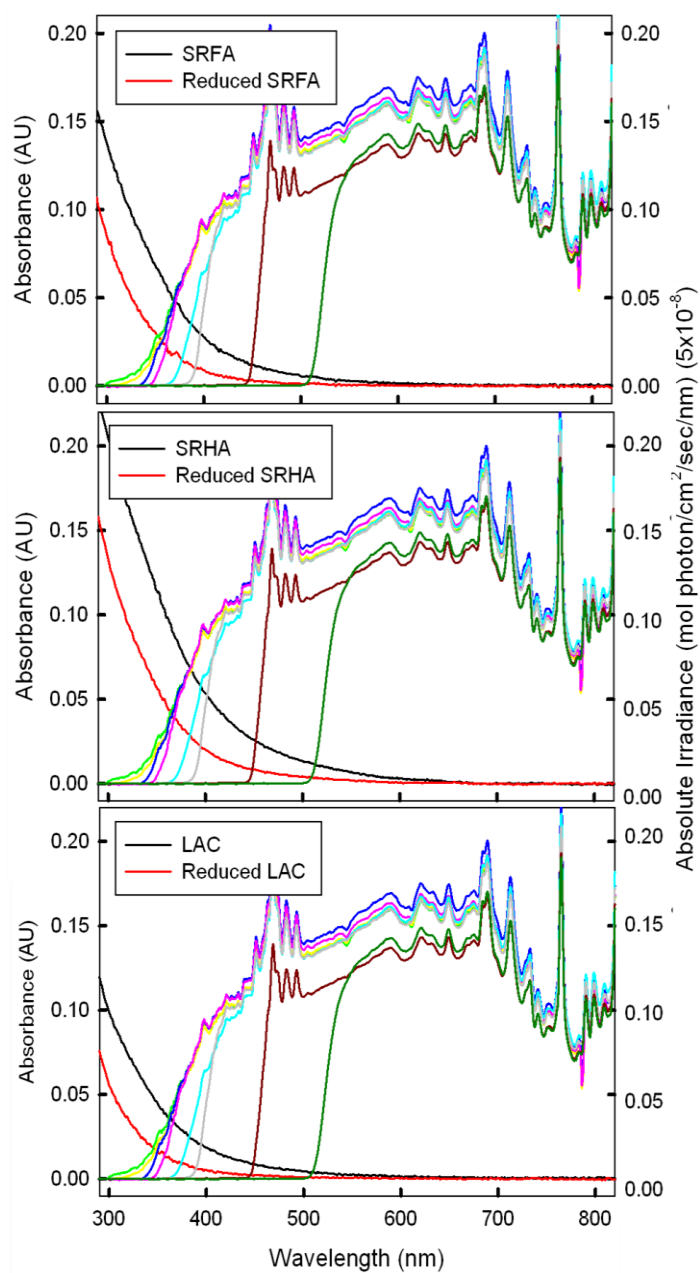
TMP analyses were performed in triplicate using RP-HPLC system consisting of a Shimadzu LC-10AS pump, 50 µL loop and a Waters RCM 8x10 cartridge which supported a Waters Nova-Pak C<sub>18</sub> column (5x100mm, 4µM pore size). Analyses were performed under isocratic conditions using a mobile phase composition of 60% methanol, 30% water and 10% dilute acetic acid (1%) at a flow rate of 1 mL min.<sup>-1</sup> TMP detection was performed using a Dionex AD25 absorbance detector set to 280 nm.

Samples were irradiated in a 1 cm quartz cuvette using a 300 W high pressure xenon arc lamp following passage through 8 cm of water to remove infrared radiation. A series of longpass wavelength filters at  $\lambda = 305, 325, 345, 360, 385, 400, 455$  and  $515$  nm (50% transmittance at  $\lambda$ ) were employed to simulate the solar spectrum and selectively alter the light field. The spectral output of the lamp at each wavelength range was measured using an Ocean Optics USB2000 spectroradiometer and is provided in Fig. III.1.



**Figure III.1:** Average absolute irradiance (left panel) of the high pressure xenon arc lamp in combination with the various wavelength cutoff filters employed in this study (left panel) and expansion plot from 300-400 nm (right panel). Error bars represent  $\pm 1$  standard deviation of at least three measurements.

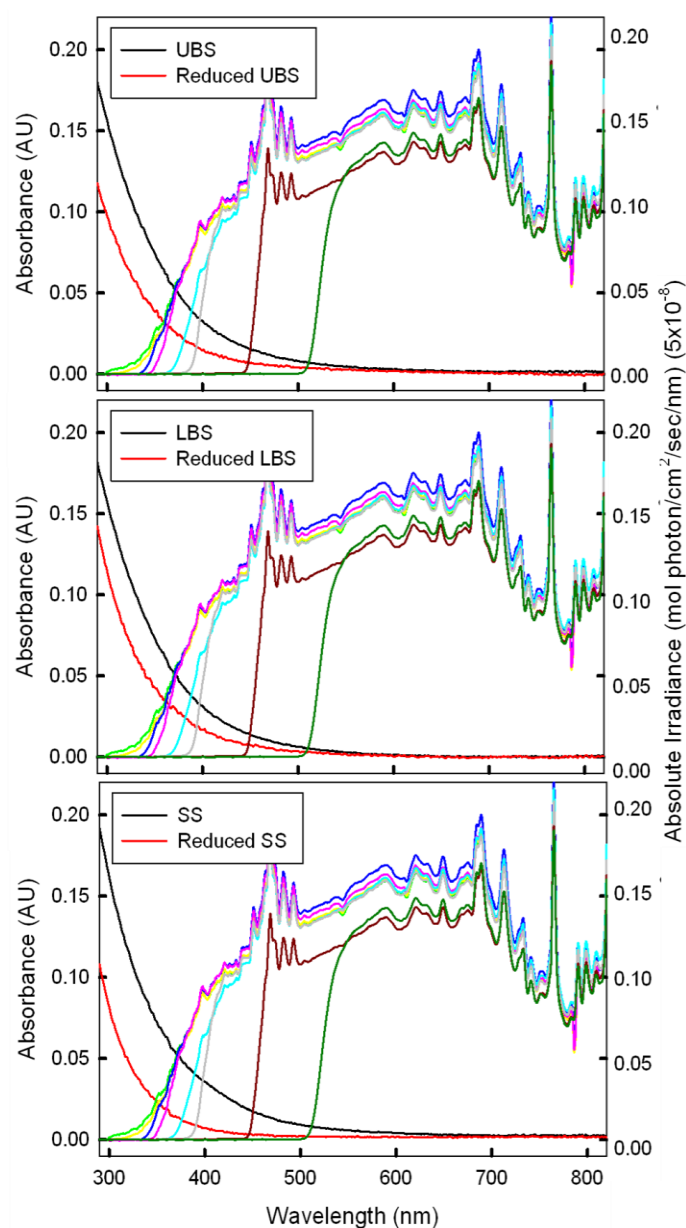
The integrated intensities for filters  $\lambda > 305$  nm to  $\lambda > 515$  nm were approximately  $88\text{-}53 \text{ mW/cm}^2$  and did not change significantly ( $< 5\%$ ) throughout the study period. An overlay of the absorption spectra of untreated and borohydride-reduced SRFA, SRHA, LAC and  $C_{18}$  extracts and the absolute irradiance for each wavelength cutoff filter are provided in Appendix III (Figs. III.2-3).



— > 305 nm    — > 325 nm    — > 345 nm    — > 360 nm  
— > 385 nm    — > 400 nm    — > 515 nm    — > 455 nm

Figure III.2: Absorbance spectra of untreated (black trace) and borohydride-reduced (red trace) SRFA, SRHA and LAC at  $10 \text{ mg L}^{-1}$ . Samples are in PB at pH=7.0. Overlaid are the absolute irradiance profiles of the xenon arc lamp with each long pass wavelength filter employed in this study.





— > 305 nm    — > 325 nm    — > 345 nm    — > 360 nm  
— > 385 nm    — > 400 nm    — > 515 nm    — > 455 nm

**Figure III.3:** Absorbance spectra of untreated (black trace) and borohydride-reduced (red trace) Upper Bay Sample (UBS), Lower Bay Sample (LBS) and Shelf Sample (SS) Samples were in PB at pH=7.0. Overlaid are the absolute irradiance profiles of the xenon arc lamp with each long pass wavelength filter employed in this study.

Ultraviolet/visible absorption measurements employed a Shimadzu 2401-PC dual beam spectrophotometer. Spectra were collected versus air over the range 190-820 nm and corrected by subtraction of a Milli-Q water spectrum. Total organic carbon (TOC) was determined using high temperature oxidation (680°C) on a Shimadzu 5000A TOC analyzer calibrated using KHP. Specific absorption coefficients,  $a^*(\lambda)$ , were obtained using equation III.1

$$a^*(\lambda) = 2.303 \cdot A(\lambda) / (b \cdot C) \quad (\text{III.1})$$

where  $A(\lambda)$  is the absorbance at a given wavelength,  $b$  is the pathlength in meters and  $C$  is the concentration of total organic carbon in mg carbon  $L^{-1}$ . The spectral slope parameter ( $S$ ) was obtained by a non-linear least squares fitting of the spectra over the range from 290 to 820 nm to equation III.2

$$a^*(\lambda) = a^*(\lambda_{\text{Ref}}) e^{-S(\lambda - \lambda_{\text{Ref}})} \quad (\text{III.2})$$

where  $a^*(\lambda_{\text{Ref}})$  is the specific absorption coefficient at the reference wavelength, 350 nm.

### 3.2.3 NaBH<sub>4</sub> Reduction

Stock solutions of SRFA, SRHA and LAC were prepared at 500 mg/L in MQ and the pH was adjusted to pH=10 using 0.25 N NaOH. To a five milliliter (mL) aliquot of SRFA, SRHA or LAC a 5, 10, 25, 50 or 100-fold mass excess of sodium borohydride (NaBH<sub>4</sub>) was added (see Table III.1) and the solution gently stirred.

Mass Excess NaBH <sub>4</sub>	Concentration of HS (mg/L)	Mass NaBH <sub>4</sub> (mg)
0X	500	0
5X		12.5
10X		25
25X		62.5
50X		125
100X		250

**Table III.1:** Mass excess of NaBH<sub>4</sub> added to 500 mg/L SRFA, SRHA or LAC.

Samples were reduced under aerobic conditions, sealed with Parafilm and stored in the dark at room temperature for the duration of the study. See Appendix II for kinetic data and additional information. In order to remove excess borate and borohydride and adjust the pH to neutral, solutions were passed over a 2.5 cm x 8 cm Sephadex G-10 (40 – 120  $\mu\text{m}$ ) column equilibrated with Milli-Q water. TOC analysis was employed in order to provide carbon-matched optical spectra and solutions for photochemical experiments. Control samples (0X) represent untreated samples, which were only passed over a Sephadex G-10 column (Figure III.2, red trace).

### 3.2.4 Photochemical Experiments

Stock solutions of 500  $\text{mg L}^{-1}$  LAC, SRHA and SRFA and 500  $\mu\text{M}$  TMP were prepared in MQ water. The SRHA stock solution was passed through a 0.2  $\mu\text{m}$  filter prior to use. The absorbance of the  $\text{C}_{18}$  extracts were matched at 350 nm to a spectrum of 10  $\text{mg L}^{-1}$  ([DOC] = 4.5  $\text{mg C L}^{-1}$ ) SRFA at pH=7.0, the concentration used in the irradiations. All stock solutions and samples were stored in the dark at 4°C when not in use. Just prior to irradiation, final solutions containing SRFA, SRHA, LAC (10  $\text{mg L}^{-1}$ ) or the  $\text{C}_{18}$  extracts and TMP (5-100  $\mu\text{M}$ ) were prepared in 50 mM phosphate buffer at pH=7.0 (PB). Control samples contained TMP alone in PB. Samples were transferred to a 1 cm quartz cuvette and were irradiated for 15 minutes under 5% ( $\sim 63 \mu\text{M}$ )  $[\text{O}_2]$  achieved through mixing ultra-high purity (UHP) nitrogen and air in a dual flow rotameter. Samples reduced with sodium borohydride (see below) were treated in a similar manner. Aerated solutions were kept open to the atmosphere, whereas analyses performed under controlled dioxygen conditions were sparged for 5 minutes prior to

irradiation followed by flushing of the headspace of the closed vial during irradiation. Quantification of TMP was performed using RP-HPLC at 5 minute intervals during the 15 minute irradiation time in which [TMP] decreased linearly. The direct photochemical loss of TMP was negligible (<5%) over this time period.

Estimated (polychromatic) apparent quantum efficiencies ( $\Phi$ ) of TMP loss for both untreated and borohydride-reduced samples were calculated using equation III.3,

$$\Phi = R_{\text{TMP}} / R_{\text{EX}} \quad (\text{III.3})$$

where  $R_{\text{TMP}}$  is the initial rate of TMP loss at 100  $\mu\text{M}$  TMP and 63  $\mu\text{M}$   $\text{O}_2$  (air-saturated), and  $R_{\text{EX}}$  is the rate of light excitation given by equation III.4,

$$R_{\text{EX}} = \int_{190}^{820} a(\lambda) \cdot I(\lambda) d\lambda = \int_{190}^{820} R(\lambda) d\lambda \quad (\text{III.4})$$

where  $a(\lambda)$  is the absorption coefficient of the sample,  $I(\lambda)$  is the spectral photon irradiance at the front face of the cuvette as measured with the Ocean Optics spectroradiometer and  $R(\lambda)$  provides the wavelength dependence of the light excitation rate (see Figs. III.6-7). To obtain an estimate of the apparent quantum efficiency of the species eliminated by borohydride reduction, equation 3.5 was employed (Golanoski et. al. 2012),

$$\Phi_{\text{diff}} = (R_{\text{TMP}}^{\text{U}} - R_{\text{TMP}}^{\text{R}}) / (R_{\text{EX}}^{\text{U}} - R_{\text{EX}}^{\text{R}}) \quad (\text{III.5})$$

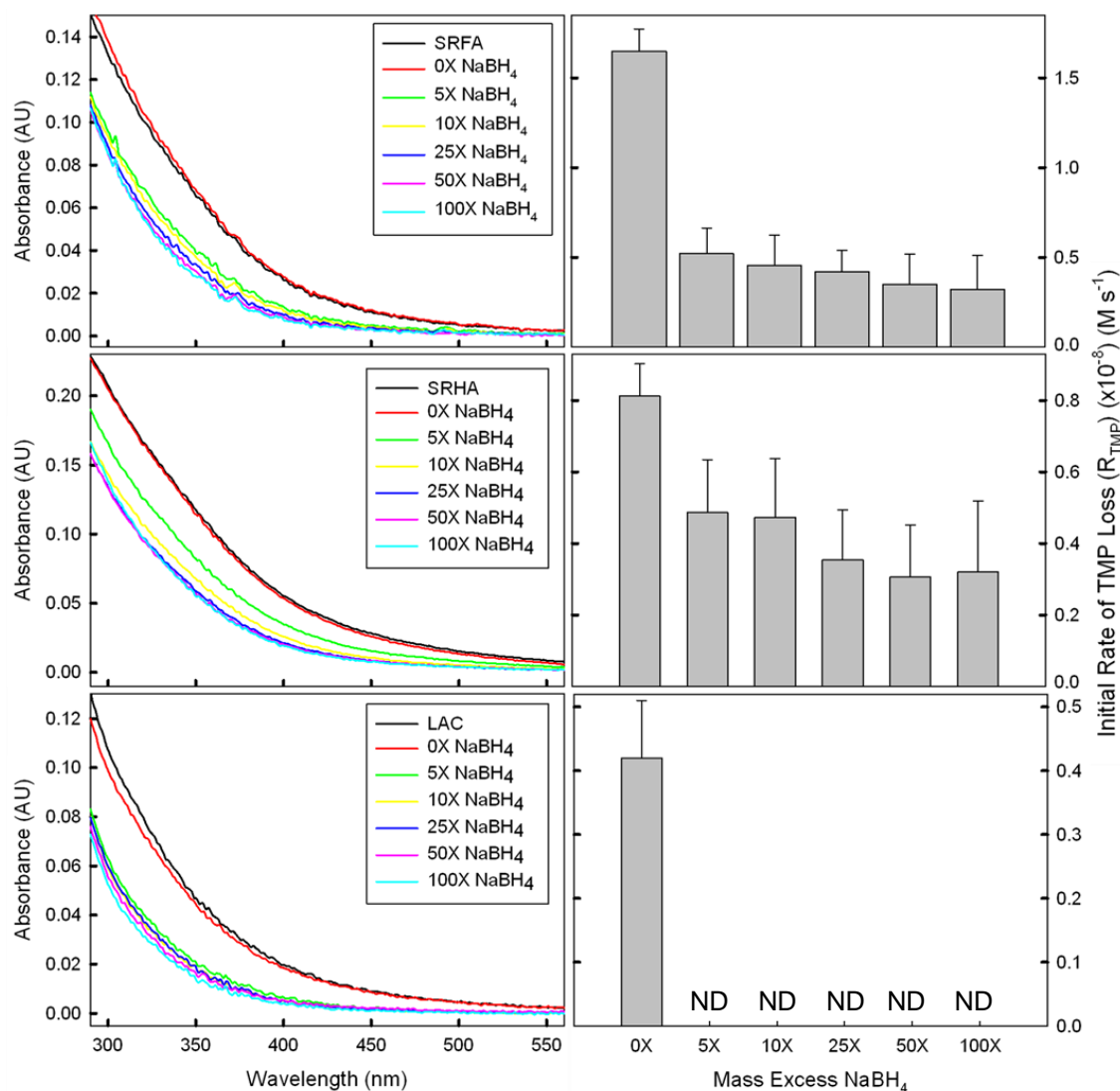
where the superscripts U and R denote untreated and borohydride-reduced samples.

### 3.3 Results and Discussion

#### 3.3.1 Effect of $\text{NaBH}_4$ on the Optical, Photochemical Properties of HS and CDOM

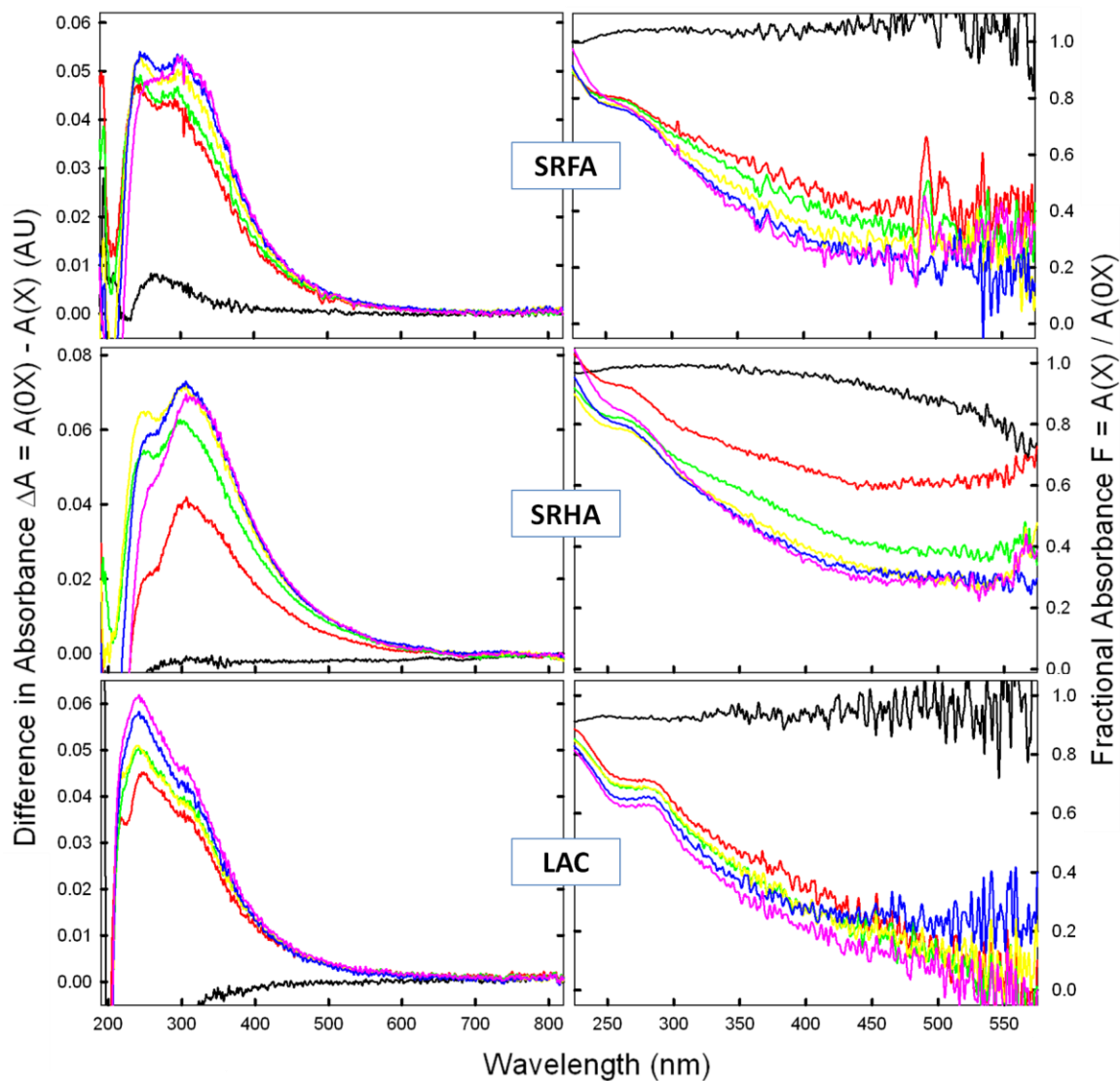
The dependence of the optical and photochemical properties of HS on 5, 10, 25, 50 and 100-fold mass excesses of sodium borohydride were examined for SRFA, SRHA and LAC. The effect of increasing the mass excess of  $\text{NaBH}_4$  from five-fold (5X) to 100-

fold (100X) resulted in larger losses of absorbance for all samples (Fig. III.4, left panel) and additional decreases in  $R_{\text{TMP}}$  for SRFA and SRHA (Fig. III.4, right panel).



**Figure III.4:** Absorbance spectra (left panel) and initial rate of TMP loss (right panel) for untreated (black trace) and sodium borohydride-reduced SRFA, SRHA and LAC. Samples were reduced using 5, 10, 25, 50 or 100-fold mass excess of sodium borohydride (all other conditions as in Appendix II). Control samples (0X, red trace) represent untreated samples passed over a Sephadex G-10 column then normalized by TOC to account for dilution.  $R_{\text{TMP}}$  as determined under aerated conditions ( $\sim 250 \mu\text{M O}_2$ ),

$[TMP] = 100 \mu M$  and  $\lambda > 325 \text{ nm}$  where ND = not detected. Error bars represent  $\pm 1$  standard deviation of at least three independent determinations.



**Figure III.5:** Difference in absorbance (left panel) and fractional absorbance (right panel) for sodium borohydride-reduced SRFA, SRHA and LAC using 0X (control, black trace), 5X (red trace), 10X (green trace), 25X (yellow trace), 50X (blue trace) and 100X (purple trace) mass excess  $\text{NaBH}_4$ . All other conditions as in Figure III.4.

Consistent with prior results, the largest absolute loss of absorbance occurred in the UV (Fig. III.5, left panel) and the largest fractional loss was observed in the visible (Fig. III.5, right panel) (Tinnacher and Honeyman, 2007; Ma et al, 2010; Andrew et. al, 2013; Golanoski et. al, 2012; Zhang et. al, 2012). Absorbance spectra of control samples (0X) (Fig III.4, red trace) did not vary significantly from untreated HS indicating that passage over a Sephadex G-10 column neither contributes nor detracts from the optical properties when compared on a carbon-matched basis.

Values of spectral slope ( $S$ ), specific absorption coefficient at 350 nm ( $a^*(350)$ ) were determined from the absorbance spectra of SRFA, SRHA and LAC which were untreated (0X) or treated with a 5X, 10X, 25X, 50X or 100X mass excess of  $\text{NaBH}_4$  are presented in Table III.2 along with  $R_{\text{TMP}}$  for each sample. Increasing the mass excess of  $\text{NaBH}_4$  from five- to fifty-fold produced an additional 22-32% decrease in  $a^*(350)$ , 17-27% increase in  $S$  and 33-35% decrease in  $R_{\text{TMP}}$  (except LAC). However, increasing the mass excess of  $\text{NaBH}_4$  to 100-fold produced negligible (<10%) additional changes in these three parameters. Further, the addition of 250 mg  $\text{NaBH}_4$  produces an overwhelming volume of  $\text{H}_2$  gas, often leading to cracking of the Sephadex column and sample loss. In light of this, all samples used in this study were reduced using a fifty-fold mass excess of  $\text{NaBH}_4$ .

		$a^*(350)$ ( $\text{m}^{-1} \text{mg}^{-1} \text{C L}^{-1}$ )	$S$ ( $\text{nm}^{-1}$ )	$R_{\text{TMP}}$ ( $\text{M s}^{-1}$ ) ( $\times 10^{-8}$ )
SRFA	0X	3.51	0.014	$1.65 \pm 0.12$
	5X	2.00	0.016	$0.52 \pm 0.14$
	10X	1.90	0.019	$0.45 \pm 0.17$
	25X	1.72	0.021	$0.42 \pm 0.12$
	50X	1.56	0.022	$0.35 \pm 0.17$
	100X	1.43	0.023	$0.32 \pm 0.19$
SRHA	0X	7.30	0.012	$0.81 \pm 0.09$
	5X	5.20	0.015	$0.49 \pm 0.15$
	10X	4.38	0.015	$0.47 \pm 0.28$
	25X	3.77	0.017	$0.35 \pm 0.14$
	50X	3.55	0.018	$0.31 \pm 0.15$
	100X	3.42	0.019	$0.32 \pm 0.20$
LAC	0X	4.00	0.016	$0.42 \pm 0.09$
	5X	1.79	0.020	$0.00 \pm 0.08$
	10X	1.62	0.024	$0.00 \pm 0.09$
	25X	1.63	0.024	$0.00 \pm 0.10$
	50X	1.40	0.025	$0.00 \pm 0.09$
	100X	1.20	0.026	$0.00 \pm 0.10$

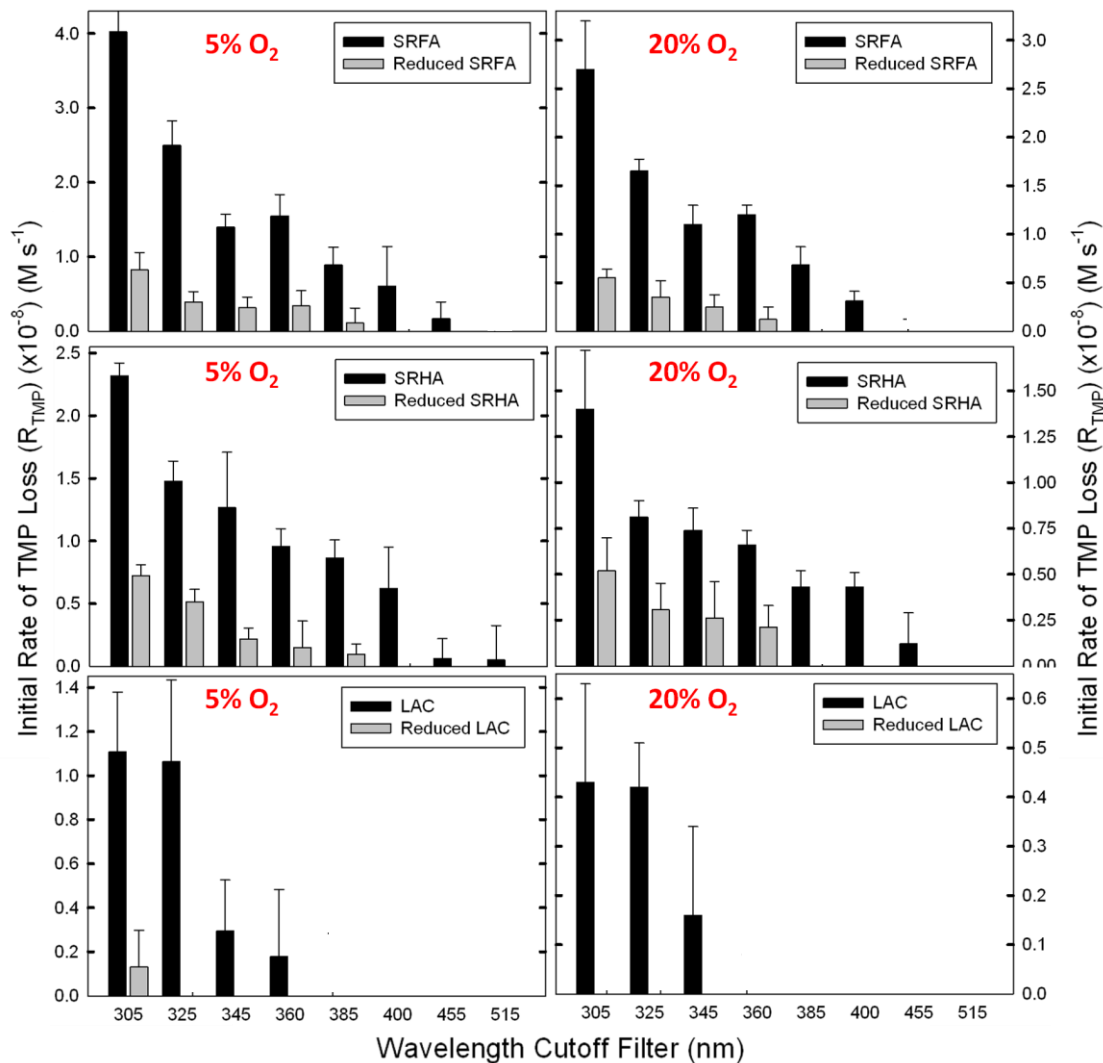
**Table III.2:** Values of specific absorbance coefficient at 350 nm ( $a^*(350)$ ), spectral slope ( $S$ ) and initial rate of TMP loss ( $R_{\text{TMP}}$ ) for untreated and borohydride-reduced SRFA, SRHA and LAC using 5, 10, 25, 50 and 100-fold mass excess of  $\text{NaBH}_4$ .  $R_{\text{TMP}}$  was determined at  $[\text{TMP}] = 100 \mu\text{M}$  and  $[\text{O}_2] = 250 \mu\text{M}$  and the uncertainty for  $S = 0.01 \text{ nm}^{-1}$  and  $a^*(350) = 0.01 \text{ m}^{-1} \text{mg}^{-1} \text{C L}$ .

### 3.3.2: Wavelength dependence of $R_{\text{TMP}}$ for untreated and borohydride reduced HS

The spectral dependence of  $R_{\text{TMP}}$  was examined for untreated and borohydride-reduced SRFA, SRHA and LAC at a constant  $[\text{TMP}] = 100 \mu\text{M}$  and under aerated (20%, right panel) and low (5%, left panel)  $\text{O}_2$  conditions. Values of  $R_{\text{TMP}}$  increased by a factor

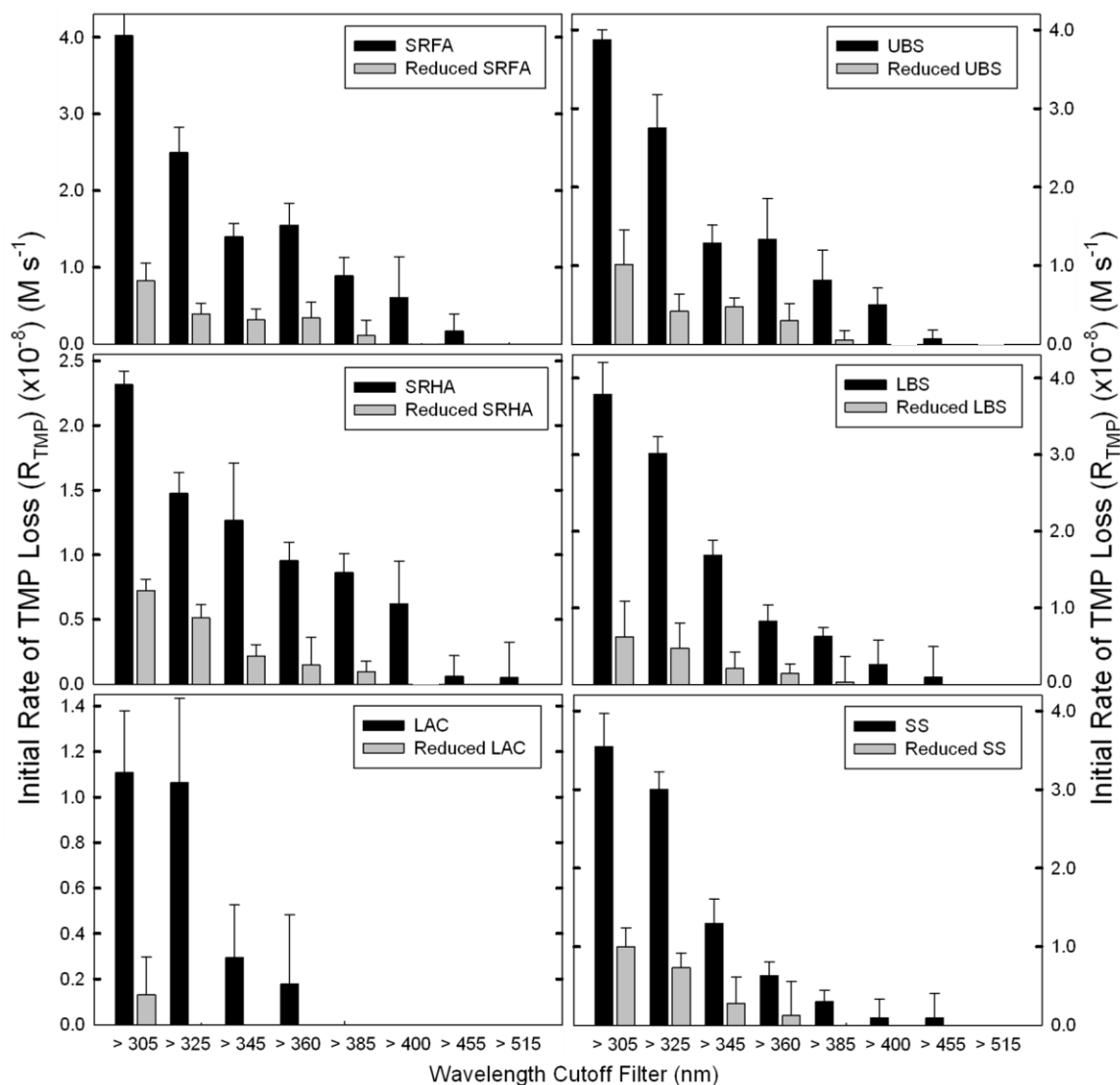


of  $\sim 2$  for untreated and by  $\sim 1.5$  for borohydride-reduced samples for a four-fold decrease in  $[O_2]$ . This result is consistent with prior results which were attributed to reduced quenching of triplet excited states by molecular oxygen at lower  $[O_2]$  (Figure III.4) (Golanoski, et.al., 2012). Further, the magnitude of this increase in  $R_{TMP}$  from 20% to 5%  $[O_2]$  was approximately constant across all wavelengths at which  $R_{TMP}$  was detected.



**Figure III.6:** Dependence of the initial rate of TMP loss ( $R_{TMP}$ ) on wavelength for both untreated (black bars) and borohydride-reduced (gray bars) SRFA, SRHA and LAC under 5% (left panel) and 20% (right panel) conditions.  $R_{TMP}$  as determined at  $[TMP] =$

100  $\mu\text{M}$  and all other conditions as in Figures III.2-3. Error bars represent  $\pm 1$  standard deviation of at least three independent measurements. Measurements not appearing on this graph were not detected above the detection limit.



**Figure III.7:** Dependence of the initial rate of TMP loss ( $R_{\text{TMP}}$ ) on wavelength for both untreated (black bars) and borohydride-reduced (gray bars) SRFA, SRHA, LAC, UBS, LBS and SS.  $R_{\text{TMP}}$  as determined at 5% ( $\sim 63 \mu\text{M}$ )  $\text{O}_2$  and  $[\text{TMP}] = 100 \mu\text{M}$  conditions where ND = not detected. All other conditions as in Figures III.2-3. Error bars represent  $\pm 1$  standard deviation of at least three independent measurements.

Due to sample limitations, the wavelength dependence of  $R_{\text{TMP}}$  for the  $\text{C}_{18}$  extracts of the Delaware Bay were only performed under 5%  $\text{O}_2$  conditions and the results are compared to SRFA, SRHA and LAC determined under similar conditions in Figure III.6. The largest values of  $R_{\text{TMP}}$  occur with the 305 nm filter, then decreased with increasing wavelength of the cut-off filter, becoming undetectable at 360 nm for LAC, above ~400 nm for SRFA, UBS, LBS and SS and ~455 nm for SRHA.

To provide a comparison of the wavelength dependence among the samples, a simple linear regression analysis was performed on log-transformed values of  $R_{\text{TMP}}$  for untreated and borohydride-reduced samples (Figure III.8).

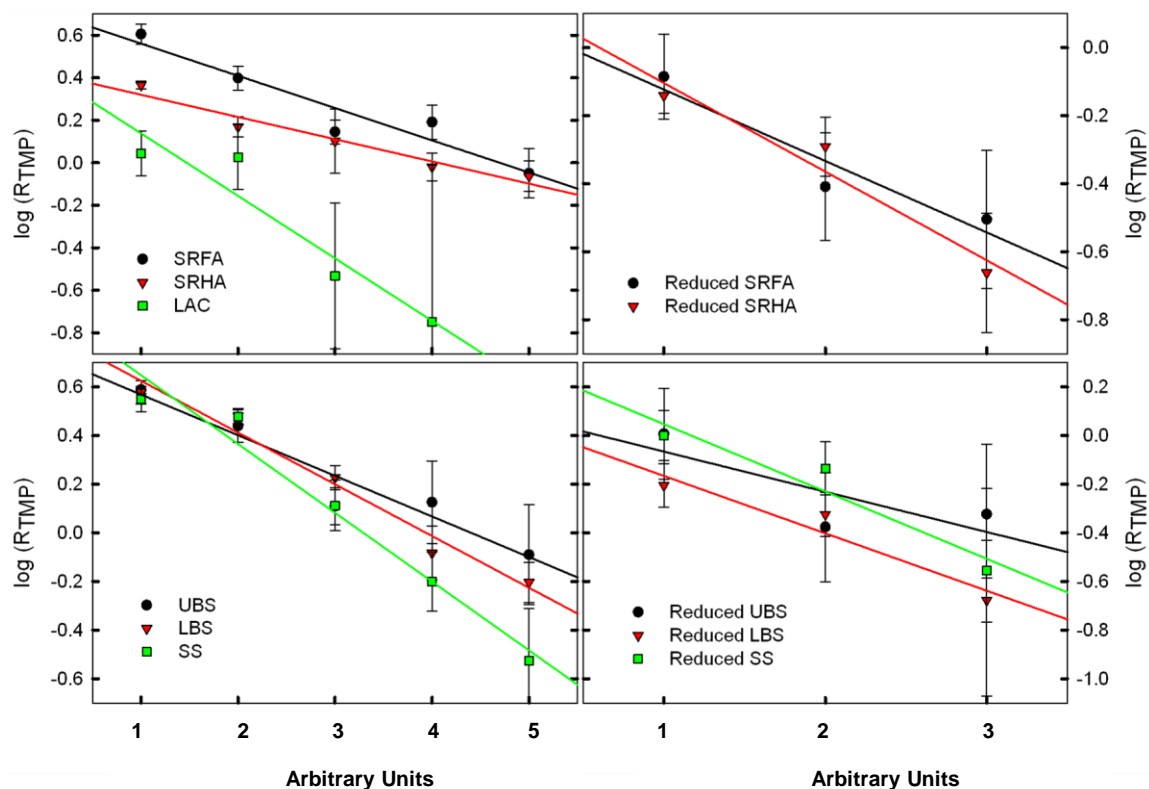


Figure III.8: Log-transformed values of  $R_{\text{TMP}}$  for untreated and borohydride-reduced SRFA, SRHA, LAC, UBS, LBS and SS. For simplicity, the x-axis is arbitrary.

For simplicity, data were fit using an arbitrary x-axis (i.e. 1, 2, 3, etc) with all slopes normalized to the value obtained for SRFA. The rate at which  $R_{TMP}$  decreased followed the order:  $LAC > SS > LBS > UBS > SRFA > SRHA$  for untreated samples, whereas for borohydride-reduced samples similar rates were observed for all samples except borohydride-reduced UBS where the fit was relatively poor ( $R^2 = 0.63$ ) (Table III.3). For untreated samples, this result is proportional to the trend observed for the spectral slope parameter,  $S$ , which describes the rate at which absorbance decreases with increasing wavelength where  $LAC > C_{18} \text{ extracts} \approx SRFA > SRHA$  (Table III.2; Golanoski et. al., 2012).

	Slope	$R^2$		Slope	$R^2$
SRFA	$1.0 \pm 0.2$	0.91	Reduced SRFA	$1.4 \pm 0.5$	0.91
SRHA	$0.67 \pm 0.07$	0.95	Reduced SRHA	$1.7 \pm 0.4$	0.94
LAC	$1.9 \pm 0.5$	0.90			
			Reduced UBS	$1.1 \pm 0.9$	0.63
UBS	$1.1 \pm 0.2$	0.93	Reduced LBS	$1.6 \pm 0.5$	0.92
LBS	$1.4 \pm 0.1$	0.97	Reduced SS	$1.9 \pm 0.5$	0.92
SS	$1.9 \pm 0.2$	0.97			

**Table III.3:** Values of slope (normalized to SRFA) and coefficients of determination ( $R^2$ ) for the simple linear regression of log-transformed  $R_{TMP}$  for untreated and borohydride-reduced SRFA, SRHA, LAC, UBS, LBS and SS. All other conditions as in Figure III.8.

Compared to untreated samples, borohydride reduction decreases  $R_{TMP}$  by ~65-88% at  $\lambda > 305$  nm then decreases with increasing wavelength, becoming undetectable at 325 nm for LAC and at 385 nm for SRFA, SRHA, and the  $C_{18}$  extracts. The remaining  $R_{TMP}$  following borohydride reduction exhibited a similar dependence on wavelength as the untreated samples consistent with the results observed for the dependence of  $R_{TMP}$  on

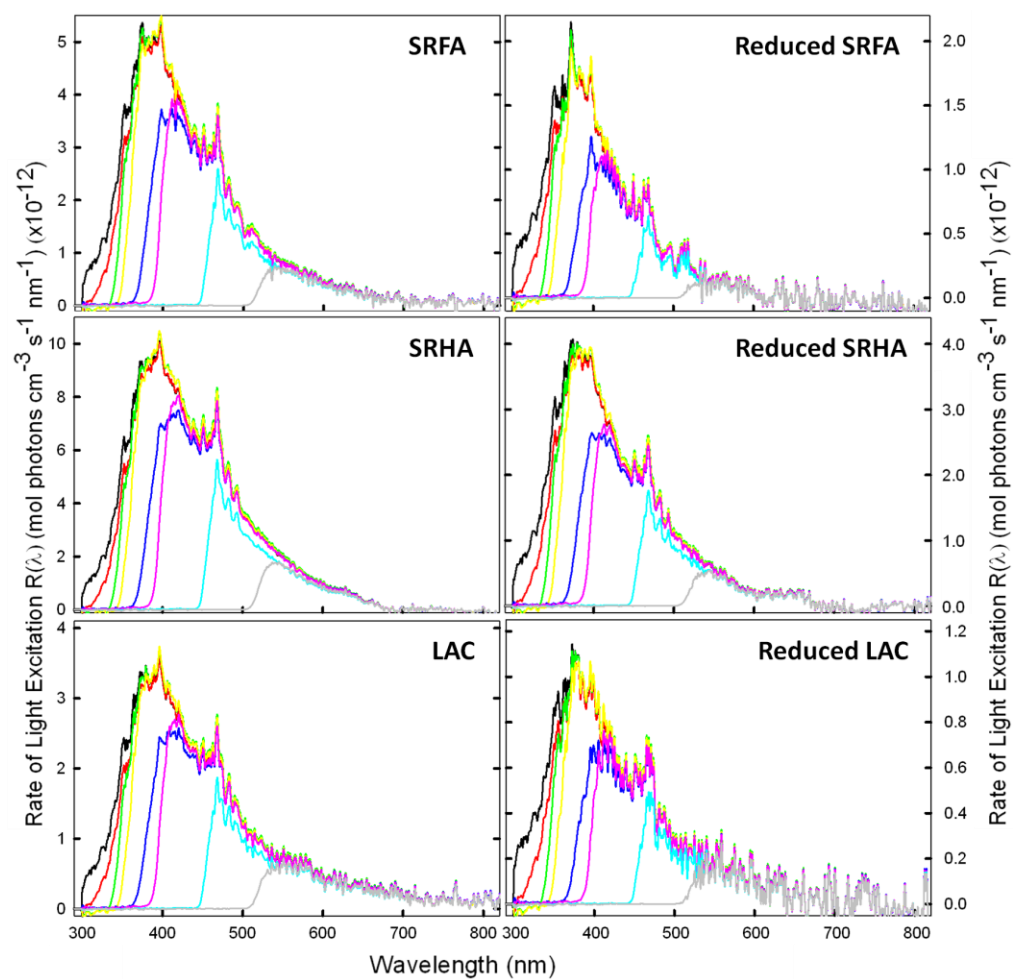
[O<sub>2</sub>] suggesting that a similar class of oxidants was remaining, perhaps quinones (Golanoski et. al., 2012).

However,  $R_{\text{TMP}}$  was not measureable for most untreated and borohydride-reduced samples above ~400 nm and ~ 385 nm, respectively, suggesting that either the sensitizing species have insufficient rates of light absorption or that the light absorbing moieties do not contribute efficiently to TMP sensitization across the visible.

### **3.3.3 Wavelength dependence of $R(\lambda)$ for untreated and borohydride-reduced HS**

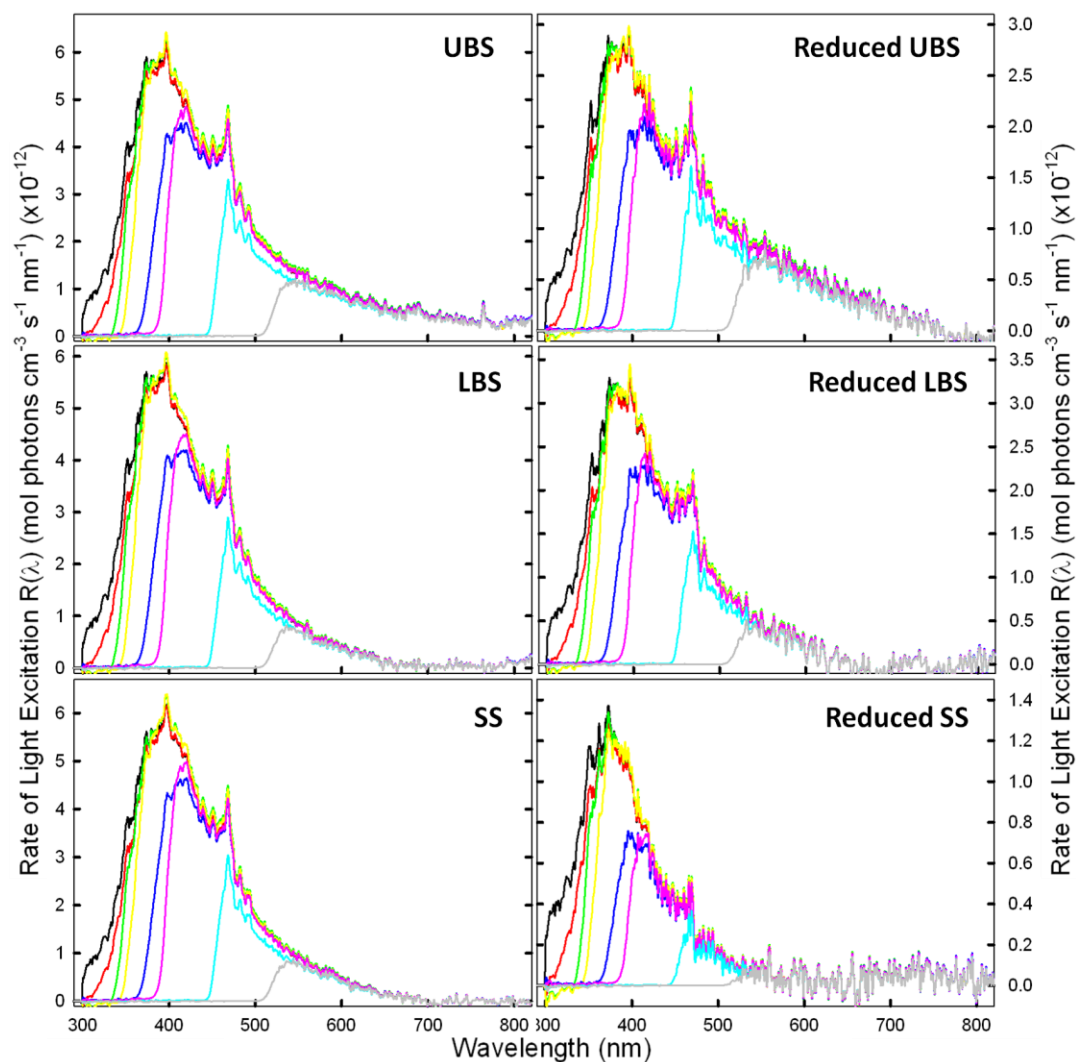
To further examine this possibility, the wavelength dependence of  $R(\lambda)$  (Eqn. III.4) and apparent polychromatic quantum yields ( $\Phi$ ) (Eqn. III.3) for all wavelength cutoff filters employed in this study was determined for untreated and borohydride-reduced SRFA, SRHA and LAC and C<sub>18</sub> extracts of the Delaware Bay at an Upper Bay Station (UBS), Lower Bay Station (LBS) and Shelf Station (SS).

A maximum value of  $R(\lambda)$  was observed for untreated samples at ~400 nm, where this dependence is a result of the product of the HS absorption spectrum (high absorbance at short wavelengths) and the absolute irradiance of the xenon arc lamp and selected cutoff filters (largest photon flux at long wavelengths) (Eqn. III.4) (Figs. III.2-3). Sodium borohydride, a selective reductant of carbonyl-containing moieties in HS and CDOM, produces a preferential loss of long wavelength absorption thus decreasing substantially the absolute values of  $R(\lambda)$  by more than two-fold, as well as decreasing the wavelength at which the maximum in  $R(\lambda)$  is observed (~375 nm) (Figs. III.9-10, right panels).



**Figure III.9:** Wavelength dependence of  $R(\lambda) = a(\lambda) \cdot I(\lambda)$  for untreated (left panel) and borohydride-reduced (right panel) SRFA, SRHA and LAC employing selected wavelength cutoff filters to alter  $I(\lambda)$  at

—  $> 305$  nm    —  $> 325$  nm    —  $> 345$  nm    —  $> 360$  nm  
 —  $> 385$  nm    —  $> 400$  nm    —  $> 455$  nm    —  $> 515$  nm



**Figure III.10:** Wavelength dependence of  $R(\lambda) = a(\lambda) \cdot I(\lambda)$  for untreated (left panel) and borohydride-reduced (right panel) Upper Bay Station (UBS), Lower Bay Station (LBS) and Shelf Station (SS) employing selected wavelength cutoff filters to alter  $I(\lambda)$  at

— > 305 nm    — > 325 nm    — > 345 nm    — > 360 nm    — > 385 nm    — > 400 nm  
 — > 455 nm    — > 515 nm

Moreover, examination of  $R_{TMP}$  and  $R_{EX}$  across wavelengths in the UVB and UVA reveals that  $R_{TMP}$  decreases far faster than  $R_{EX}$  providing additional evidence that these wavelengths are primarily responsible for the sensitization (Tables III.4-5).

	$R_{TMP} (\times 10^{-8}) (M s^{-1})$		$R_{EX} (\times 10^{-7}) (M s^{-1})$	
	SRFA	Reduced SRFA	SRFA	Reduced SRFA
> 305 nm	$4.0 \pm 0.5$	$0.82 \pm 0.24$	$3.7 \pm 0.2$	$1.1 \pm 0.1$
> 325 nm	$2.5 \pm 0.3$	$0.39 \pm 0.14$	$3.5 \pm 0.1$	$0.95 \pm 0.1$
> 345 nm	$1.4 \pm 0.2$	$0.31 \pm 0.15$	$3.5 \pm 0.2$	$0.91 \pm 0.1$
> 360 nm	$1.6 \pm 0.3$	$0.34 \pm 0.21$	$3.3 \pm 0.2$	$0.82 \pm 0.1$
> 385 nm	$0.89 \pm 0.24$	$0.11 \pm 0.21$	$2.4 \pm 0.2$	$0.53 \pm 0.1$
> 400 nm	$0.61 \pm 0.52$	ND	$2.2 \pm 0.1$	$0.45 \pm 0.02$
> 455 nm	$0.17 \pm 0.23$	ND	$0.93 \pm 0.06$	$0.13 \pm 0.01$
> 500 nm	ND	ND	$0.39 \pm 0.04$	$0.04 \pm 0.01$

	SRHA	Reduced SRHA	SRHA	Reduced SRHA
> 305 nm	$2.3 \pm 0.1$	$0.72 \pm 0.09$	$9.7 \pm 0.4$	$3.3 \pm 0.1$
> 325 nm	$1.5 \pm 0.2$	$0.51 \pm 0.10$	$9.3 \pm 0.3$	$3.1 \pm 0.1$
> 345 nm	$1.3 \pm 0.4$	$0.22 \pm 0.09$	$9.3 \pm 0.5$	$3.0 \pm 0.2$
> 360 nm	$0.96 \pm 0.14$	$0.15 \pm 0.21$	$8.8 \pm 0.4$	$2.8 \pm 0.1$
> 385 nm	$0.87 \pm 0.14$	$0.10 \pm 0.08$	$6.8 \pm 0.4$	$2.0 \pm 0.1$
> 400 nm	$0.62 \pm 0.33$	ND	$6.3 \pm 0.4$	$1.8 \pm 0.1$
> 455 nm	$0.06 \pm 0.16$	ND	$3.0 \pm 0.2$	$0.71 \pm 0.12$
> 500 nm	ND	ND	$1.4 \pm 0.1$	$0.24 \pm 0.02$

	LAC	Reduced LAC	LAC	Reduced LAC
> 305 nm	$1.1 \pm 0.3$	$0.13 \pm 0.17$	$4.7 \pm 0.1$	$1.3 \pm 0.1$
> 325 nm	$1.1 \pm 0.4$	ND	$4.4 \pm 0.1$	$1.2 \pm 0.1$
> 345 nm	$0.29 \pm 0.23$	ND	$4.4 \pm 0.2$	$1.1 \pm 0.1$
> 360 nm	$0.18 \pm 0.30$	ND	$4.1 \pm 0.1$	$1.0 \pm 0.1$
> 385 nm	ND	ND	$3.1 \pm 0.1$	$0.75 \pm 0.03$
> 400 nm	ND	ND	$2.8 \pm 0.1$	$0.67 \pm 0.02$
> 455 nm	ND	ND	$1.3 \pm 0.1$	$0.28 \pm 0.01$
> 500 nm	ND	ND	$0.54 \pm 0.1$	$0.11 \pm 0.01$

**Table III.4:** Values of  $R_{TMP}$  and  $R_{EX}$  for SRFA, SRHA and LAC at all wavelength cutoff filters employed. ND = not detected. All conditions as in Figures III.5 and 6.



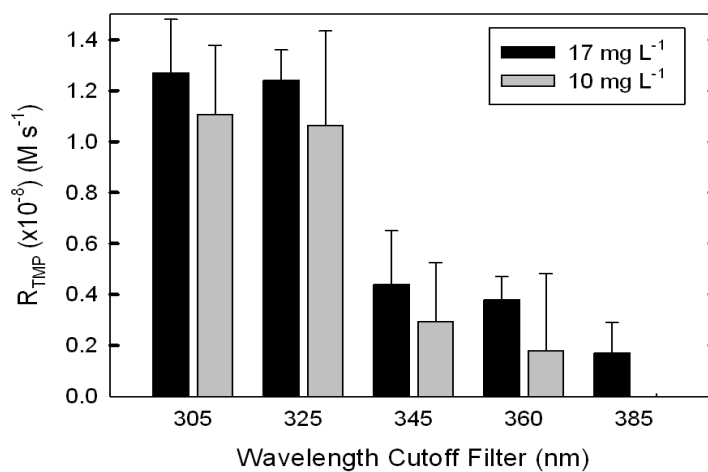
	$R_{\text{TMP}} (\times 10^{-8}) (\text{M s}^{-1})$		$R_{\text{EX}} (\times 10^{-7}) (\text{M s}^{-1})$	
	UBS	Reduced UBS	UBS	Reduced UBS
> 305 nm	$3.9 \pm 0.1$	$1.0 \pm 0.4$	$2.6 \pm 0.3$	$1.3 \pm 0.1$
> 325 nm	$2.8 \pm 0.4$	$0.42 \pm 0.22$	$2.5 \pm 0.2$	$1.2 \pm 0.1$
> 345 nm	$1.3 \pm 0.2$	$0.47 \pm 0.12$	$2.5 \pm 0.3$	$1.2 \pm 0.1$
> 360 nm	$1.3 \pm 0.5$	$0.30 \pm 0.22$	$2.4 \pm 0.2$	$1.1 \pm 0.1$
> 385 nm	$0.81 \pm 0.38$	$0.05 \pm 0.12$	$1.8 \pm 0.2$	$0.86 \pm 0.1$
> 400 nm	$0.50 \pm 0.21$	ND	$1.7 \pm 0.2$	$0.79 \pm 0.1$
> 455 nm	$0.07 \pm 0.12$	ND	$0.85 \pm 0.06$	$0.41 \pm 0.07$
> 500 nm	ND	ND	$0.47 \pm 0.04$	$0.22 \pm 0.04$

	LBS	Reduced LBS	LBS	Reduced LBS
> 305 nm	$3.8 \pm 0.4$	$0.62 \pm 0.46$	$2.0 \pm 0.2$	$1.1 \pm 0.1$
> 325 nm	$3.0 \pm 0.2$	$0.47 \pm 0.33$	$1.8 \pm 0.1$	$0.99 \pm 0.08$
> 345 nm	$1.7 \pm 0.2$	$0.21 \pm 0.21$	$1.8 \pm 0.2$	$0.97 \pm 0.09$
> 360 nm	$0.83 \pm 0.21$	$0.14 \pm 0.13$	$1.7 \pm 0.2$	$0.90 \pm 0.03$
> 385 nm	$0.63 \pm 0.12$	$0.03 \pm 0.34$	$1.3 \pm 0.2$	$0.65 \pm 0.05$
> 400 nm	$0.26 \pm 0.12$	ND	$1.1 \pm 0.1$	$0.58 \pm 0.06$
> 455 nm	$0.09 \pm 0.40$	ND	$0.46 \pm 0.05$	$0.22 \pm 0.03$
> 500 nm	ND	ND	$0.17 \pm 0.04$	$0.067 \pm 0.02$

	SS	Reduced SS	SS	Reduced SS
> 305 nm	$3.5 \pm 0.4$	$1.0 \pm 0.24$	$0.95 \pm 0.09$	$0.17 \pm 0.03$
> 325 nm	$3.0 \pm 0.2$	$0.73 \pm 0.18$	$0.90 \pm 0.07$	$0.15 \pm 0.02$
> 345 nm	$1.3 \pm 0.3$	$0.28 \pm 0.33$	$0.89 \pm 0.04$	$0.14 \pm 0.06$
> 360 nm	$0.63 \pm 0.18$	$0.12 \pm 0.44$	$0.84 \pm 0.05$	$0.13 \pm 0.03$
> 385 nm	$0.30 \pm 0.15$	ND	$0.63 \pm 0.07$	$0.085 \pm 0.02$
> 400 nm	$0.09 \pm 0.24$	ND	$0.57 \pm 0.08$	$0.072 \pm 0.02$
> 455 nm	$0.09 \pm 0.24$	ND	$0.22 \pm 0.10$	$0.026 \pm 0.01$
> 500 nm	ND	ND	$0.078 \pm 0.04$	$0.012 \pm 0.01$

**Table III.5:** Values of  $R_{\text{TMP}}$  and  $R_{\text{EX}}$  for UBS, LBS and SS at all wavelength cutoff filters employed. ND = not detected. All conditions as in Figures III.5 and 7.

Interestingly,  $R_{\text{TMP}}$  is not detected for LAC at wavelengths greater than 360 nm despite comparable values to SRFA of  $R_{\text{EX}}$  at  $\lambda > 385, 400, 455$  and  $515$  nm (Table III.4). To determine whether there exists no sensitization at these wavelengths, or whether  $R_{\text{TMP}}$  is simply undetectable at the concentrations of LAC employed, the concentration of LAC was increased to  $17 \text{ mg L}^{-1}$  ( $a(350) = 0.1 \text{ OD}$ ) and the wavelength dependence of  $R_{\text{TMP}}$  was determined. Although absorption at 350 nm was increased by almost two-fold, only a small ( $\sim 15\%$ ) increase in  $R_{\text{TMP}}$  was observed for LAC at 305 nm and the range of wavelengths at which  $R_{\text{TMP}}$  was detected was extended from 360 nm to 385 nm (Fig III.11).



**Figure III.11:** Wavelength dependence of  $R_{\text{TMP}}$  for  $10 \text{ mg L}^{-1}$  (left panel) and  $17 \text{ mg L}^{-1}$  (right panel) LAC as determined at  $[\text{TMP}] = 100 \mu\text{M}$  and under  $5\% [\text{O}_2]$  conditions.

The relatively low  $R_{\text{TMP}}$  observed at 305 nm for both  $10$  and  $17 \text{ mg L}^{-1}$  LAC suggest that 1)  $R_{\text{TMP}}$  is smaller because of a low yield of triplet excited states or 2) that LAC simply contains fewer sensitizing carbonyl moieties.

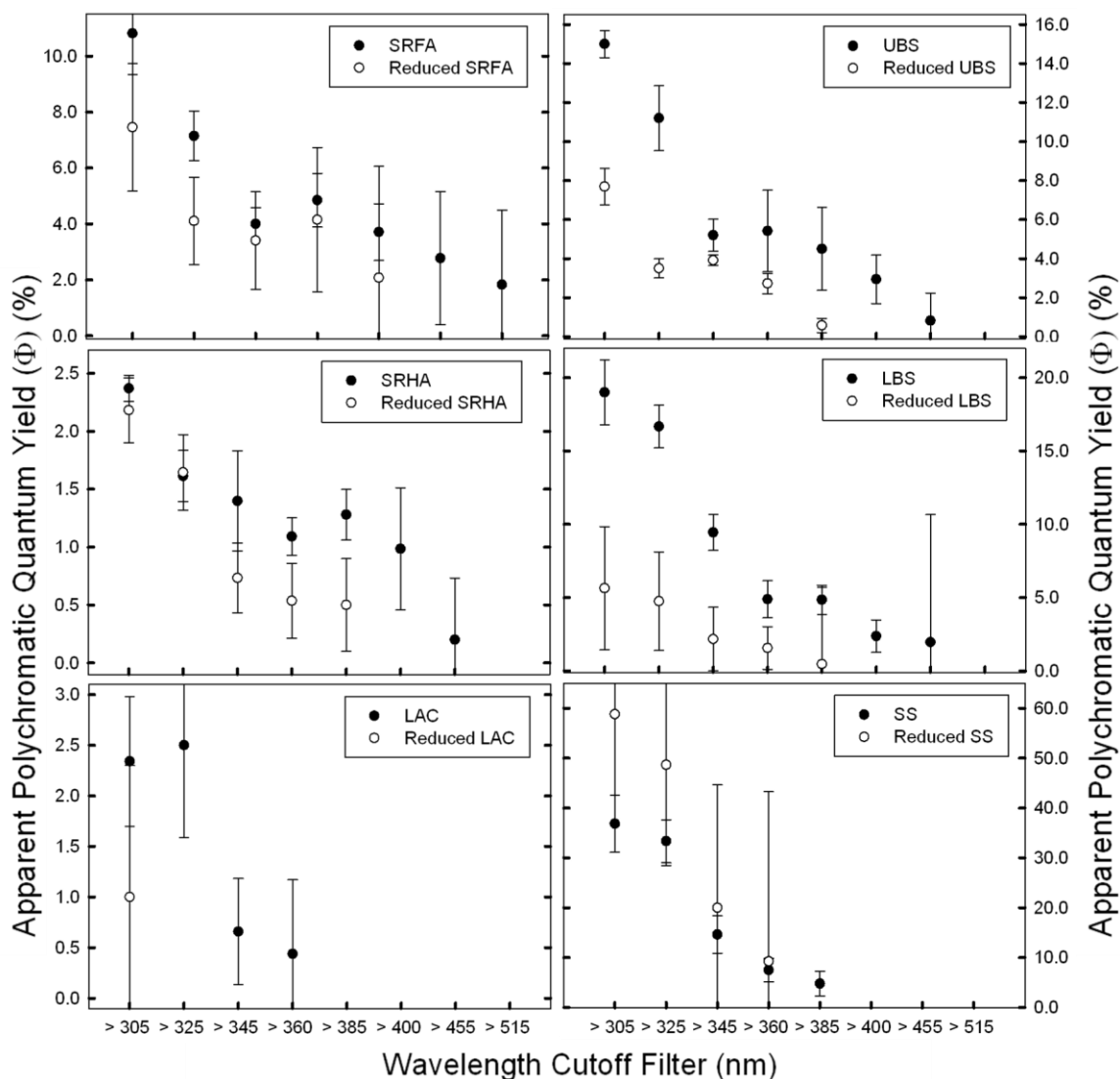
### 3.3.4: Wavelength dependence of $\Phi$ for untreated and borohydride-reduced HS

Apparent polychromatic quantum efficiencies ( $\Phi$ ) were determined for untreated and borohydride reduced SRFA, SRHA, LAC and C18 extracts of the Delaware Bay at an Upper Bay Station (UBS), Lower Bay Station (LBS) and Shelf Station (SS) to make a comparison between samples, account for the decrease in  $R_{EX}$  with increasing wavelength, and the effect of reduction by sodium borohydride.

Similar to the wavelength dependence of  $R_{TMP}$ , the largest values of  $R_{TMP}$  were noted at 305 nm then decreased with increasing wavelength (Figure III.12). Values of  $\Phi$  at 305 nm vary from 2.5 to 35% with the trend:  $LAC \approx SRHA < SRFA < UBS < LBS < SS$ . These results are consistent with previously published values of apparent quantum efficiencies for  $^1O_2$  production, whose reaction with HS and CDOM is also thought to proceed via a triplet mechanism (Aguer et. al., 1997; Sandvik et. al., 2000; Paul et. al., 2004).

Prior work presented values of  $\Phi$  (determined under aerated conditions) which were thought to represent a lower bound to the maximum efficiencies expected for triplet excited states of ketones/aldehydes (Golanoski et. al., 2012). That values of  $\Phi$  under low (5%)  $[O_2]$  conditions increase by roughly two-fold provides support for the previously proposed idea that quantitative reaction of TMP with the intermediate initiating oxidation was not attained. However, the values reported herein are also negatively impacted by the fact that maximum rates of light excitation occurring near 400 nm, where ketones and aldehydes are not expected to absorb thus reducing  $R_{TMP}$ . Interestingly, a small increase in  $\Phi$  is observed with the 360 and 385 nm cutoff filters for SRFA, SRHA, UBS and LBS

which may be correlated to maxima of  $R(\lambda)$  for these samples, although additional data points would be needed.



**Figure III.12:** Dependence of the apparent polychromatic quantum efficiencies ( $\Phi$ ) for TMP loss on wavelength for both untreated (black bars) and borohydride-reduced SRFA, SRHA, LAC, UBS, LBS and SS under 5% ( $\sim 63 \mu\text{M}$ )  $\text{O}_2$  conditions. All other conditions as in Figures 3.3 and 3.4. Error bars represent  $\pm 1$  standard deviation of at least three independent measurements.

Values of  $\Phi$  for borohydride reduced samples remained similar (given the uncertainties) to untreated values for SRHA, SRFA and SS, were lower for UBS, LBS and LAC (Figure III.12). Consistent with prior results, values of  $\Phi$  for borohydride-reduced SRHA remained very similar to untreated values. However, for borohydride-reduced UBS and LBS, values of  $\Phi$  which were previously reported to remain similar to untreated samples are now shown in Figure III.9 to have smaller values of  $\Phi$  compared to untreated samples. This may be attributable to the larger mass excess of  $\text{NaBH}_4$  employed, which further reduced  $R_{\text{TMP}}$  and thereby decreased  $\Phi$ .

For all samples, the largest value of  $R_{\text{TMP}}$  observed for the 305 nm filter followed by a decrease in  $R_{\text{TMP}}$  with increasing wavelength, becoming undetectable for most samples at  $\lambda > 400$  nm. The effect of borohydride reduction of HS and CDOM samples decreased  $R_{\text{TMP}}$  by 65-88%; the remaining sensitization showed similar wavelength dependence, indicating that the remaining sensitization may arise from a similar pool of oxidizing triplets. For a four-fold decrease in  $[\text{O}_2]$ , values of  $R_{\text{TMP}}$  increased by a factor of  $\sim 2$  for untreated samples and by  $\sim 1.5$  for borohydride-reduced samples, consistent with the idea that at low  $[\text{O}_2]$ , quenching of triplet states by dioxygen decreases allowing for enhancement in  $R_{\text{TMP}}$ . The fact that  $R_{\text{TMP}}$  decreases much faster than  $R_{\text{EX}}$  and the apparent polychromatic quantum yields rapidly decrease with increasing wavelength provide strong evidence that long-wavelength absorbing moieties within HS and CDOM do not contribute significantly to the photosensitization. This result, however, would appear to preclude as triplet sensitizers quinones that absorb significantly into the visible. This study provides additional evidence for the role of triplet excited states of short-

wavelength absorbing moieties (such as aromatic ketones and quinones) within HS and CDOM in the photosensitized loss of TMP.

## **Chapter IV: Effects of Borohydride Reduction and [O<sub>2</sub>] on the sensitized loss of a series of phenols by Suwannee River Fulvic Acid (SRFA).**

### **Abstract**

The dependence of the initial rate of phenol probe loss ( $R_{\text{probe}}$ ) on [phenol], [O<sub>2</sub>] and sodium borohydride reduction of SRFA was determined for a series of substituted phenols of varying one-electron reduction potentials ( $E^\circ(\text{PhO}\cdot/\text{PhO}^-)$ ) vs NHE. Similar dependencies on [O<sub>2</sub>] were noted for 2,4,6-trimethylphenol (TMP) and 4-methoxyphenol (4-MOP) with untreated and borohydride-reduced SRFA however DMOP exhibited saturation of the initial rate at high [O<sub>2</sub>] in contrast to the inverse dependence observed for TMP and 4-MOP in this regime. This data, in addition to apparent polychromatic quantum yields and rate constants and obtained from fitting of the [O<sub>2</sub>] dependence support the idea that triplet excited states of CDOM play a major role in the photosensitized loss of TMP and 4-MOP however a separate pathway may be important to the mechanism for DMOP. Borohydride reduction decreased  $R_{\text{probe}}$  by 35-75% while exhibiting similar dependencies to untreated SRFA, indicating that a similar pool of photooxidants may be responsible for the remaining sensitization.

### **4.1 Introduction**

Despite having been studied for several decades, the underlying structural basis of the observed photochemical properties of chromophoric dissolved organic matter (CDOM) remain unclear, due in large part to the spatial and temporal variations in CDOM composition. The sunlight-mediated phototransformation of organic pollutants,

particularly substituted phenols, was found to occur readily in natural waters but not in pure water (Zafiriou *et. al.*, 1985). The ability of CDOM to act as the sensitizer to initiate this degradation reaction is well documented in the literature (Zepp *et. al.*, 1981a,b; Canonica, 2007; Guerard *et. al.*, 2009; Halladja *et. al.* 2007).

Early reports identified reactive oxygen species (ROS) such as singlet dioxygen ( $^1\text{O}_2$ ), hydroxyl radical ( $\bullet\text{OH}$ ) or peroxy radicals ( $\text{RO}_2$ ) which are photoproduced upon irradiation of CDOM, as the intermediates initiating oxidation. However, more recent studies strongly implicate triplet excited states of carbonyl moieties within CDOM in this process. Canonica (1995a) reported evidence of a strong correlation between CDOM and aromatic ketones (as model sensitizers) in the photochemical sensitization of phenols and phenylurea herbicides (Gerecke, 2009; Canonica, 2006). This research suggested a direct oxidation mechanism between phenols and triplet excited states of CDOM but did not preclude the involvement of long-lived species such as peroxy radicals. Further, other researchers observed an increase in CDOM-mediated sensitization of trimethylphenol (TMP) (Golanoski, *et. al.*, 2012), monuron (Vialaton *et. al.*, 1997), bisphenol-A (Zhan *et. al.* 2006; Chin *et. al.*, 2004) and sulfa drugs (Boreen *et. al.*, 2005) upon deoxygenation, consistent with a triplet mechanism but not one dominated by ROS. The question remains whether the general mechanism of phenol photooxidation proceeds predominantly by direct reaction with triplet excited states or by photogenerated reactive oxygen species.

Substituted phenols are easily oxidizable compounds and are expected to react with a variety of photooxidants in natural waters, making them excellent candidates to probe the photochemical properties of CDOM. By utilizing a series of phenols with



varying one-electron reduction potentials, the nature of the photooxidants produced by irradiated CDOM may be better characterized. Substituted phenols with the lowest one-electron oxidation potential have more electron donating character and thus are expected to have enhanced reactivity with the oxidant. The one-electron reduction potentials are defined for the phenolate ion ( $\text{PhO}^-$ ) and phenoxy radical ( $\text{PhO}^\bullet$ ) versus a normal hydrogen electrode (NHE) and were selected for comparison to results published by Canonica (1995b).

Alkyl phenols such as 2,4,6-trimethylphenol (TMP) and 4-methylphenol (4-MP) have been reported to be best-suited for reaction with short-lived species such as triplet excited states of CDOM whereas long-lived photooxidants such as peroxy radicals have been suggested as more easily detected using alkoxy-type phenols such as 3,4-dimethoxyphenol (DMOP) or 4-methoxyphenol (4-MOP) (Cannonica, 1995a,b). Although phenolate ions have been reported to undergo facile reaction with  $^1\text{O}_2$  ( $k_{\text{ArO}^-} \approx 1 \times 10^8$ ) (Tratnyek, et. al., 1991), this reaction pathway is unimportant for non-dissociated phenols that predominate under the environmental relevant conditions employed in this study.

For these reasons, DMOP, TMP, 4-MOP, 4-MP and phenol were employed to examine the dependence of the initial rate of phenol probe loss ( $R_{\text{probe}}$ ) on [phenol] and/or  $[\text{O}_2]$  for both untreated and borohydride-reduced Suwanee River Fulvic Acid (SRFA). We find that the decrease in  $R_{\text{probe}}$  following borohydride-reduction for all samples supports the role of triplet excited states in the oxidation of the substituted phenols evaluated in this study. However, evidence supporting the role of a pathway separate from triplets was observed for DMOP, namely: 1) lower than expected values of  $R_{\text{probe}}$

for DMOP and 4-MOP at low  $[O_2]$  2) markedly high values of  $R_{\text{probe}}$  for DMOP at high  $[O_2]$  where quenching of triplets by dioxygen is expected to dominate and 3) Values of  $\Phi$  for DMOP fall outside the inverse, linear dependence of  $\Phi$  on one-electron reduction potentials where  $DMOP \approx TMP > 4-MOP > 4-MP > \text{phenol}$ .

## **4.2 Materials and Methods**

### **4.2.1 Materials**

All chemicals were used as received and were of the highest purity available unless otherwise noted. Analytical grade 2,4,6-trimethylphenol (TMP) was obtained from Fluka, 3,4-dimethoxyphenol (DMOP), 4-methoxyphenol (4-MOP), 4-methylphenol (4-MP) and phenol were obtained from Sigma Aldrich. Suwannee River Fulvic Acid (SRFA) was obtained from the International Humic Substances Society. Water was obtained from a Millipore Milli-Q purification system. Dipotassium hydrogen phosphate ( $K_2HPO_4$ ) was obtained from Sigma Aldrich whereas potassium dihydrogen phosphate ( $KH_2PO_4$ , sodium borohydride ( $NaBH_4$ ) were obtained from Fischer Scientific. Ultra-high purity compressed gases were obtained from Airgas. Potassium hydrogen phthalate (KHP) was obtained from Nacalai Tesque, Inc.

### **4.2.2 Apparatus**

Phenol probe analyses were performed in triplicate using a RP-HPLC system consisting of a Shimadzu LC-20AP pump, 50  $\mu\text{L}$  loop and a Waters RCM 8x10 cartridge which supported a Waters Nova-Pak C18 column (5x100mm, 4  $\mu\text{m}$  pore size). Analyses were performed under isocratic conditions using the appropriate mobile phase

composition for each probe (Table III.1). Probe detection was performed using a Shimadzu LC-AD absorbance detector set to the appropriate detection wavelength for each probe (Table IV.1).

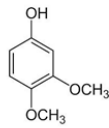
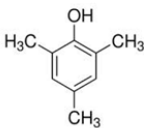
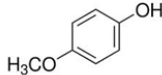
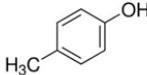

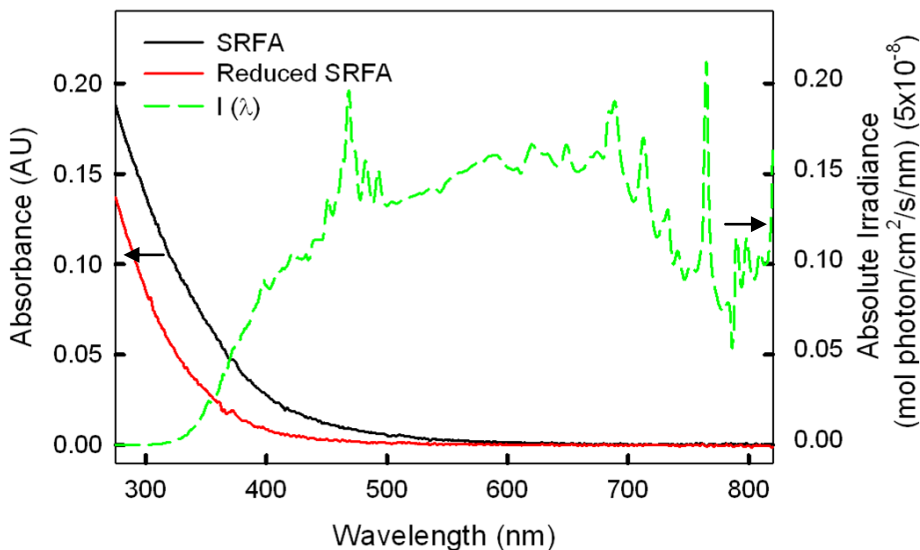
	DMOP	TMP	4-MOP	4-MP	phenol
					
<b>pK<sub>a</sub><sup>a</sup></b>	<b>10.0</b>	<b>10.9</b>	<b>10.5</b>	<b>10.3</b>	<b>10.0</b>
<b>λ<sub>det</sub> (nm)<sup>b</sup></b>	<b>285</b>	<b>280</b>	<b>288</b>	<b>277</b>	<b>270</b>
<b>MP Comp. (% ACN / % H<sub>2</sub>O)</b>	<b>15 / 85</b>	<b>45 / 55</b>	<b>20 / 80</b>	<b>40 / 60</b>	<b>25 / 75</b>
<b>E° (PhO•/PhO<sup>-</sup>) (V)</b>	<b>0.30</b>	<b>0.49</b>	<b>0.54</b>	<b>0.68</b>	<b>0.79</b>

Table VI.1: Structures, values of acid dissociation constant ( $pK_a$ ) ( $a$  = Liptak et. al., 2002), absorbance detector wavelength ( $b$  = Canonica and Frieburghaus, 2001), mobile phase composition employed in this study and one-electron reduction potential ( $E^\circ$ ) ( $c$  = Lind et. al., 1990; Jonsson et. al., 1993). The potential for DMOP was roughly estimated according to its reactivity with excited triplet states ( $d$  = Canonica et. al., 1995).

Samples were irradiated in a 1 cm quartz cuvette using a 300 W high pressure xenon arc lamp following passage through 8 cm of water to remove infrared radiation and a longpass wavelength filter (50% transmission at 325 nm) to simulate the solar spectrum. The spectral output of the lamp was measured using an Ocean Optics USB2000 spectroradiometer and is provided in Fig. IV.1. Ultraviolet/visible absorption measurements employed a Shimadzu 2401-PC dual beam spectrophotometer. Spectra were collected versus air over the range 190-820 nm and corrected by subtraction of a

Milli-Q water spectrum. Total organic carbon (TOC) was determined using high-temperature oxidation (680°C) on a Shimadzu 5000A TOC analyzer calibrated with KHP.



*Figure IV.1: Absorbance spectra of untreated (black trace) and borohydride-reduced (red trace) SRFA at  $10 \text{ mg L}^{-1}$  in PB at  $\text{pH}=7.0$ . Overlaid is the spectral irradiance profile of the xenon arc lamp with a 325 nm long pass wavelength filter employed in this study (green trace).*

#### 4.2.3 Photochemical Experiments

Stock solutions of  $1000 \text{ mg L}^{-1}$  SRFA and  $500 \text{ }\mu\text{M}$  3,4-DMOP, TMP, 4-MOP, 4-MP and phenol were prepared in Milli-Q water where a small volume of acetonitrile (<5% v/v) was employed to increase the solubility of some phenol solutions. All stock solutions and samples were stored in the dark at  $4^\circ\text{C}$  when not in use. Just prior to irradiation, final solutions containing untreated or borohydride reduced (see below) SRFA ( $10 \text{ mg L}^{-1}$ ) and probe ( $10\text{-}250 \text{ }\mu\text{M}$ ) were prepared in  $10 \text{ mM}$  phosphate buffer at

pH=7 (PB). Control samples contained probe alone in PB. Samples were transferred to a 1 cm quartz cuvette and were irradiated for 15 minutes under differing dioxygen concentrations achieved through mixing ultra-high purity (UHP) nitrogen, dioxygen or air in a dual flow rotameter. Aerated solutions were kept open to the atmosphere, whereas analyses performed under controlled dioxygen conditions were sparged for 5 minutes prior to irradiation followed by flushing of the headspace of a closed vial during irradiation. Quantification of each probe was performed using RP-HPLC at 5 minute intervals during the 15 minute irradiation in which the probe decreased linearly. The direct photochemical loss of each probe was negligible (<5%) over this time period.

Estimated (polychromatic) apparent quantum efficiencies ( $\Phi$ ) of probe loss for untreated and borohydride-reduced samples were calculated using equation IV.1,

$$\Phi = R_{\text{probe}} / R_{\text{EX}} \quad (\text{IV.1})$$

where  $R_{\text{probe}}$  is the initial rate of probe loss at 100  $\mu\text{M}$  probe concentration and 250  $\mu\text{M}$   $\text{O}_2$  (air-saturated) and  $R_{\text{EX}}$  is the rate of light excitation given by equation IV.2,

$$R_{\text{EX}} = I(\lambda) \cdot a(\lambda) = \int_{190}^{820} R(\lambda) d\lambda \quad (\text{IV.2})$$

where  $I(\lambda)$  is the spectral photon irradiance at the front face of the cuvette as measured with an Ocean Optics spectroradiometer and  $a(\lambda)$  is the absorbance coefficient of the sample and  $R(\lambda)$  gives the spectral dependence of the light excitation (see Fig. IV.2).

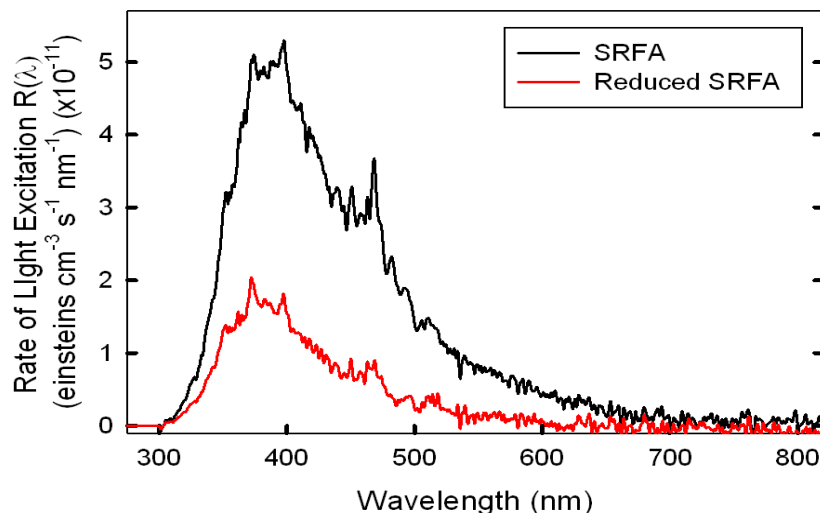


Figure IV.2: Wavelength dependence of the rate of light excitation ( $R(\lambda) = a(\lambda) \cdot I(\lambda)$ ) for untreated (black trace) and borohydride reduced (red trace) SRFA.

#### 4.2.4 Sodium Borohydride ( $\text{NaBH}_4$ ) Reduction

Sodium borohydride ( $\text{NaBH}_4$ ) was employed to reduced SRFA as previously reported (Tinnacher and Honeyman, 2007; Ma *et. al.*, 2010; Golanoski *et. al.*, 2012). Briefly, 4 milliliters (mL) of a 1000 mg  $\text{L}^{-1}$  solution of SRFA was transferred to a 1 cm quartz cuvette and purged with UHP nitrogen for 15 minutes to exclude dioxygen. A fifty-fold excess by weight of  $\text{NaBH}_4$  was added and the sample was immediately placed under nitrogen purge. The reduction was considered to be complete when no further changes in the optical properties were observed, usually after 24 hours. The borohydride-reduced sample was passed over a 2.5 x 8 cm Sephadex G-10 (40 - 120  $\mu\text{m}$ ) column equilibrated with Milli-Q water to remove excess borate and borohydride and adjust the pH to neutral. Note that upon re-introduction of dioxygen, any quinones previously reduced to hydroquinones by borohydride under anaerobic conditions are expected to be re-oxidized to quinones within 24 hours (Tinnacher and Honeyman, 2007; Ma *et. al.*, 2010, Aeschbacher *et. al.*, 2010) and thus would not be removed by this procedure.

## 4.3 Results and Discussion

### 4.3.1 Dependence of $R_{\text{probe}}$ on [probe] and $\text{NaBH}_4$ reduction of SRFA

The dependence of the initial rate of phenol probe loss ( $R_{\text{probe}}$ ) on [phenol] was determined for DMOP, TMP, 4-MOP, 4-MP and phenol with untreated and borohydride-reduced SRFA (Fig. IV.3).

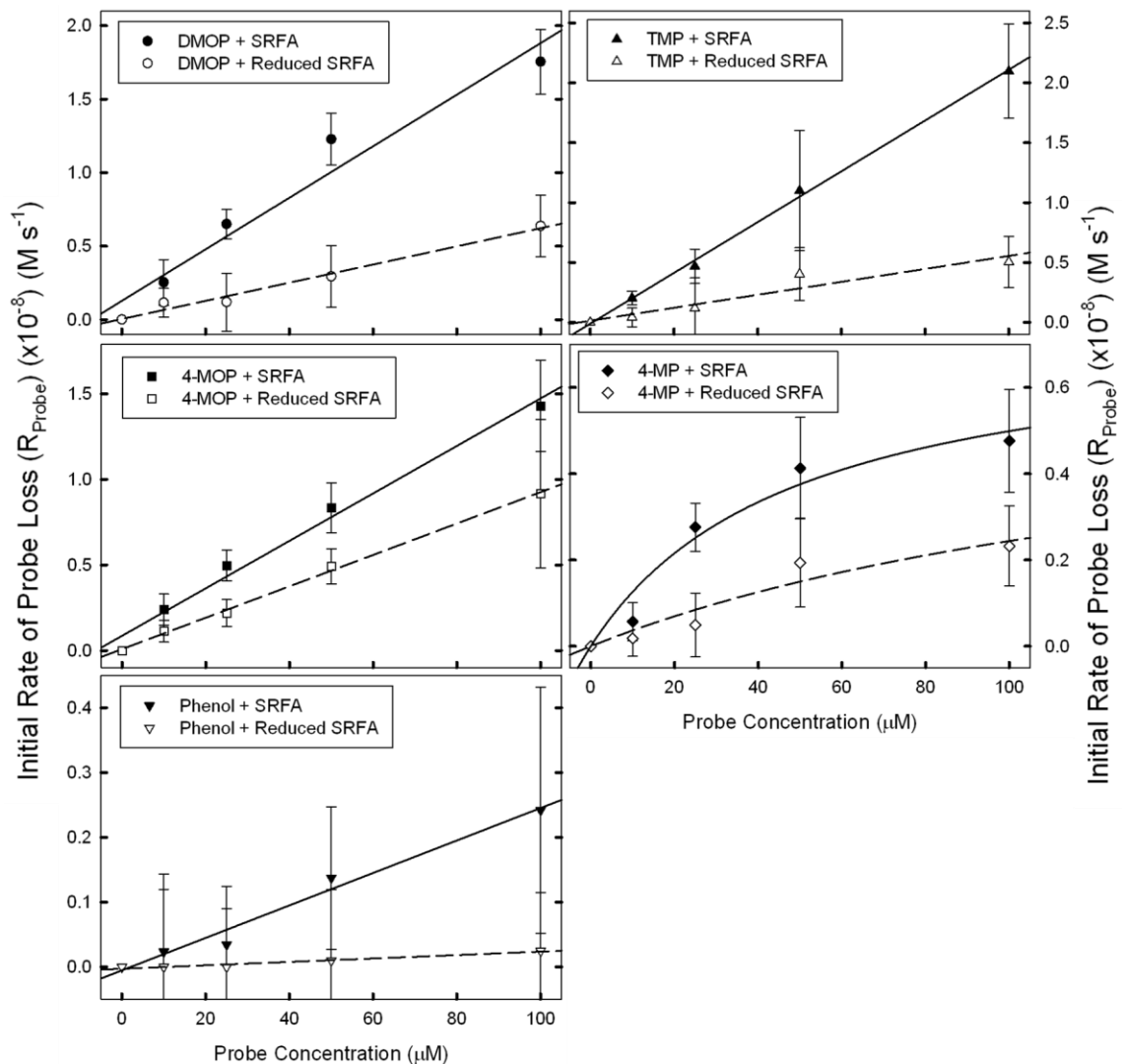


Figure IV.3: Dependence of the initial rate of probe loss ( $R_{\text{probe}}$ ) on [probe] for both untreated or borohydride-reduced SRFA at  $10 \text{ mg L}^{-1}$  in  $10 \text{ mM PB}$  under aerated

conditions (250  $\mu\text{M}$   $\text{O}_2$ ). Error bars represent  $\pm 1$  standard deviation of at least three independent determinations.

Except for 4-MP where curvature was observed,  $R_{\text{probe}}$  increased linearly from 10 to 100  $\mu\text{M}$  (Fig. IV.3) for all probe phenols in the presence of untreated SRFA under aerated conditions (250  $\mu\text{M}$   $\text{O}_2$ ).

A closer examination of the phenol and 4-MP data reveals only a 6 – 9% loss of initial phenol or 4-MP concentration over the course of a 15 minute irradiation. Typically, a  $\geq 20\%$  decrease in initial probe concentration over the course of the irradiation is desired to obtain reliable initial rate data, which was readily attained for DMOP, TMP and 4-MOP at the concentrations employed in this study under aerated conditions. Although a linear increase in  $R_{\text{probe}}$  was observed for phenol, the small ( $\leq 5\%$ ) loss of initial concentration led to initial rates which approached the limit of detection and large error with respect to  $R_{\text{probe}}$ , making the determination of a trend difficult.

Nevertheless, at 100  $\mu\text{M}$  probe,  $R_{\text{probe}}$  increased with decreasing oxidation potential of the probes in the order: phenol < 4-MP < 4-MOP < DMOP < TMP (Figure IV.3, Table IV.2). This result is inconsistent with prior results (Canonica *et. al.*, 1995) where the rate constant for reaction of DMOP with SRFA was two-fold larger than for TMP when [probe] = 5  $\mu\text{M}$  under aerated conditions. Examination of  $R_{\text{probe}}$  for DMOP and TMP at concentrations  $\leq 25$   $\mu\text{M}$  is consistent with the trend reported by Canonica where  $R_{\text{probe}}$  increased in the order: phenol < 4-MP < 4-MOP < TMP < DMOP. One explanation for the differences observed is that  $R_{\text{probe}}$  for DMOP appears to be suppressed at high DMOP concentrations. .



Samples containing borohydride reduced SRFA also increased linearly with probe concentration. However, compared to untreated samples  $R_{\text{probe}}$  was decreased by 35-75% for all probes (with the smallest decrease observed for 4-MOP and the largest for TMP) except phenol for which  $R_{\text{probe}}$  became undetectable. Excluding 4-MP and phenol (because of very low signal) inhibition followed the order  $\text{TMP} > \text{DMOP} > \text{4-MOP}$  suggesting that more easily oxidized phenols are more substantially inhibited by borohydride. The loss of UV and visible absorbance (Figure IV.1) and decrease in  $R_{\text{probe}}$  upon borohydride reduction of SRFA is consistent with prior results which attribute these changes to the reduction of aromatic ketone and aldehyde moieties within SRFA to their corresponding alcohols (Golanoski *et. al.*, 2012).

[DMOP] ( $\mu\text{M}$ )	$R_{\text{DMOP, SRFA}}$ ( $\times 10^{-8}$ ) ( $\text{M s}^{-1}$ )	$R_{\text{DMOP, Reduced SRFA}}$ ( $\times 10^{-8}$ ) ( $\text{M s}^{-1}$ )	[TMP] ( $\mu\text{M}$ )	$R_{\text{TMP, SRFA}}$ ( $\times 10^{-8}$ ) ( $\text{M s}^{-1}$ )	$R_{\text{TMP, Reduced SRFA}}$ ( $\times 10^{-8}$ ) ( $\text{M s}^{-1}$ )
10	$0.25 \pm 0.16$	$0.12 \pm 0.10$	10	$0.20 \pm 0.04$	$0.04 \pm 0.13$
25	$0.65 \pm 0.10$	$0.12 \pm 0.20$	25	$0.47 \pm 0.06$	$0.12 \pm 0.08$
50	$1.2 \pm 0.2$	$0.30 \pm 0.21$	50	$1.1 \pm 0.1$	$0.40 \pm 0.25$
100	$1.8 \pm 0.2$	$0.64 \pm 0.21$	100	$2.1 \pm 0.5$	$0.51 \pm 0.22$
250	$2.1 \pm 0.2$	$0.71 \pm 0.17$	250	$3.3 \pm 0.4$	$0.62 \pm 0.21$

[4-MOP] ( $\mu\text{M}$ )	$R_{\text{4-MOP, SRFA}}$ ( $\times 10^{-8}$ ) ( $\text{M s}^{-1}$ )	$R_{\text{4-MOP, Reduced SRFA}}$ ( $\times 10^{-8}$ ) ( $\text{M s}^{-1}$ )	[4-MP] ( $\mu\text{M}$ )	$R_{\text{4-MP, SRFA}}$ ( $\times 10^{-8}$ ) ( $\text{M s}^{-1}$ )	$R_{\text{4-MP, Reduced SRFA}}$ ( $\times 10^{-8}$ ) ( $\text{M s}^{-1}$ )
10	$0.24 \pm 0.09$	$0.11 \pm 0.06$	10	$0.06 \pm 0.04$	$0.02 \pm 0.04$
25	$0.49 \pm 0.09$	$0.22 \pm 0.08$	25	$0.10 \pm 0.06$	$0.05 \pm 0.07$
50	$0.83 \pm 0.15$	$0.49 \pm 0.10$	50	$0.41 \pm 0.12$	$0.19 \pm 0.10$
100	$1.4 \pm 0.3$	$0.91 \pm 0.43$	100	$0.48 \pm 0.12$	$0.23 \pm 0.09$
250	$1.9 \pm 0.4$	$1.4 \pm 0.3$	250	$0.73 \pm 1.5$	$0.28 \pm 0.14$

[Phenol] ( $\mu\text{M}$ )	$R_{\text{Phenol, SRFA}}$ ( $\times 10^{-8}$ ) ( $\text{M s}^{-1}$ )	$R_{\text{Phenol, Reduced SRFA}}$ ( $\times 10^{-8}$ ) ( $\text{M s}^{-1}$ )
10	$0.02 \pm 0.12$	ND
25	$0.03 \pm 0.09$	ND
50	$0.13 \pm 0.11$	$0.01 \pm 0.09$
100	$0.24 \pm 0.19$	$0.01 \pm 0.11$
250	$0.25 \pm 0.20$	$0.02 \pm 0.08$

Table IV.2: Values of initial rate of probe loss ( $R_{\text{probe}}$ ) for both untreated and borohydride-reduced SRFA.  $R_{\text{probe}}$  was determined at  $[\text{probe}] = 10 - 250 \mu\text{M}$  and  $\text{O}_2 =$

250  $\mu\text{M}$ . Error bars represent  $\pm 1$  standard deviation of at least three independent determinations. ND = not detected.

Further evidence for the involvement of triplet excited states in the loss of TMP was provided by the dependence of  $R_{\text{TMP}}$  on  $[\text{TMP}]$  at low (22  $\mu\text{M}$ ) and aerated (250  $\mu\text{M}$ )  $\text{O}_2$  (Figure IV.4, middle panel).

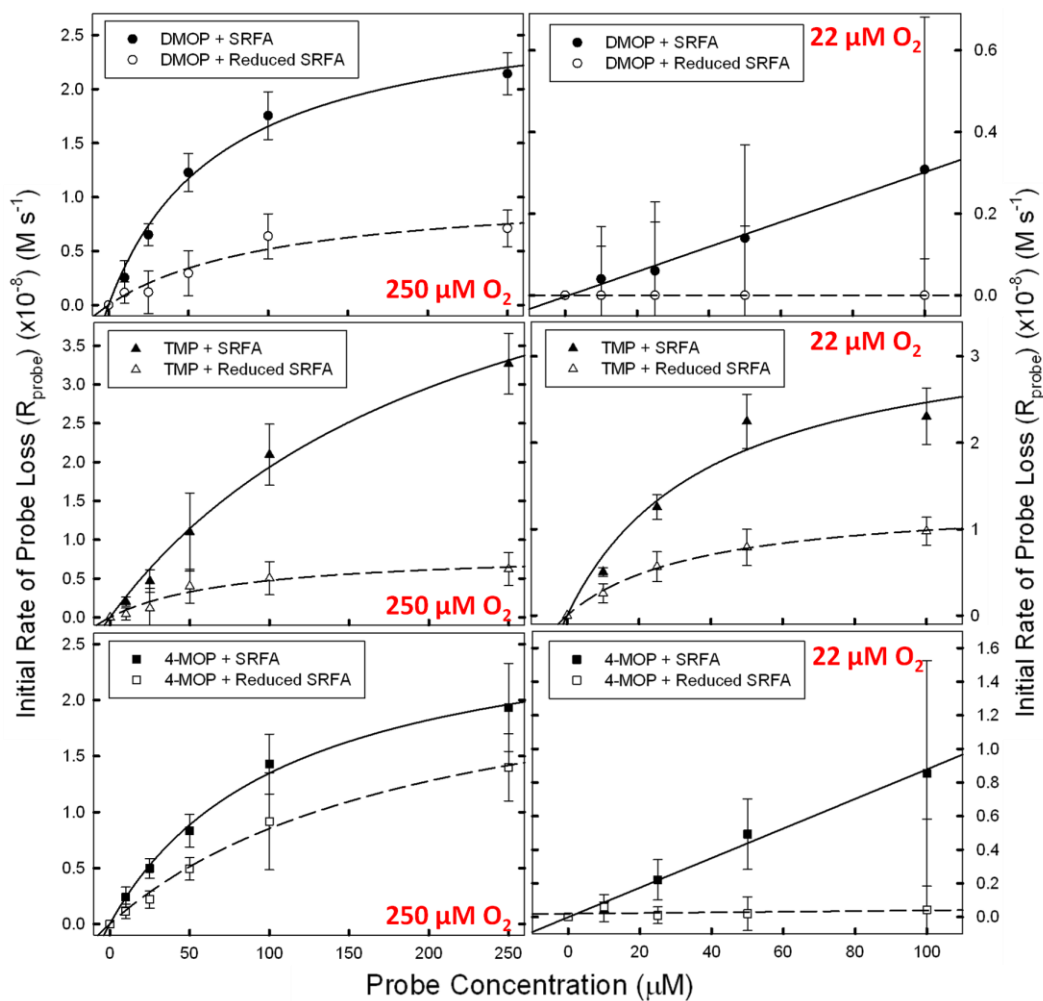


Figure IV.4: Dependence of  $R_{\text{probe}}$  on  $[\text{probe}]$  for both untreated and borohydride-reduced SRFA at high (250  $\mu\text{M}$ ) and low (22  $\mu\text{M}$ )  $[\text{O}_2]$ . The data were fit to the equation  $R_{\text{probe}} = a \cdot [\text{Probe}] / (b + \text{Probe})$  using a non-linear least squares fitting routine except

*under low [O<sub>2</sub>] for DMOP and 4-MOP for which a linear least squares fitting routine was employed.*

At 22  $\mu\text{M}$  [O<sub>2</sub>], where triplet state quenching by O<sub>2</sub> would be greatly reduced, R<sub>TMP</sub> showed evidence of saturation at [TMP]  $\leq$  100  $\mu\text{M}$  (Figure IV.4, right panel) for both untreated and borohydride-reduced samples whereas saturation occurred at [TMP]  $\geq$  100  $\mu\text{M}$  under aerated conditions (Figure IV.4, left panel). Values of half-saturation of the initial rate (b) occurred for TMP at low and high [O<sub>2</sub>] at 40 and 230  $\mu\text{M}$  TMP, respectively (Table IV.3). This result is consistent with a competition between TMP and O<sub>2</sub> for a common intermediate such as a triplet. This work was extended to DMOP and 4-MOP where half-saturation of the initial rate (b) occurred under aerated conditions at  $\approx$  70 and 110  $\mu\text{M}$ , respectively (Table IV.3) however no saturation of the initial rate was observed under 22  $\mu\text{M}$  O<sub>2</sub> conditions (Figure IV.4, right panel) where markedly lower values of R<sub>probe</sub> were observed. This result, namely for DMOP, suggests that a separate pathway at low [O<sub>2</sub>] may be important for this substituted phenol. Upon borohydride-reduction, R<sub>probe</sub> became undetectable for DMOP and 4-MOP whereas for TMP R<sub>probe</sub> was decreased by 50-97% under low and high [O<sub>2</sub>], respectively.

Probe	HS	a ( $\times 10^{-8}$ ) (M s <sup>-1</sup> )	b ( $\mu$ M)	R <sup>2</sup>
3,4-DMOP	SRFA	2.8 $\pm$ 0.2	71 $\pm$ 12	0.99
	Reduced SRFA	1.1 $\pm$ 0.2	108 $\pm$ 53	0.97
TMP	SRFA	6.3 $\pm$ 0.8	230 $\pm$ 51	0.99
	Reduced SRFA	0.86 $\pm$ 0.16	81 $\pm$ 35	0.97
4-MOP	SRFA	2.8 $\pm$ 0.1	110 $\pm$ 13	0.99
	Reduced SRFA	2.6 $\pm$ 0.9	198 $\pm$ 39	0.99

250  $\mu$ M [O<sub>2</sub>]; 0 - 250  $\mu$ M [Probe]

Probe	HS	a ( $\times 10^{-8}$ ) (M s <sup>-1</sup> )	b ( $\mu$ M)	R <sup>2</sup>
TMP	SRFA	3.5 $\pm$ 0.7	40 $\pm$ 19	0.98
	Reduced SRFA	1.3 $\pm$ 0.1	37 $\pm$ 4	0.99

22  $\mu$ M [O<sub>2</sub>]; 0 - 100  $\mu$ M [Probe]

Table IV.3: Values of half-saturation rate (a) and maximal rate (b) from data in Figure IV.4 where the data were fit to the equation  $R_{probe} = a \cdot [Probe] / (b + [Probe])$ .

#### 4.3.2 Dependence of R<sub>probe</sub> on [O<sub>2</sub>] for untreated and borohydride-reduced SRFA

The dependence of R<sub>probe</sub> on [O<sub>2</sub>] for both untreated and borohydride-reduced SRFA was determined for DMOP, TMP and 4-MOP (Fig. IV.5).

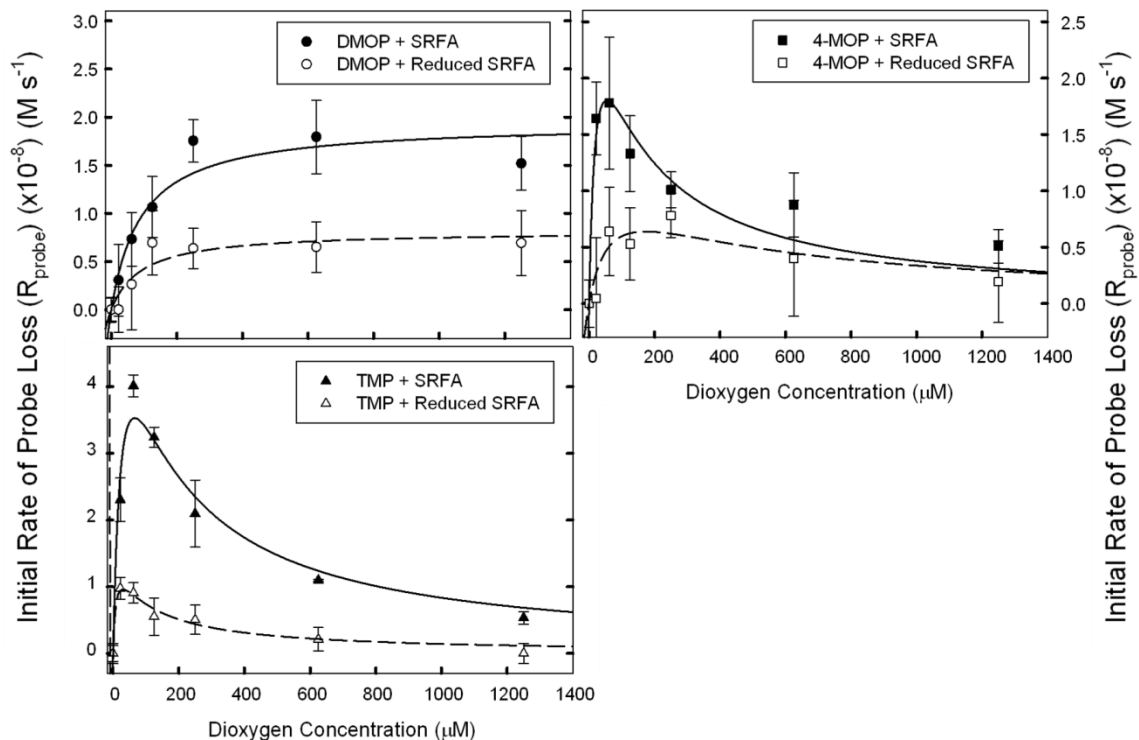


Figure IV.5: Dependence of  $R_{probe}$  on  $[O_2]$  at a fixed  $[probe] = 100 \mu M$  for DMOP and TMP and  $50 \mu M$  for 4-MOP in the presence of untreated or borohydride-reduced SRFA. Data were fit to the Eqn. II.12 employing a non-linear least squares fitting routine of  $k_t = 6.64 \times 10^4 s^{-1}$ ,  $k_{TMP} = 2.5 \times 10^9 M^{-1} s^{-1}$  and  $k_Q = 2.0 \times 10^9 M^{-1} s^{-1}$  were utilized in the fitting.

$R_{probe}$  was determined at  $100 \mu M$  for DMOP and TMP and at  $50 \mu M$  for 4-MOP where the irradiation data for 4-MOP was restricted to the first ten minutes of irradiation to improve the fit of the data (Fig. IV.6).

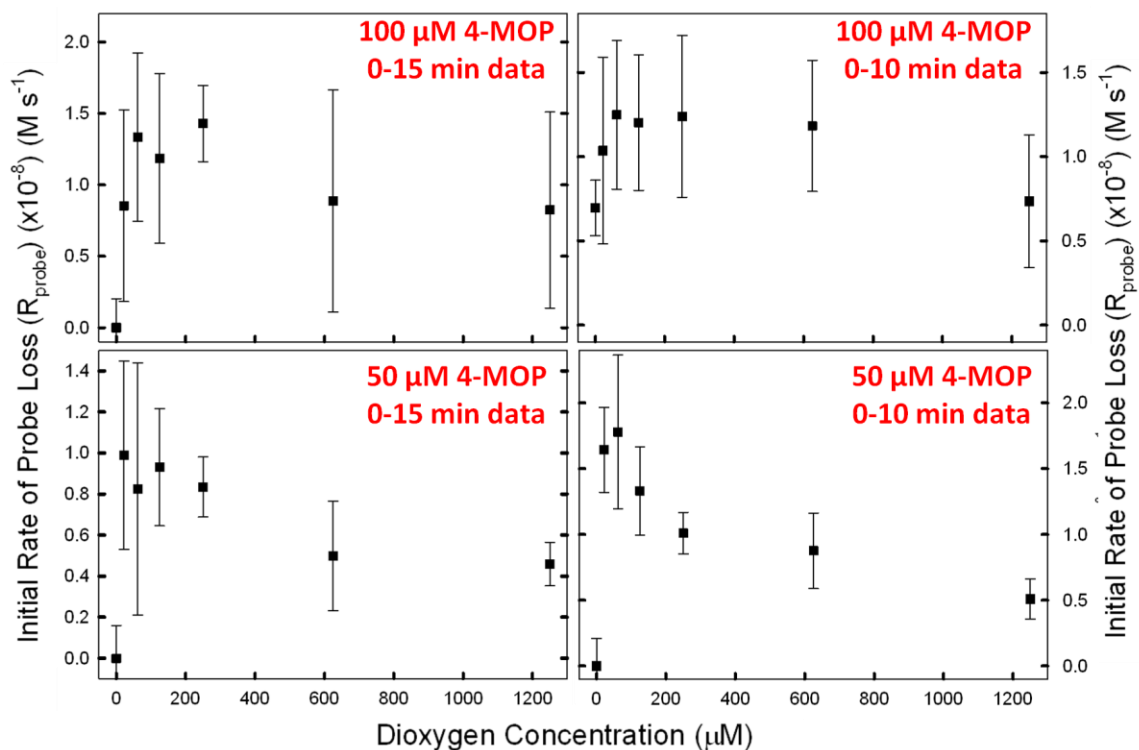


Figure III.6: Dependence of  $R_{probe}$  on  $[O_2]$  for 100  $\mu M$  and 50  $\mu M$  4-MOP (top and bottom panels, respectively) employing data from 15 minutes of irradiation (left panel) compared to restricting the analysis to the first 10 minutes of irradiation data (right panel).

For DMOP,  $R_{probe}$  increased with increasing  $[O_2]$  over the range 0 – 250  $\mu M$  followed by a saturation in the initial rate with increasing  $[O_2]$  to 1.2 mM. For TMP and 4-MOP,  $R_{probe}$  decreases with increasing  $[O_2]$  for 50  $\mu M$  to 1.2 mM, however below 50  $\mu M$   $O_2$ ,  $R_{probe}$  decreases rapidly becoming undetectable under anaerobic conditions. For samples with borohydride-reduced SRFA,  $R_{probe}$  was decreased by 58-72% yet exhibited a similar dependence to untreated SRFA, indicating that the remaining sensitization also arises from a similar pool of intermediates.

For DMOP, the high  $R_{\text{probe}}$  observed at high  $[\text{O}_2]$  and fixed  $[\text{DMOP}]$  in addition to the substantial remaining sensitization following borohydride-reduction indicates that a pathway separate from triplets may be important to the mechanism of photooxidation of this substituted phenol.

The dependence of  $R_{\text{TMP}}$  on  $[\text{O}_2]$  was previously modeled as a competition between triplet state reaction with TMP at low  $[\text{O}_2]$  and triplet state quenching by  $\text{O}_2$  at high  $[\text{O}_2]$  leading to an expression that relates the initial rate of TMP loss to  $[\text{TMP}]$  and  $[\text{O}_2]$  (see Chapter II, section 2.3.4).

$$R_{\text{TMP}} = \left( -\frac{d[\text{TMP}]}{dt} \right)_0 = \left( \frac{\phi \bar{k}_f \bar{k}_{\text{TMP}} [\text{TMP}]}{\bar{k}_t + \bar{k}_{\text{TMP}} [\text{TMP}] + \bar{k}_Q [\text{O}_2]} \right) \cdot \left( 1 - \frac{1}{1 + (\bar{k}_{\text{RXN}}/\bar{k}_{\text{REC}}) [\text{O}_2]} \right) \quad (\text{IV.4})$$

where  $\phi$  is the branching ratio of chemical to physical quenching of the triplet and  $\bar{k}_{\text{TMP}} =$  is the sum of these processes,  $\bar{k}_f$  is the rate constant for triplet formation,  $\bar{k}_t$  is the rate constant for radiationless transition to the ground state and  $\bar{k}_{\text{RXN}}/\bar{k}_{\text{REC}}$  is the ratio of further reaction of the radical species  $\bullet\text{CH}$  and  $\bullet\text{TMP}_{(-\text{H})}$  to form products to that of recombination. Estimated values of  $\bar{k}_t$  and  $\bar{k}_{\text{TMP}}$  were obtained as described in Chapter II, Section 2.3.4. Briefly, the data for TMP in Figure IV.4 were fit using a non-linear least squares routine to the equation  $y = a \cdot x / (b+x)$ , where  $y = R_{\text{TMP}}$ ,  $a = \phi \cdot \bar{k}_f$ ,  $x = [\text{TMP}]$  and  $b = (\bar{k}_t + \bar{k}_Q [\text{O}_2]) / \bar{k}_{\text{TMP}}$ . The values of  $b$  (half-saturation) obtained at high and low  $[\text{O}_2]$  were utilized along with their respective  $[\text{O}_2]$  and a fixed value of  $\bar{k}_Q = 2.0 \times 10^9 \text{ M}^{-1} \text{ s}^{-1}$  (Zepp et. al., 1985; Paul et. al., 2004; Muvrov et. al., 1993) to calculate  $\bar{k}_t$  and  $\bar{k}_{\text{TMP}}$  for both untreated and borohydride-reduced SRFA. As no saturation in  $R_{\text{probe}}$  was

observed under low  $[O_2]$  for DMOP and 4-MOP,  $b$  values were not obtained and thus rate constant for reaction of DMOP or 4-MOP with untreated or borohydride-reduced SRFA could not be determined.

### 4.3.3 Apparent polychromatic quantum yields

Apparent (polychromatic) quantum yields ( $\Phi$ ) were calculated for all phenols at 100 and 250  $\mu M$  under 250  $\mu M$   $[O_2]$  for untreated and borohydride-reduced SRFA (Table IV.4).

		SRFA			Reduced SRFA		
		$R_{probe}$ ( $\times 10^{-8}$ ) (M s $^{-1}$ )	$R_{EX}$ ( $\times 10^{-7}$ ) (M s $^{-1}$ )	$\Phi$ (%)	$R_{probe}$ ( $\times 10^{-8}$ ) (M s $^{-1}$ )	$R_{EX}$ ( $\times 10^{-7}$ ) (M s $^{-1}$ )	$\Phi$ (%)
DMOP ( $\mu M$ )	100	$1.8 \pm 0.2$	$6.9 \pm 0.1$	$2.6 \pm 0.3$	$0.64 \pm 0.21$	$1.9 \pm 0.1$	$3.4 \pm 1.1$
	250	$2.1 \pm 0.2$	$6.9 \pm 0.1$	$3.1 \pm 0.3$	$0.71 \pm 0.17$	$1.9 \pm 0.1$	$3.8 \pm 0.9$
TMP ( $\mu M$ )	100	$2.1 \pm 0.5$	$6.9 \pm 0.1$	$3.0 \pm 0.7$	$0.51 \pm 0.22$	$1.9 \pm 0.1$	$2.7 \pm 1.2$
	250	$3.3 \pm 0.4$	$6.9 \pm 0.1$	$4.8 \pm 0.6$	$0.62 \pm 0.21$	$1.9 \pm 0.1$	$3.3 \pm 1.1$
4-MOP ( $\mu M$ )	100	$1.4 \pm 0.3$	$6.9 \pm 0.1$	$2.0 \pm 0.4$	$0.91 \pm 0.43$	$1.9 \pm 0.1$	$4.9 \pm 2.3$
	250	$1.9 \pm 0.4$	$6.9 \pm 0.1$	$2.8 \pm 0.6$	$1.4 \pm 0.3$	$1.9 \pm 0.1$	$7.5 \pm 1.6$
4-MP ( $\mu M$ )	100	$0.48 \pm 0.12$	$6.9 \pm 0.1$	$0.7 \pm 0.2$	$0.23 \pm 0.09$	$1.9 \pm 0.1$	$1.2 \pm 0.5$
	250	$0.73 \pm 1.5$	$6.9 \pm 0.1$	$1.1 \pm 2.2$	$0.28 \pm 0.14$	$1.9 \pm 0.1$	$1.5 \pm 0.8$
Phenol ( $\mu M$ )	100	$0.24 \pm 0.19$	$6.9 \pm 0.1$	$0.35 \pm 0.28$	$0.01 \pm 0.11$	$1.9 \pm 0.1$	$0.05 \pm 0.59$
	250	$0.25 \pm 0.20$	$6.9 \pm 0.1$	$0.36 \pm 0.29$	$0.02 \pm 0.08$	$1.9 \pm 0.1$	$0.11 \pm 0.43$

Table IV.4: Values of initial rate of probe loss ( $R_{probe}$ ), rate of light excitation ( $R_{EX}$ ) and apparent polychromatic quantum yield ( $\Phi$ ) for  $[probe] = 100$  and  $250 \mu M$  and untreated or borohydride-reduced SRFA at  $10 \text{ mg L}^{-1}$  under  $[O_2] = 250 \mu M$ .

Values of  $\Phi$  ranged from 0.35 to 3.0 % for untreated SRFA and 0.5 to 4.9 % for borohydride-reduced SRFA for  $[probe] = 100 \mu M$  (Table IV.4). For  $[probe] = 250 \mu M$ ,



where quantitative reaction between the probe and intermediate was attained, values of  $\Phi$  remained the same or exhibited a small increase for all phenols and untreated and borohydride-reduced SRFA. Overall, these efficiencies are similar in magnitude to apparent quantum yields for  $^1\text{O}_2$  production for a variety of humic substances (Aguer and Richard, 1996; Sandvik, et. al., 2000; Zepp et. al., 1985; Paul et. al., 2004). At both probe concentrations employed, no change in  $\Phi$ , within the error of the measurement, was observed for borohydride reduced SRFA compared to untreated SRFA.

In order to make a comparison among samples, values of  $\Phi$  for [probe] = 100  $\mu\text{M}$  and  $[\text{O}_2]$  = 250  $\mu\text{M}$  were plotted against their corresponding one-electron reduction potential of the probe phenol employed (Table IV.1, Figure IV.7).

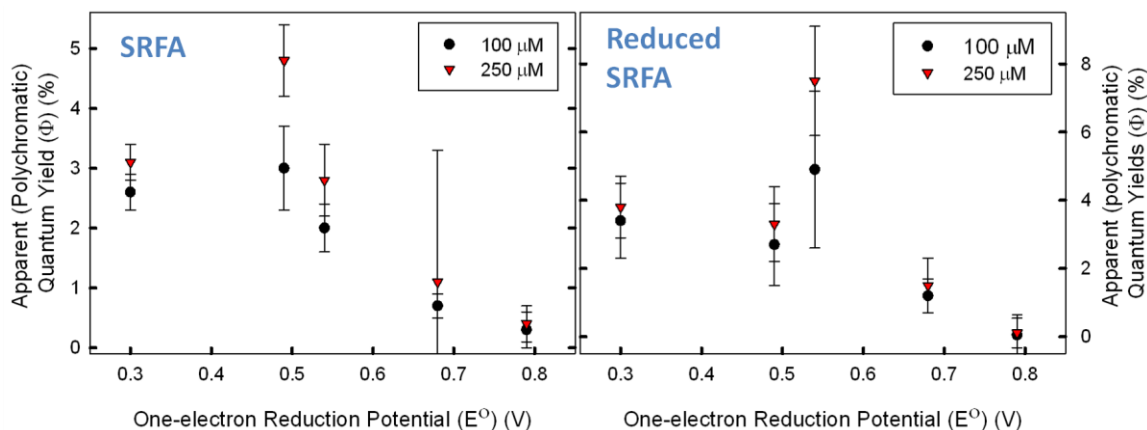


Figure IV.7: Values of apparent polychromatic quantum yields ( $\Phi$ ) for 100  $\mu\text{M}$  and 250  $\mu\text{M}$  DMOP, TMP, 4-MOP, 4-MP and phenol with untreated and borohydride-reduced SRFA under aerated conditions.

For untreated SRFA at [probe] = 100 and 250  $\mu\text{M}$ , values of  $\Phi$  for DMOP (0.30 V) were equivalent or slightly lower than TMP (0.49 V) followed by a linear decrease in values with increasing one-electron reduction potential for 4-MOP (0.54 V), 4-MP (0.68 V) and phenol (0.79 V) (Figure IV.7, left panel).

For borohydride-reduced SRFA at  $[\text{probe}] = 100$  and  $250 \mu\text{M}$ ,  $\Phi$  decreased linearly with increasing one-electron reduction potential except for 4-MOP which exhibited the largest value of  $\Phi$  for all phenols with borohydride-reduced SRFA (Figure IV.7, right panel). This result indicates that triplet excited states of aromatic ketones/aldehydes may not be as important to the mechanism of degradation for DMOP as for other phenol probes.

In conclusion, the decrease in  $R_{\text{probe}}$  following borohydride-reduction for all samples supports the role of triplet excited states in the oxidation of the substituted phenols evaluated in this study. However, evidence supporting the role of a pathway separate from triplets was observed for DMOP, namely: 1) lower than expected values of  $R_{\text{probe}}$  for DMOP and 4-MOP at low  $[\text{O}_2]$  2) markedly high values of  $R_{\text{probe}}$  for DMOP at high  $[\text{O}_2]$  where quenching of triplets by dioxygen is expected to dominate and 3) Values of  $\Phi$  for DMOP fall outside the inverse, linear dependence of  $\Phi$  on one-electron reduction potentials where  $\text{DMOP} \approx \text{TMP} > 4\text{-MOP} > 4\text{-MP} > \text{phenol}$ .

## Chapter V: Summary and Future Work

### 5.1 Summary

It is well established that organic pollutants such as phenols are degraded in the presence of chromophoric dissolved organic matter (CDOM) and sunlight in natural waters. Early work attributed this reaction to the involvement of reactive oxygen species (ROS) such as singlet oxygen ( $^1\text{O}_2$ ), hydroxyl radical ( $\bullet\text{OH}$ ) or peroxy radicals ( $\text{RO}_2\bullet$ ). However, evidence for the involvement of triplet excited states of aromatic ketones and aldehydes and not for ROS has accumulated in the literature.

To probe the mechanism of the photosensitized loss of phenols by humic substances (HS), the dependence of the initial rate of 2,4,6-trimethylphenol (TMP) loss ( $R_{\text{TMP}}$ ) on dioxygen concentration was examined both for a variety of untreated as well as borohydride-reduced HS and  $\text{C}_{18}$  extracts from the Delaware Bay and Mid-Atlantic Bight.  $R_{\text{TMP}}$  was inversely proportional to dioxygen concentration at  $[\text{O}_2] > 50 \mu\text{M}$ , a dependence consistent with reaction with triplet excited states, but not with  $^1\text{O}_2$  or  $\text{RO}_2$ . Modeling the dependence of  $R_{\text{TMP}}$  on  $[\text{O}_2]$  provided rate constants for TMP reaction,  $\text{O}_2$  quenching and lifetimes compatible with a triplet intermediate. Borohydride reduction significantly reduced TMP loss, supporting the role of aromatic ketone triplets in this process. However, for most samples, the incomplete loss of sensitization following borohydride reduction, as well as the inverse dependence of  $R_{\text{TMP}}$  on  $[\text{O}_2]$  for these samples, suggests that there remains another class of oxidizing triplet sensitizer, perhaps quinones.

To further probe the mechanism of the CDOM-sensitized oxidation of phenols, we examined the spectral dependence of the initial rate of 2,4,6-trimethylphenol loss

( $R_{\text{TMP}}$ ) for untreated and borohydride-reduced SRFA, SRHA, LAC and  $C_{18}$  extracts of the Delaware Bay. We find that 1) increasing the mass excess of borohydride leads to additional losses of absorbance and decreases in  $R_{\text{TMP}}$ , but except for LAC,  $R_{\text{TMP}}$  is never completely eliminated 2) Decreasing  $[O_2]$  increases  $R_{\text{TMP}}$  for both untreated and borohydride-reduced samples by  $\sim 2$  for a four-fold reduction of  $[O_2]$  from 250  $\mu\text{M}$  to 63  $\mu\text{M}$  3)  $R_{\text{TMP}}$  drops off rapidly with increasing  $\lambda$ , far more rapidly than the rate of light excitation ( $R_{\text{EX}}$ ), for both untreated and borohydride-reduced samples indicating that UVB and UVA wavelengths are primarily responsible for the sensitization. Except for SRHA, wavelengths  $> 400$  nm give rise to little or no sensitization which argues against major sensitization by long-wavelength absorbing quinones.

Results of the dependence of initial rate of probe loss ( $R_{\text{probe}}$ ) for untreated and borohydride-reduced SRFA with a series of substituted phenols of varying one-electron reduction potential found that the decrease in  $R_{\text{probe}}$  following borohydride-reduction for all samples supports the role of triplet excited states in the oxidation of the substituted phenols evaluated in this study. However, evidence supporting the role of a pathway separate from triplets was observed for DMOP, namely: 1) lower than expected values of  $R_{\text{probe}}$  for DMOP and 4-MOP at low  $[O_2]$  2) markedly high values of  $R_{\text{probe}}$  for DMOP at high  $[O_2]$  where quenching of triplets by dioxygen is expected to dominate and 3) Values of  $\Phi$  for DMOP fall outside the inverse, linear dependence of  $\Phi$  on one-electron reduction potentials where  $\text{DMOP} \approx \text{TMP} > 4\text{-MOP} > 4\text{-MP} > \text{phenol}$ .

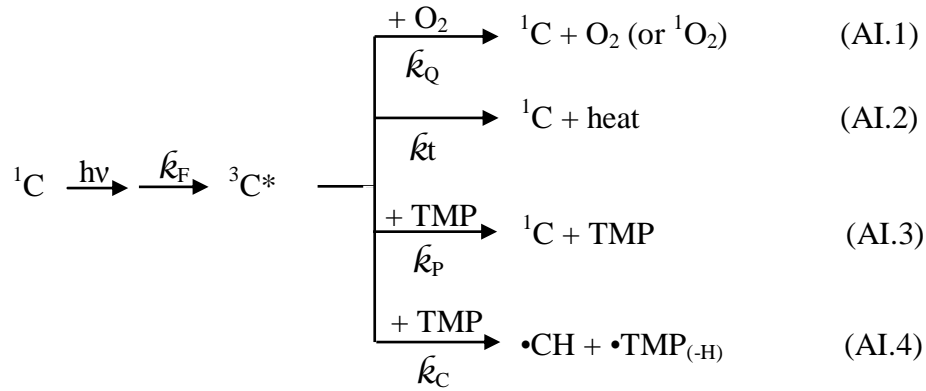
## 5.2 Future Work

The provision of meaningful results in this study was initiated by the utilization of sodium borohydride as a selective reductant of carbonyl-containing moieties such as

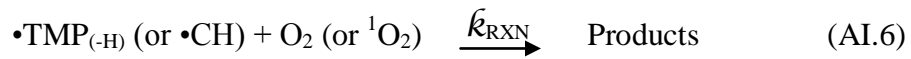
aromatic ketones and aldehydes. The application of this chemical treatment to humic substances and extracts of the Delaware Bay and Mid-Atlantic Bight and subsequent use as a probe of the photochemical properties allows for the assignment of  $\geq 50\%$  of the observed photosensitization to aromatic ketones and aldehydes. As quinones are not expected to be irreversibly reduced under this procedure, it is recommended that a selected series of experiments be done in an oxygen-free environment or that the solution be electrochemically reduced during irradiation in order to better understand the contribution of quinones in this process. Further, other selective chemical treatments such as sodium periodate, a selective oxidant of vicinal diols to two aldehyde groups, should be utilized to observe the effect of oxidation on the optical and photochemical properties of HS.

## Appendix I: Derivation of Equation II.12

Scheme I below shows the transformation of a ground state chromophore,  $^1\text{C}$ , to a triplet excited state chromophore,  $^3\text{C}^*$  with rate of formation of the excited triplet state  $\hat{k}_f$ , under a constant flux of photons from irradiation.



Transformations of  $^3\text{C}^*$  to the ground state can occur by energy transfer to molecular oxygen ( $\text{O}_2$ ) at rate  $\hat{k}_Q$  (eqn. AI.1), radiationless transition to the ground state at rate  $\hat{k}_t$  (eqn. AI.2), and physical or chemical reaction with the external donor TMP with rate  $\hat{k}_P$  or  $\hat{k}_C$ , respectively (eqns. AI.3-4). The radical intermediates produced by reaction AI.4 can be recombined at rate  $\hat{k}_{\text{RECOM}}$  (eqn. AI.5) or be further oxidized by molecular oxygen to form products with rate  $\hat{k}_{\text{RXN}}$  (eqn. AI.6).



The rate of change of the excited triplet state chromophore concentration may be written as shown in equation AI.7. From this relationship, the steady state concentration of the excited triplet state chromophore is shown in equation AI.8.

$$\frac{d[{}^3\text{C}^*]}{dt} = \bar{k}_f - \bar{k}_Q[\text{O}_2][{}^3\text{C}^*] - \bar{k}_t[{}^3\text{C}^*] - \bar{k}_p[\text{TMP}][{}^3\text{C}^*] - \bar{k}_c[\text{TMP}][{}^3\text{C}^*] \quad (\text{AI.7})$$

$$[{}^3\text{C}^*]_{ss} = \frac{\bar{k}_f}{\bar{k}_t + \bar{k}_Q[\text{O}_2] + (\bar{k}_p + \bar{k}_c)[\text{TMP}]} \quad (\text{AI.8})$$

The initial rates of change for TMP and TMP• as well as the steady state concentration of TMP• may be expressed as in equations AI.9-11.

$$-\left(\frac{d[\text{TMP}]}{dt}\right)_0 = \bar{k}_c[{}^3\text{C}^*][\text{TMP}] - \bar{k}_{\text{RECOM}}[\text{CH}\cdot][\text{TMP}\cdot_{(-\text{H})}] \quad (\text{AI.9})$$

$$\left(\frac{d[\text{TMP}\cdot]}{dt}\right)_0 = \bar{k}_c[{}^3\text{C}^*][\text{TMP}] - \bar{k}_{\text{RECOM}}[\text{CH}\cdot][\text{TMP}\cdot_{(-\text{H})}] - \bar{k}_{\text{RXN}}[\text{TMP}\cdot_{(-\text{H})}][\text{O}_2] \quad (\text{AI.10})$$

$$[\text{TMP}\cdot]_{ss} = \frac{\bar{k}_c[{}^3\text{C}^*][\text{TMP}]}{\bar{k}_{\text{RECOM}}[\text{CH}\cdot] + \bar{k}_{\text{RXN}}[\text{O}_2]} \quad (\text{AI.11})$$

$$\left(\frac{d[\text{TMP}]}{dt}\right) = \bar{k}_{\text{RECOM}}[\text{CH}\cdot][\text{TMP}\cdot_{(-\text{H})}] - \bar{k}_c[{}^3\text{C}^*][\text{TMP}] \quad (\text{AI.12})$$

$$\left(\frac{d[\text{TMP}]}{dt}\right) = \frac{\bar{k}_{\text{RECOM}}[\text{CH}\cdot] \bar{k}_c[{}^3\text{C}^*][\text{TMP}]}{\bar{k}_{\text{RECOM}}[\text{CH}\cdot] + \bar{k}_{\text{RXN}}[\text{O}_2]} - \bar{k}_c[{}^3\text{C}^*][\text{TMP}] \quad (\text{AI.13})$$

Equation AI.14 is derived from the substitution of equations AI.8 and AI.11 for the steady state concentrations of the excited triplet state of the chromophore and radical TMP in to equation AI.8.

$$-\frac{d[\text{TMP}]}{dt} = \frac{\bar{k}_f \bar{k}_c [\text{TMP}]}{\bar{k}_t + (\bar{k}_c + \bar{k}_p)[\text{TMP}] + \bar{k}_Q[\text{O}_2]} \left(1 - \frac{\bar{k}_{\text{RECOM}}[\text{CH}\cdot]}{\bar{k}_{\text{RECOM}}[\text{CH}\cdot] + \bar{k}_{\text{RXN}}[\text{O}_2]}\right) \quad (\text{AI.14})$$

The branching ratio of the chemical and physical reaction of TMP with  ${}^3\text{C}^*$  can be represented by  $\phi = \bar{k}_c / (\bar{k}_c + \bar{k}_p)$  and the sum of these processes can be defined as the

total rate constant for TMP such that  $\bar{k}_{\text{TMP}} = \bar{k}_{\text{C}} + \bar{k}_{\text{P}}$ . The terms  $[\text{CH}\bullet]$  and  $\bar{k}_{\text{RECOM}}$  are combined into a lifetime term  $\bar{k}_{\text{REC}}$  and the resultant expression is shown in eqn. AI.15.

$$-\left(\frac{d[\text{TMP}]}{dt}\right)_0 = \left(\frac{\phi \bar{k}_{\text{f}} \bar{k}_{\text{TMP}} [\text{TMP}]}{\bar{k}_{\text{t}} + \bar{k}_{\text{TMP}} [\text{TMP}] + \bar{k}_{\text{Q}} [\text{O}_2]}\right) \cdot \left(1 - \frac{1}{1 + (\bar{k}_{\text{RXN}} [\text{O}_2] / \bar{k}_{\text{REC}})}\right) \quad (\text{AI.15})$$



## **Appendix II: Dependence of the Optical Properties of Humic Substances on Mass Excess Ratios of Sodium Borohydride**

### Introduction

Prior work examined the dependence of  $R_{\text{TMP}}$  on untreated and sodium borohydride ( $\text{NaBH}_4$ ) reduced humic substances (HS) (Golanoski *et al.* 2012). It was observed that  $R_{\text{TMP}}$  decreased by ~50% for reduced HS compared to untreated HS, except for LAC which was reduced by 100%. It was suggested that another class of triplet sensitizers within HS, possibly quinones, were responsible for the remaining TMP sensitization. Interestingly, the dependence of  $R_{\text{TMP}}$  on  $[\text{O}_2]$  for reduced HS closely mirrored that of untreated HS, indicating that complete, irreversible reduction of ketone and aldehyde moieties may not have been achieved.

To test this idea, we examined the effect of  $\text{NaBH}_4$  mass excess ratios (5X – 100X) on the optical and photochemical properties for SRFA, SRHA and LAC at low (100 mg/L) and high (500 mg/L and 1000 mg/L) concentrations.

Reductions were previously performed using highly concentrated stock solutions of HS (500 mg/L or 1000 mg/L) and a 5-fold mass excess of sodium borohydride. Samples were adjusted to pH=10 using 0.25 N NaOH and were deoxygenated using ultra high purity nitrogen in order to limit consumption of  $\text{NaBH}_4$  by acidic water. The reduction was considered complete when no further changes in the absorption spectra were observed (usually at 24 hours). For comparison to the original spectrum, the pH was re-adjusted to neutral using 0.25N HCl, where additional losses of absorbance were observed. (Ma *et al.* 2010; Golanoski *et al.* 2012; Zhang *et al.* 2012, Baluha *et al.* 2013)

Due to the large number of samples (36) each requiring a threaded quartz cuvette and a UHP nitrogen line in close proximity to the UV-Vis spectrophotometer, samples were left open to air for the duration of the reduction. Prior studies have investigated the kinetics of the borohydride reduction of HS, but only until no further changes in the optical properties were observed (usually 24 hours) (Ma *et. al.* 2010). However, recent findings have shown that further changes occur beyond this time, namely for reactions at low HS concentrations ( $\leq 100$  mg/L). For this reason, the absorbance spectra were monitored at 1, 24, 48 and 72 hours.

## **Methods and Materials**

### **Materials**

All chemicals were used as received. Lignin, alkali extracted and carboxylated (LAC), was obtained from Sigma Aldrich (Lot #19714DS). Suwanee River humic acid (SRHA) and Suwanee River fulvic acid (SRFA) were obtained from the International Humic Substances Society. Potassium hydrogen phthalate (KHP) was obtained from Nacalai Tesque, Inc. Sodium borohydride ( $\text{NaBH}_4$ ) was obtained from Fischer Scientific.

### **Methods**

Stock solutions of SRFA, SRHA and LAC at 100, 500 and 1000 mg/L were prepared in MilliQ water and 0.25 N NaOH was used to adjust the solutions to pH=10. Reductions were performed in 6 mL glass vials in the dark at 25°C. To a 5 mL aliquot of each 100 and 500 mg/L HS sample, a mass of solid  $\text{NaBH}_4$  was added (see Table AI.1) and was dissolved by gently shaking the vial. All vials were tightly capped with Parafilm and a small vent hole was created to allow for the release of hydrogen gas which is

formed during the reduction. Due to sample limitations, 1000 mg/L SRFA, SRHA and LAC were reduced using only 5X and 100X NaBH<sub>4</sub> mass excess ratios.

Excess NaBH <sub>4</sub>	Concentration of HS (mg/L)	Mass NaBH <sub>4</sub> (mg)	Concentration of HS (mg/L)	Mass NaBH <sub>4</sub> (mg)
0X	100	0	500	0
5X		2.5		12.5
10X		5		25
25X		12.5		62.5
50X		25		125
100X		50		250

**Table AII.1:** Masses of NaBH<sub>4</sub> added to 100 or 500 mg/L SRFA, SRHA and LAC. Solutions of SRFA, SRHA and LAC at a concentration of 1000 mg/L were reduced only using 5-fold (25 mg NaBH<sub>4</sub>) and 100-fold (500 mg NaBH<sub>4</sub>) due to sample limitations.

UV-Vis spectra were collected using a Shimadzu 2401-PC spectrophotometer at 1, 24, 48 and 72 hours of reaction time. Spectra were corrected by subtraction of a MilliQ water spectrum. The absorbance lost during reduction,  $\Delta A$ , was calculated by subtracting the absorbance at time t, A(t), from the original spectrum at time zero, A(0). The fraction of absorbance remaining, F, was calculated by dividing A(t) by A(0). After 72 hours, the untreated (0X) and reduced (5X – 100X) 500 mg/L SRFA, SRHA and LAC samples were individually passed over a Sephadex G-10 column (2.5 x 8 cm, equilibrated with MilliQ water) in order to remove excess BH<sub>4</sub> and restore the pH to neutral. To account for the dilution factor, samples were analyzed by total organic carbon analysis (TOC) where a 50% carbon to mass ratio was used for both SRFA and SRHA and a 30% carbon to mass ratio was employed. UV-Vis spectra were obtained for

these samples at 10 mg/L where carbon concentrations were 5 mg C/L for SRFA and SRHA and 3 mg C/L for LAC (Figure III.2, left panel). Borohydride-reduced samples at 100 mg L<sup>-1</sup> were not passed over the G-10 column due to the two-fold dilution factor resulting in final concentrations which are not useful in preparation of stock solutions for use in photochemical experiments (min. conc. = 500 mg L<sup>-1</sup>). The large excess of NaBH<sub>4</sub> used to reduced the 1,000 mg L<sup>-1</sup> samples produced very large volumes of H<sub>2</sub> gas, even after long (t > 72 hours) time periods and thus these samples were not passed over the column due to cracking of the column nor were they adjusted to pH=7 due to large volume of HCl required to neutralize the samples.

## Results

For all concentrations of SRFA, SRHA and LAC, reduction by sodium borohydride produced a decrease in absorbance with the greatest absolute loss of absorbance in the ultraviolet (UV) but the largest fractional loss in the visible (VIS) (Figs. AII.1-21). These results are consistent with previously reported findings which have attributed the direct loss of absorption in the UV to the reduction of ketones and aldehydes to their corresponding alcohols and loss of absorption in the visible due to the elimination of charge-transfer contacts between short-range hydroxy- and methoxy-aromatic donor and carbonyl-containing acceptor moieties. (Ma *et. al.* 2010)

The results are summarized in Table AII.2 where for most samples the maximum decrease in absorbance ( $\Delta A_{MAX}$ ) was observed at t = 24 hours where it either remained stable or recovered. For all other samples, a maximum loss of absorbance was achieved at t = 72 hours.

		100 mg L <sup>-1</sup>	500 mg L <sup>-1</sup>	1000 mg L <sup>-1</sup>
<b>SRFA</b>	5X	24 / UV + VIS / m	24 / UV + VIS / m	24 / stable
	10X	24 / VIS / m	24 / VIS / m	
	25X	72 / NA	24 / VIS / m	
	50X	24 / VIS / m	24 / stable	
	100X	24 / stable	24 / stable	72 / NA
<b>SRHA</b>	5X	72 / VIS / m	72 / VIS / m	24 / UV + VIS / M
	10X	24 / UV + VIS / M	24 / UV + VIS / M	
	25X	24 / VIS / M	24 / UV + VIS / M	
	50X	24 / UV + VIS / M	24 / UV + VIS / M	
	100X	72 / NA	24 / UV + VIS / M	72 / NA
<b>LAC</b>	5X	24 / VIS / m	24 / VIS / m	24 / stable
	10X	24 / VIS / m	24 / VIS / m	
	25X	72 / NA	72 / NA	
	50X	24 / VIS / m	24 / stable	
	100X	24 / stable	72 / NA	24 / stable

**Table AII.2:** Summary of the optical properties observed for the sodium borohydride reduction of 100, 500 and 1,000 mg/L SRFA, SRHA and LAC using 5X, 10X, 25X, 50X and 100X mass excess ratios. All experiments were carried out at pH=10 and open to air. Legend: The first number listed indicates the time at which maximum decrease in absorbance was observed (hours). UV - increase in absorbance was observed in the ultraviolet region, VIS – increase in absorbance was observed in the visible region, m = minor increase in absorbance, M - major increase in absorbance, stable indicates that no further changes in absorbance were noted, NA – largest decrease in absorbance was observed at 72 hours therefore any subsequent changes were not able to be observed.

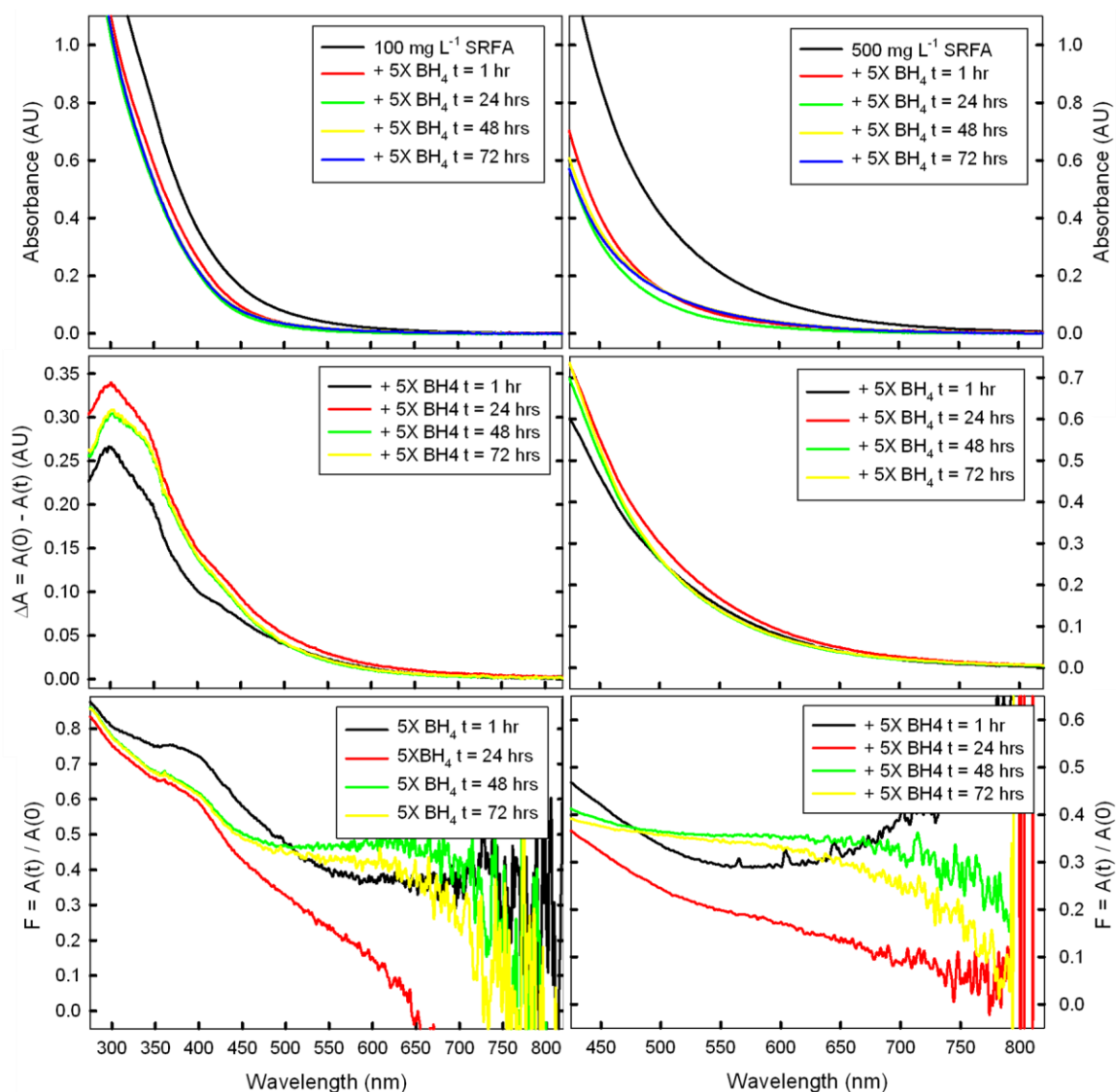
For those samples in which absorbance “recovered” (increased relative to the largest loss of absorbance but remained lower than the original absorbance) after  $t = 24$  hours, the wavelength regime (UV or VIS) was noted and qualitatively classified as minor (m) or major (M). Minor changes in absorbance were considered to be roughly indistinguishable except by examination of the difference or fractional absorbance spectra. Major changes in absorbance were easily observed in the absorbance spectra alone.

For 100 mg L<sup>-1</sup> solutions of SRFA and LAC which were treated with 5X-100X mass excesses of NaBH<sub>4</sub>, absorbance decreased with increasing borohydride mass (Figs AII.7 and 21, left panels). A similar trend is also observed for 500 and 1,000 mg/L SRFA and LAC where a 50X and 5X mass excess of NaBH<sub>4</sub>, respectively was necessary to achieve the same result. One possible explanation is that more highly concentrated solutions of HS increase the probability of interactions between HS and BH<sub>4</sub><sup>-</sup> molecules as opposed to dilute solutions, which increase the likelihood of reaction between H<sub>2</sub>O and BH<sub>4</sub><sup>-</sup> molecules thereby decreasing the effective reductive mass of NaBH<sub>4</sub> available to HS. Interestingly,  $\Delta A_{MAX}$  was observed for 1,000 mg/L LAC with 100X NaBH<sub>4</sub> mass excess but not for 1,000 mg/L SRFA indicating that perhaps additional time, NaBH<sub>4</sub> or both are required to completely reduce all or most carbonyl-containing moieties within SRFA at this concentration.

The results of the NaBH<sub>4</sub> reduction of 100, 500 and 1,000 mg L<sup>-1</sup> SRHA are curious in for most samples, a major “recovery” in absorbance (UV and VIS) were observed following  $\Delta A_{MAX}$  at 72 hours, a result not observed in SRFA or LAC under these reaction conditions. A few exceptions include the addition of 5X mass excess

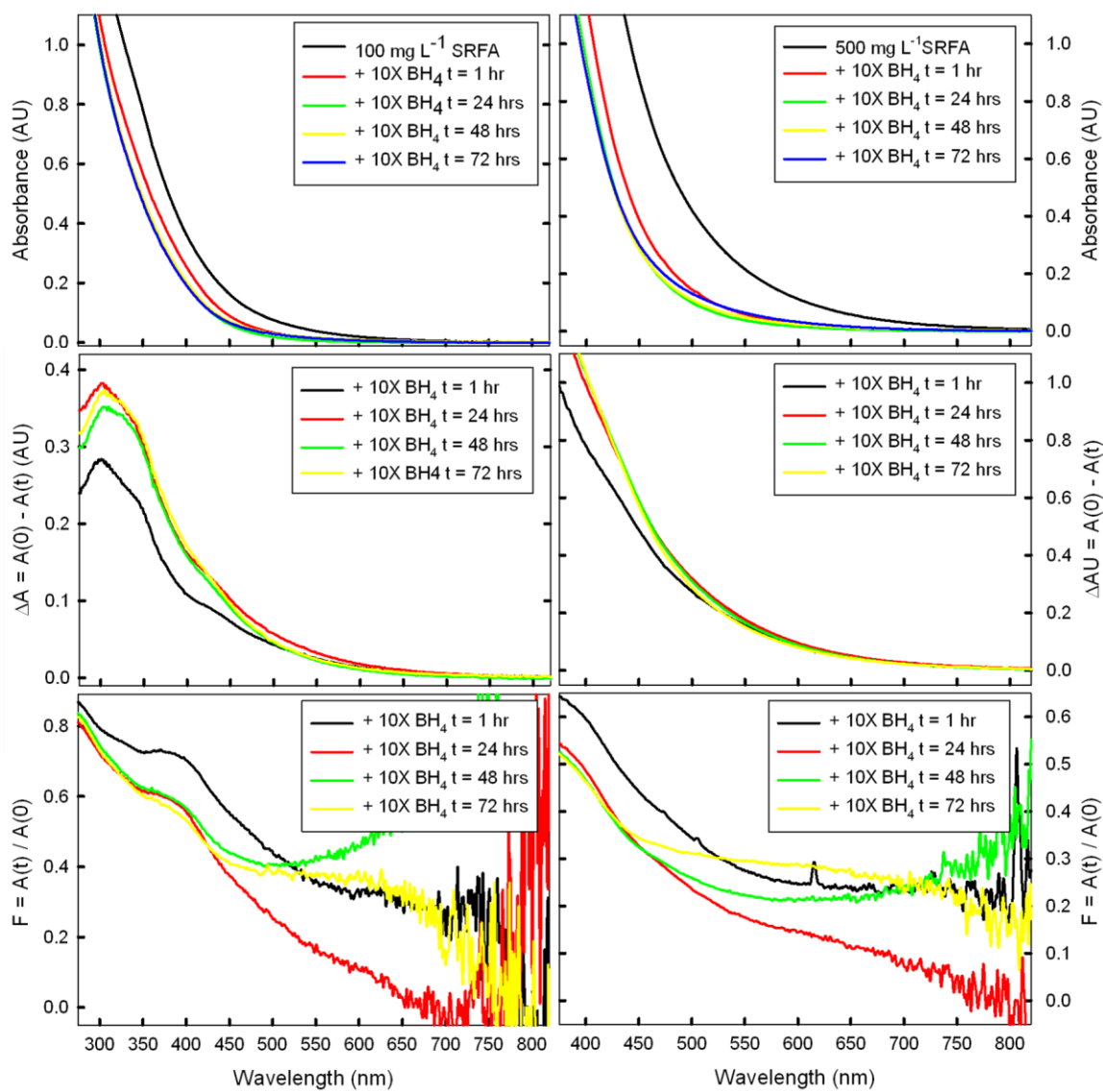
NaBH<sub>4</sub> for 100 and 500 mg L<sup>-1</sup> SRHA and addition of 100X mass excess NaBH<sub>4</sub> to 100 and 1,000 mg L<sup>-1</sup> SRHA where absorbance had not reached  $\Delta A_{MAX}$  within the 72 hour experiment period. As no clear trend exists for the parameters employed in this study, the results present a viable area of future research.

The absorbance spectra at  $\Delta A_{MAX}$  at t = 24 hours for 5X to 100X NaBH<sub>4</sub> mass excess ratios were compared for 100 and 500 mg/L SRFA, SRHA and LAC (Figs AII.6,13 and 20). Although treatment of 100 mg/L HS with 100X NaBH<sub>4</sub> produced the largest absolute loss of absorbance in the UV and largest fractional loss in the visible, the addition of large masses (250 mg) of NaBH<sub>4</sub> to small volumes (5 mL) of 500 mg/L HS was problematic. The constant evolution of gas over the course of 72 hours made acquisition of meaningful absorbance spectra difficult and interfered with the passage of these samples over a Sephadex G-10 column often led to total sample loss due to significant cracking of the column. For all HS investigated, the addition of a 50X NaBH<sub>4</sub> mass excess ratio gave similar results (within 10%) and therefore should be considered for optimum reduction of HS at concentrations of 500 mg/L or greater.

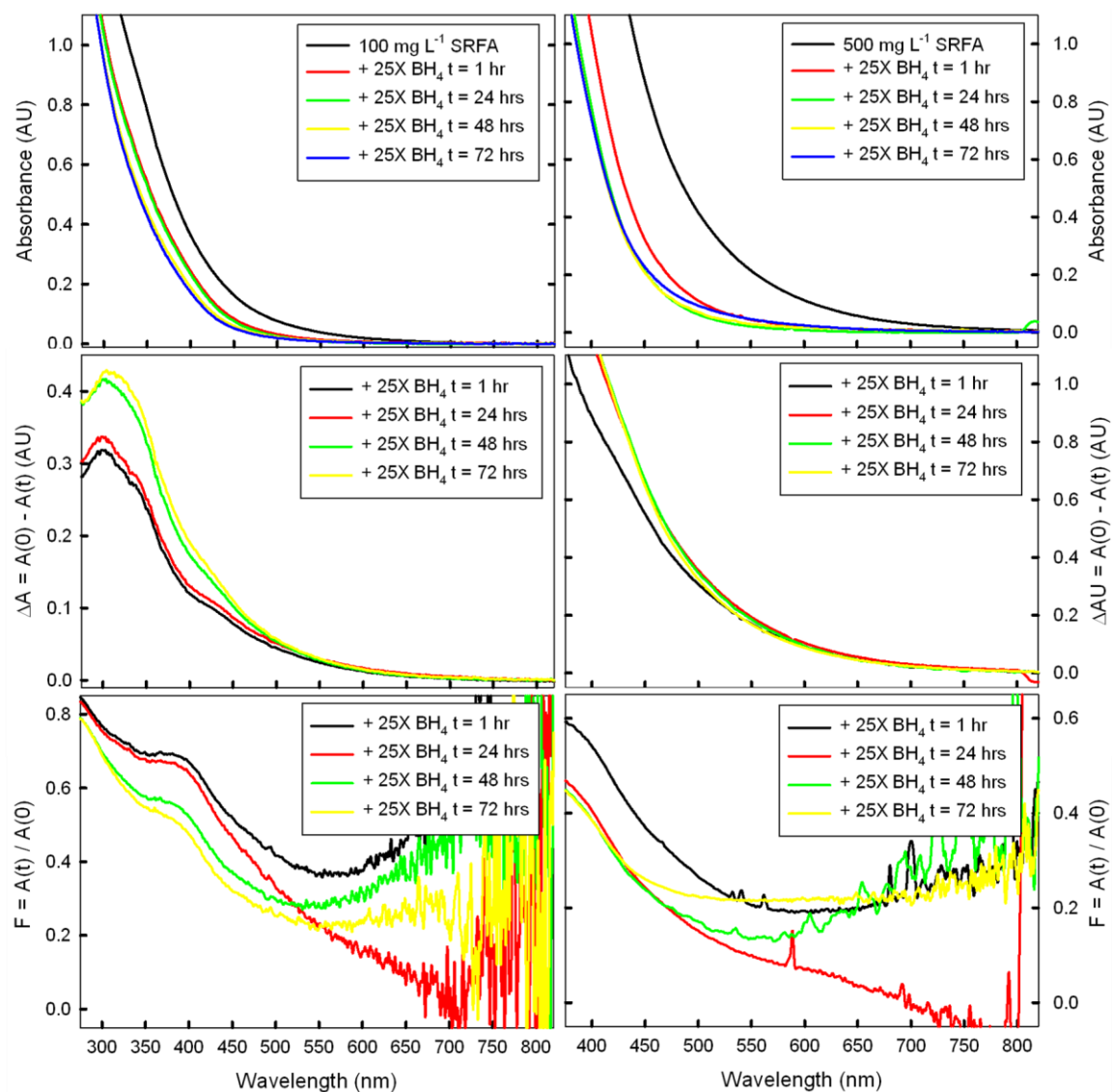


**Figure AII.1:** Time dependence of the reduction of 100 mg/L (left panel) and 500 mg/L (right panel) SRFA using a **5-fold mass excess** of sodium borohydride. Reductions were performed at an initial pH=10 and open to air. Note that  $\Delta A > 0$  represents a loss of absorbance while  $F$  represents the fraction of absorbance remaining.





**Figure AII.2:** Time dependence of the reduction of 100 mg/L (left panel) and 500 mg/L (right panel) SRFA using a **10-fold mass excess** of sodium borohydride. Reductions were performed at an initial pH=10 and open to air. Note that  $\Delta A > 0$  represents a loss of absorbance while  $F$  represents the fraction of absorbance remaining.



**Figure AII.3:** Time dependence of the reduction of 100 mg/L (left panel) and 500 mg/L (right panel) SRFA using a **25-fold mass excess** of sodium borohydride. Reductions were performed at an initial pH=10 and open to air. Note that  $\Delta A > 0$  represents a loss of absorbance while  $F$  represents the fraction of absorbance remaining.

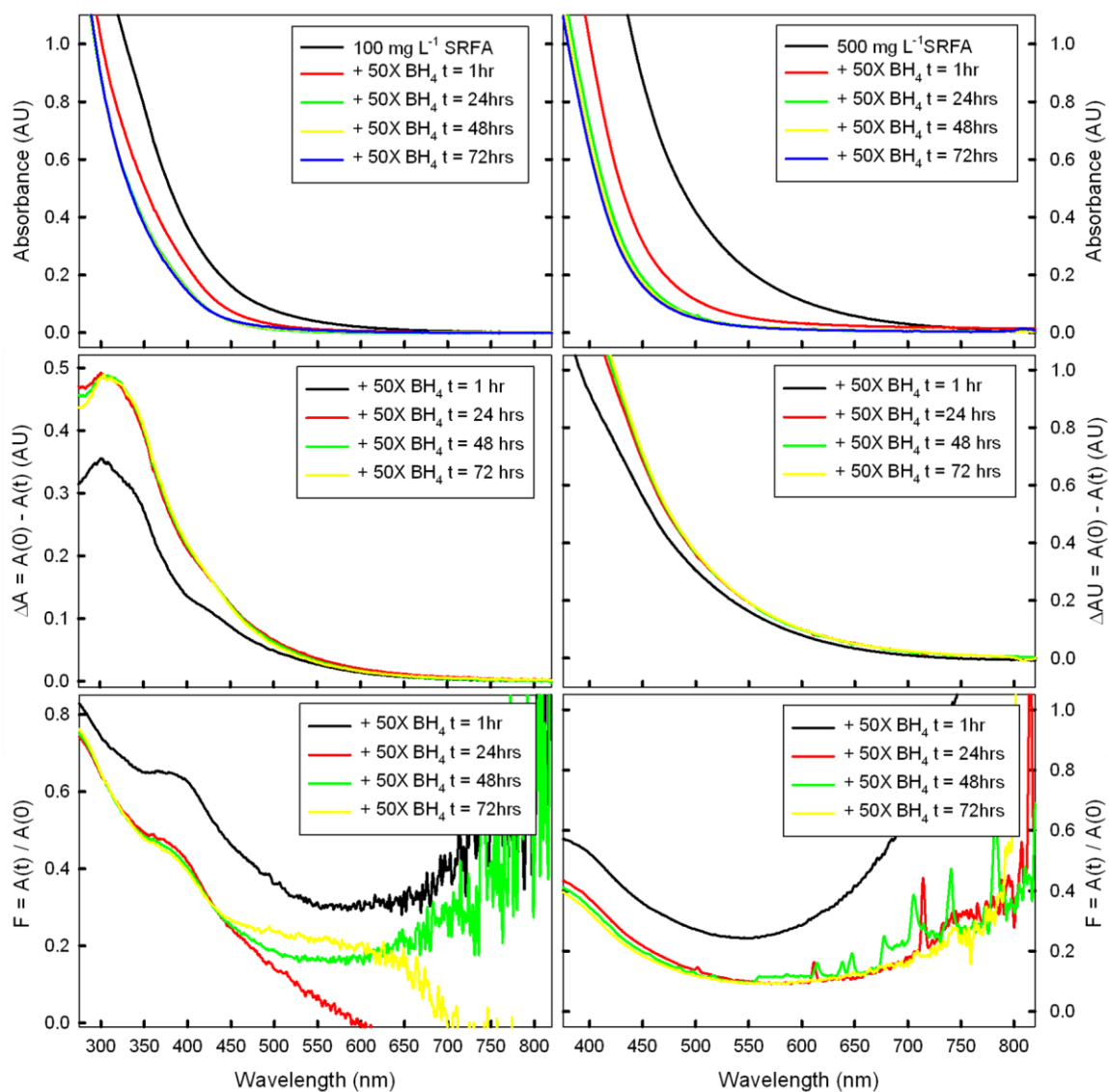
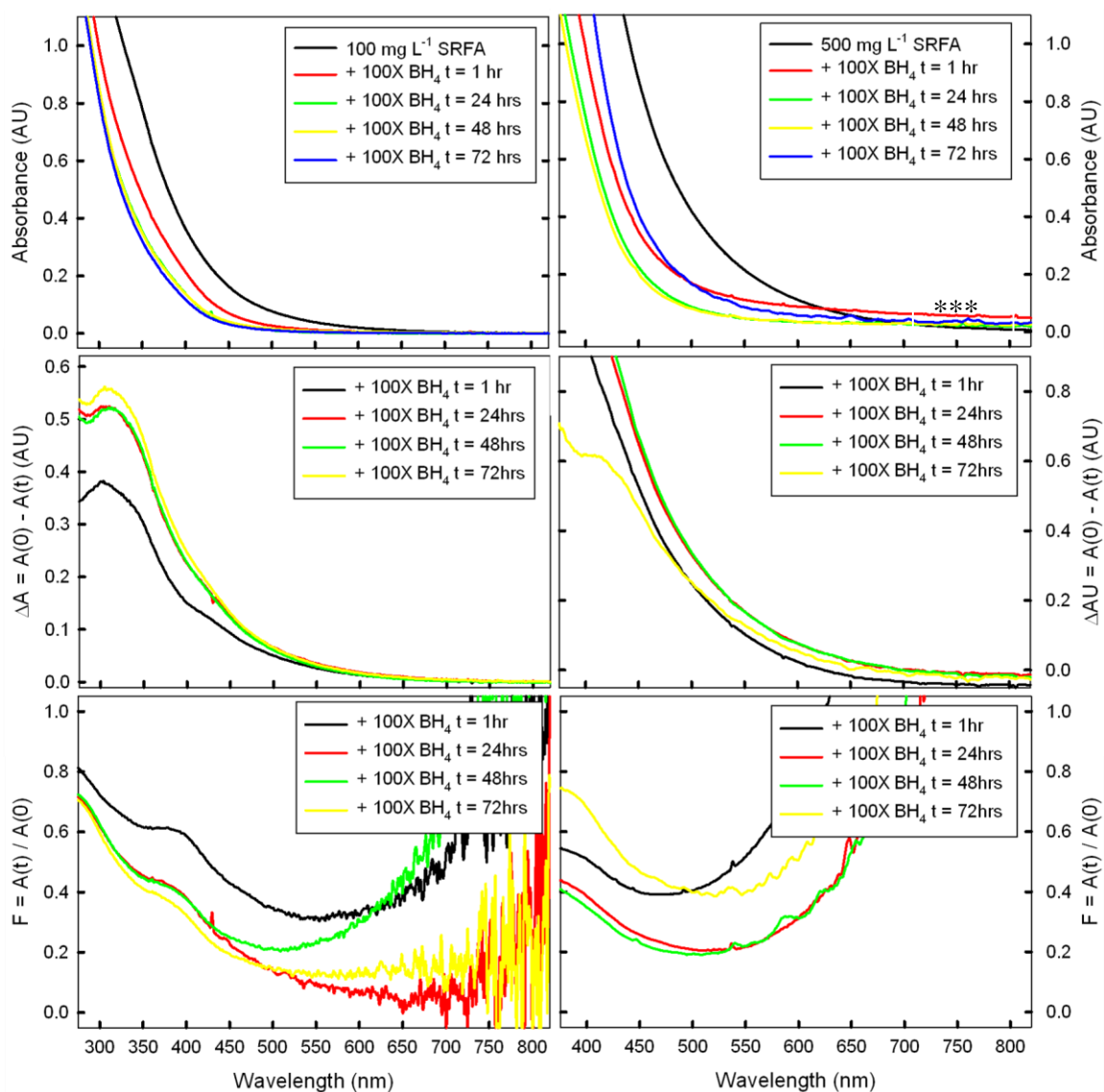
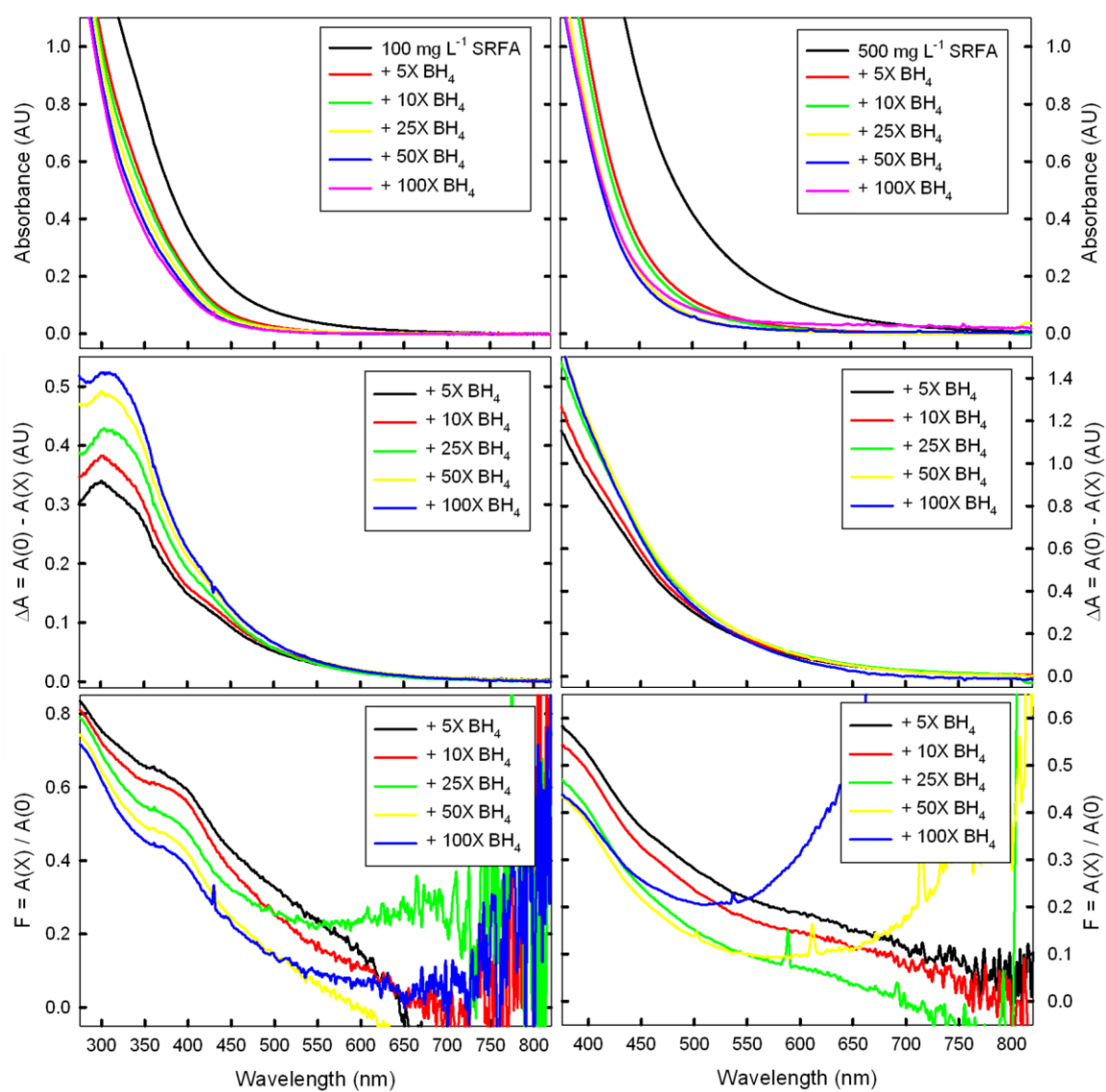


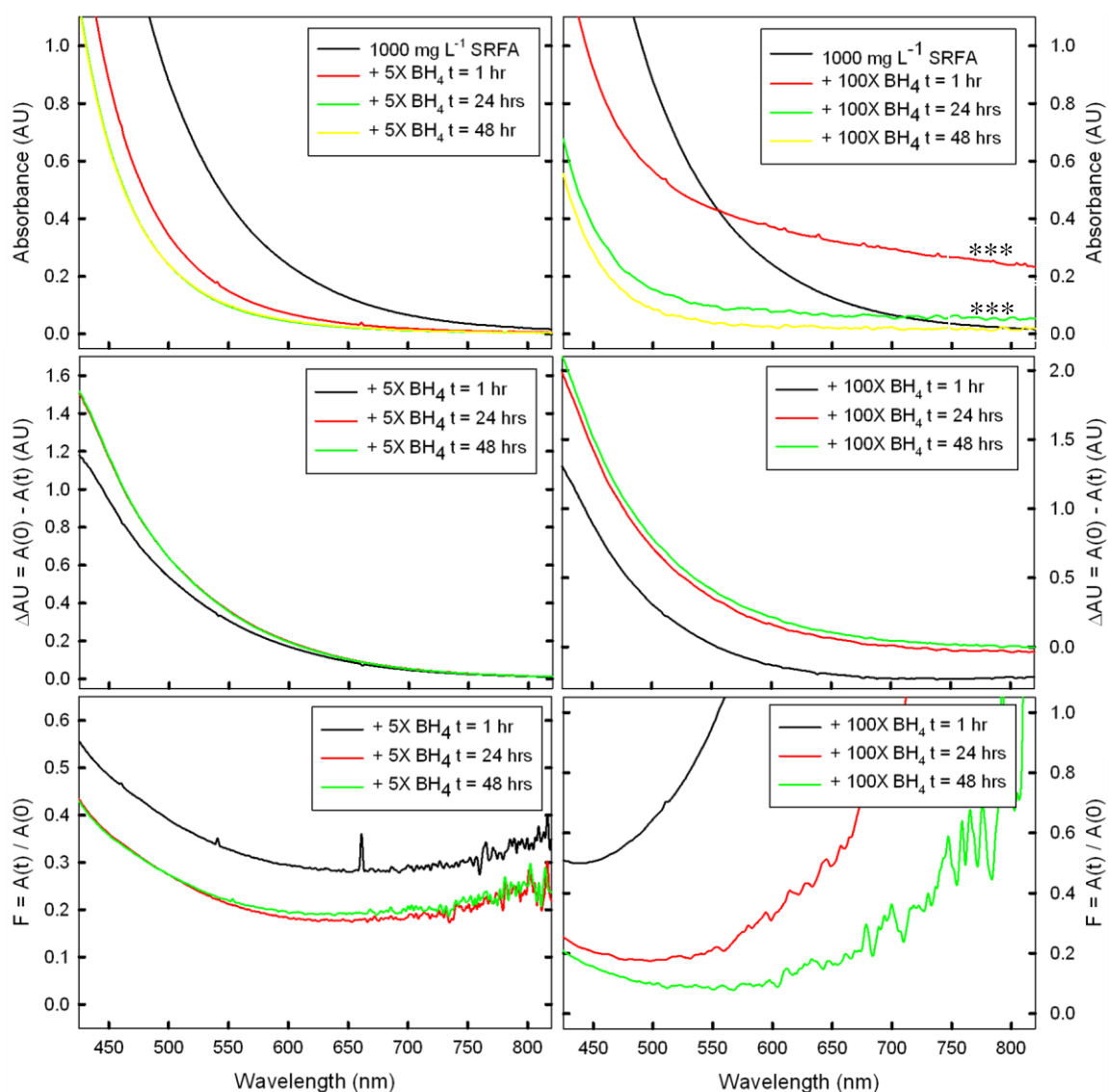
Figure AII.4: Time dependence of the reduction of 100 mg/L (left panel) and 500 mg/L (right panel) SRFA using a **50-fold mass excess** of sodium borohydride. Reductions were performed at an initial pH=10 and open to air. Note that  $\Delta A > 0$  represents a loss of absorbance while  $F$  represents the fraction of absorbance remaining.



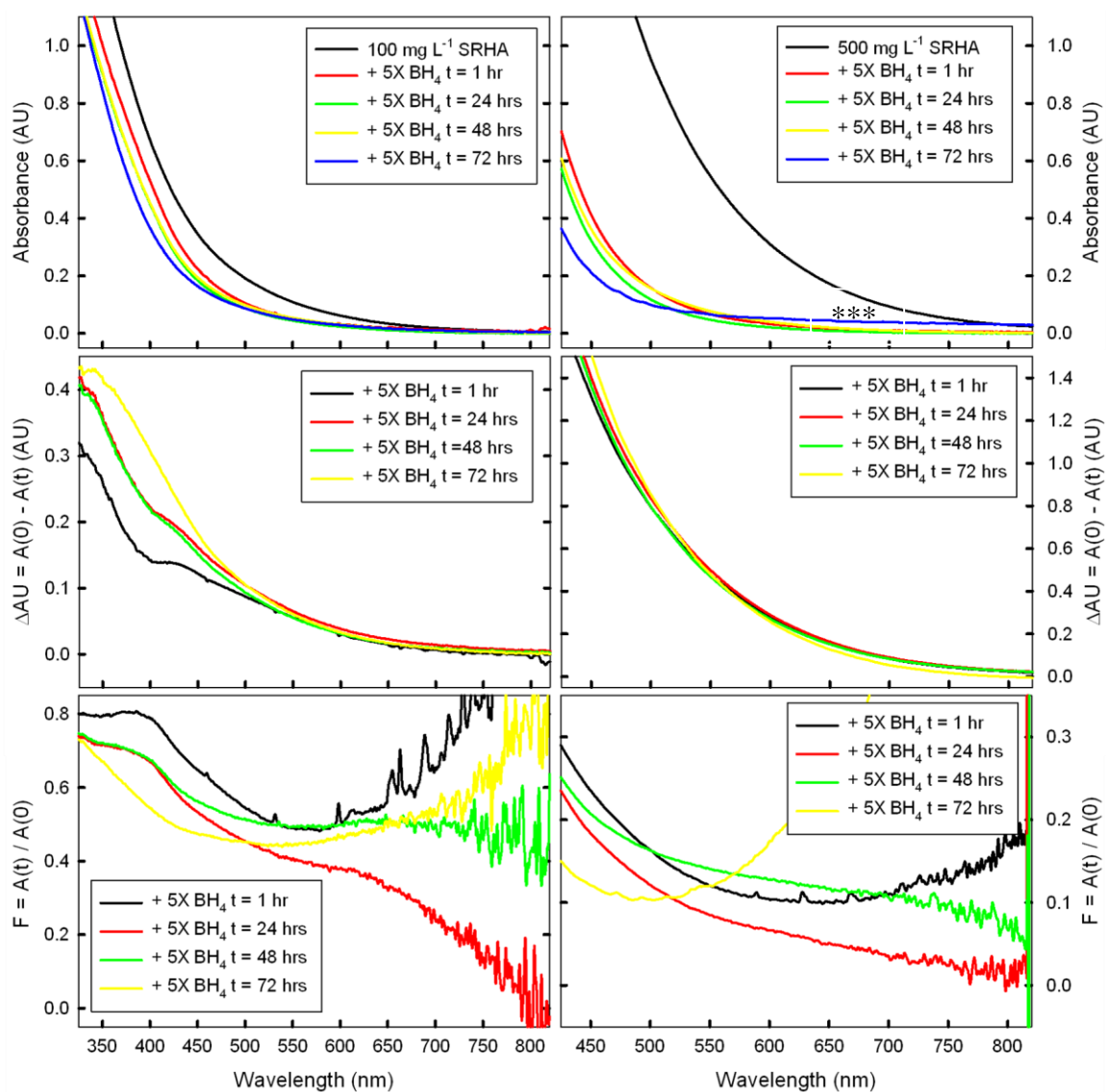
**Figure AII.5:** Time dependence of the reduction of 100 mg/L (left panel) and 500 mg/L (right panel) SRFA using a **100-fold mass excess** of sodium borohydride. Reductions were performed at an initial pH=10 and open to air. Note that  $\Delta A > 0$  represents a loss of absorbance while F represents the fraction of absorbance remaining. Spectra marked with \*\*\* are impacted by the presence of gas bubbles in solution at the time of acquisition.



**Figure AII.6:** SUMMARY of optical properties of 100 mg/L (left panel) and 500 mg/L (right panel) SRFA at the time of maximum absorbance loss (All  $t = 24$  hrs, except 25X  $t = 72$  hrs) during reduction using 5X, 10X, 25X, 50X or 100X mass excess ratio of  $\text{NaBH}_4$ : SRFA. All solutions are at pH=10 and open to air.

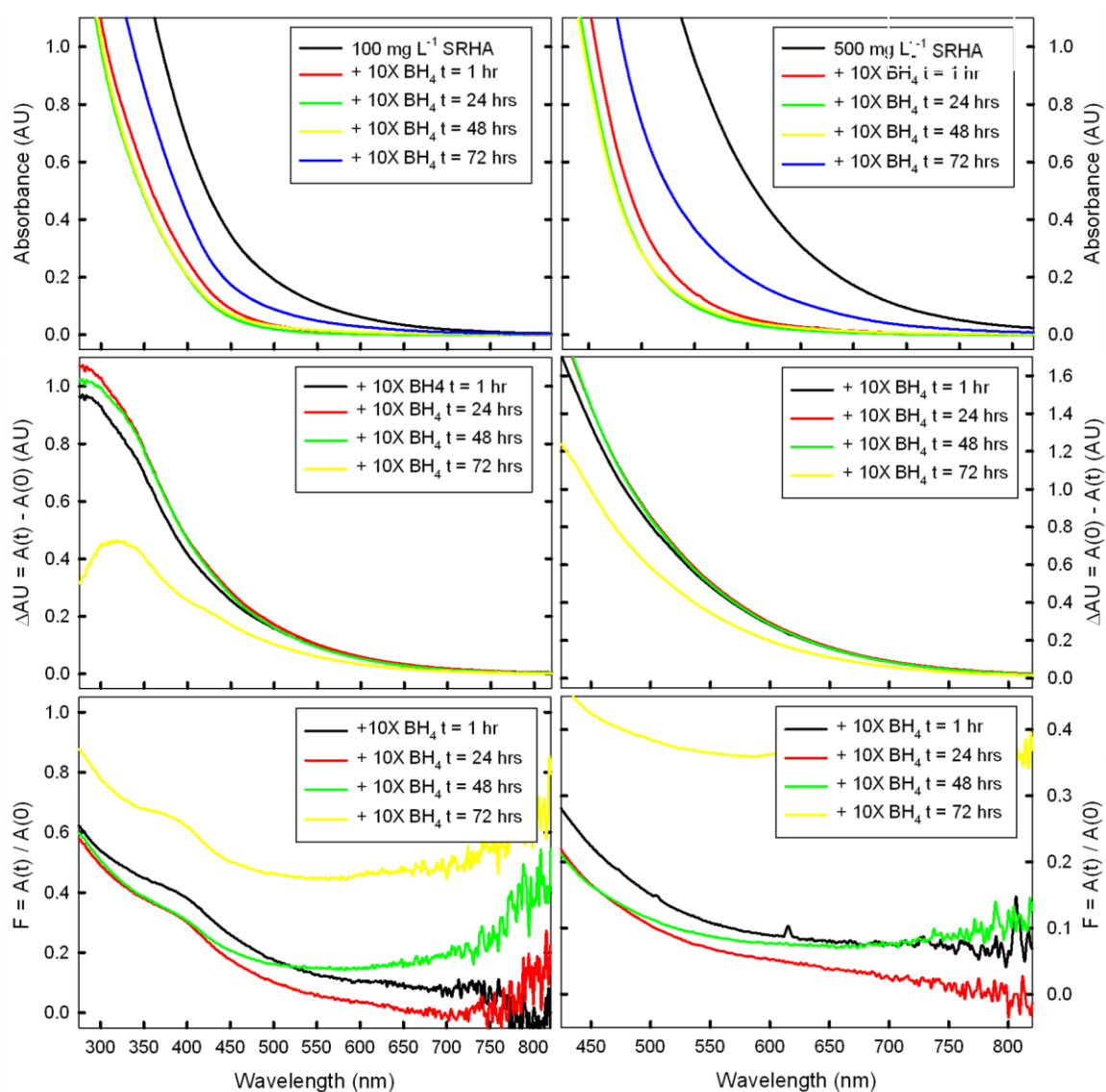


**Figure AII.7:** Time dependence of the reduction of 1000 mg/L SRFA using a **5-fold** (left panel) and **100-fold** (right panel) mass excess of sodium borohydride. Reductions were performed at initial pH=10 and open to air. Note that  $\Delta A > 0$  represents a loss of absorbance while F represents the fraction of absorbance remaining. Spectra marked with \*\*\* are impacted by the presence of gas bubbles in solution at the time of acquisition.



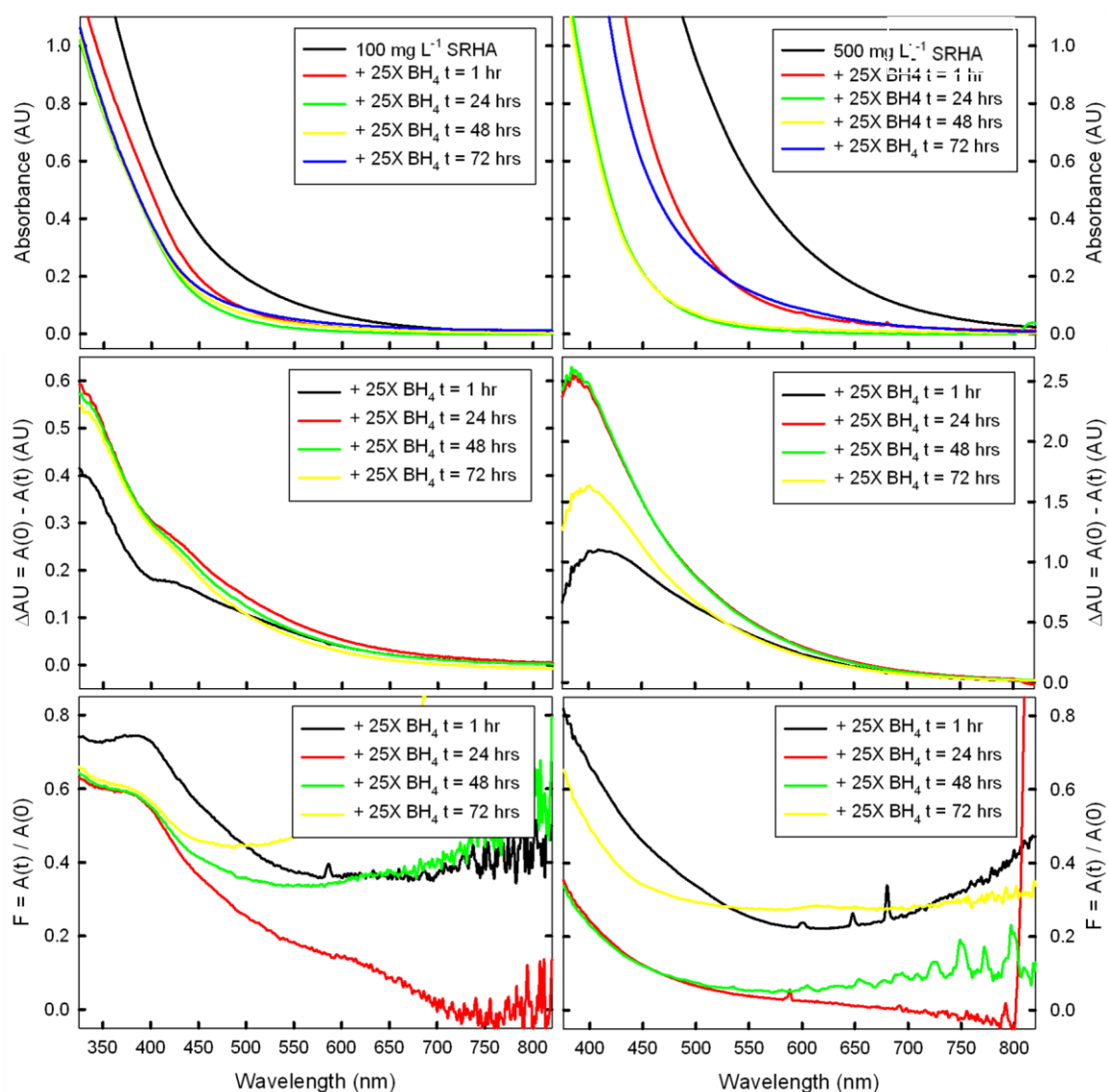
**Figure AII.8:** Time dependence of the reduction of 100 mg/L (left panel) and 500 mg/L (right panel) SRHA using a **5-fold mass excess** of sodium borohydride. Reductions were performed at initial pH=10 and open to air. Note that  $\Delta A > 0$  represents a loss of absorbance while  $F$  represents the fraction of absorbance remaining. Spectra marked with \*\*\* are impacted by the presence of gas bubbles in solution at the time of acquisition.



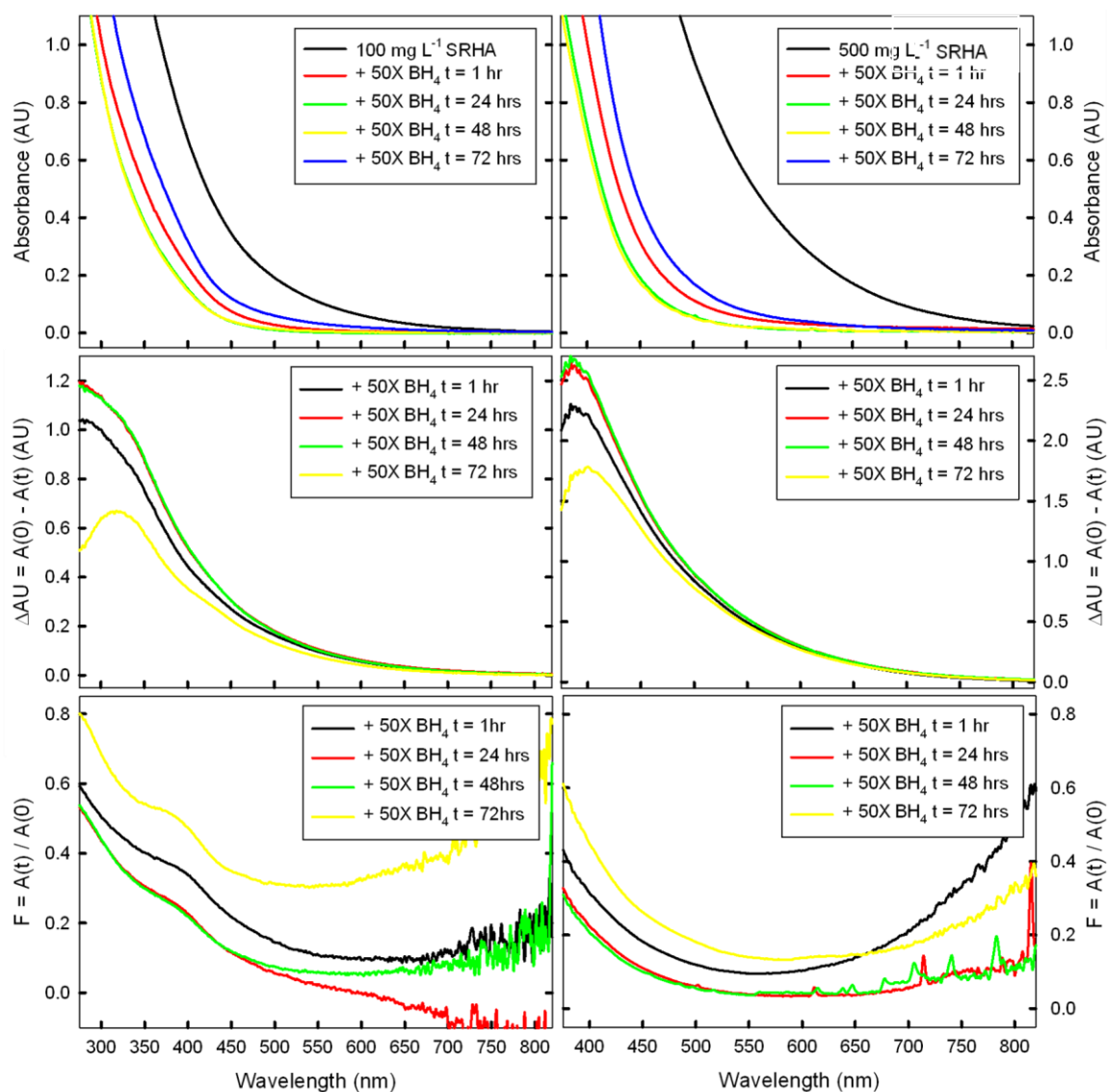


**Figure AII.9:** Time dependence of the reduction of 100 mg/L (left panel) and 500 mg/L (right panel) SRHA using a **10-fold mass excess** of sodium borohydride. Reductions were performed at initial pH=10 and open to air. Note that  $\Delta A > 0$  represents a loss of absorbance while F represents the fraction of absorbance remaining.

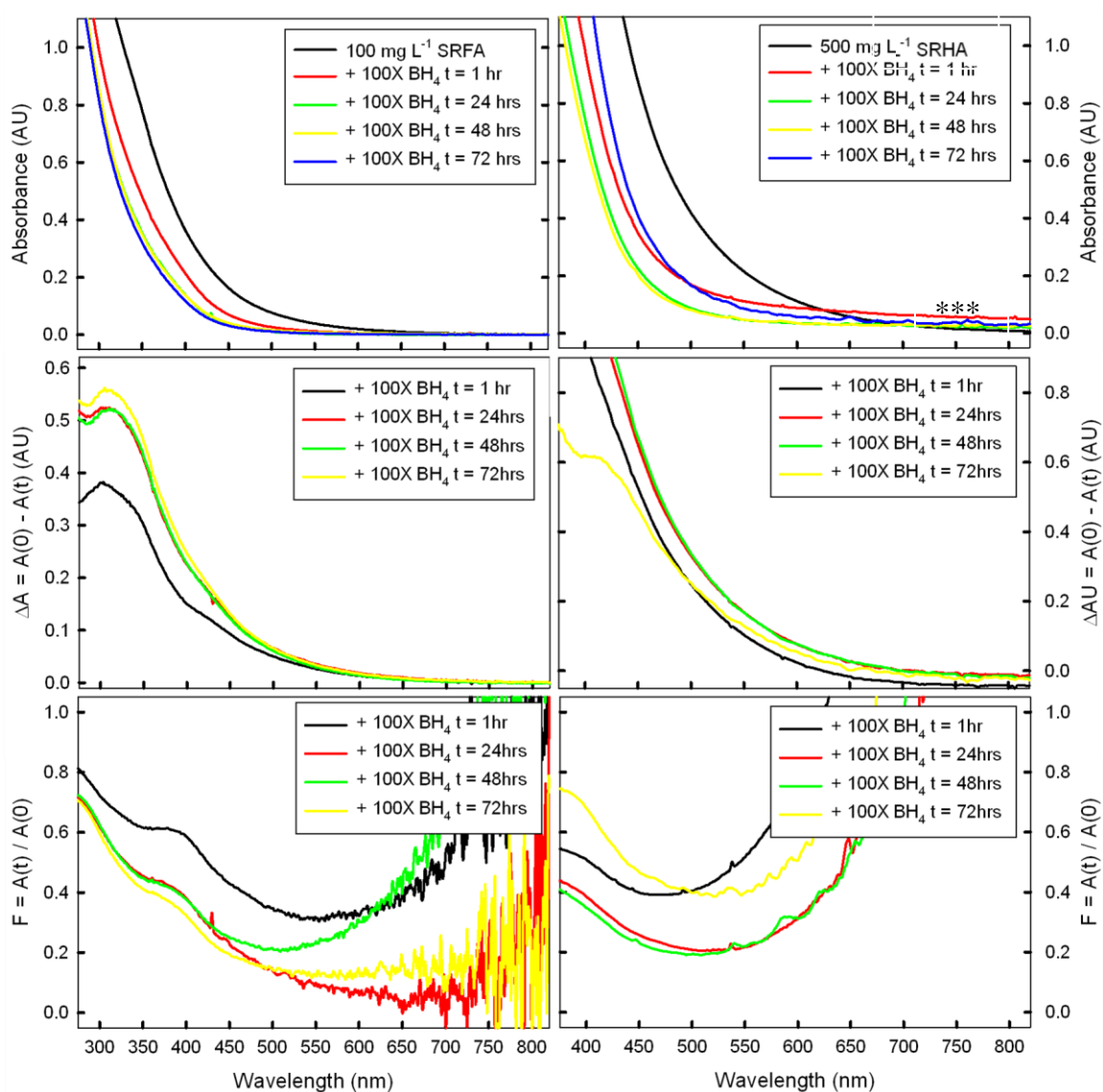




**Figure AII.10:** Time dependence of the reduction of 100 mg/L (left panel) and 500 mg/L (right panel) SRHA using a **25-fold mass excess** of sodium borohydride. Reductions were performed at initial pH=10 and open to air. Note that  $\Delta A > 0$  represents a loss of absorbance while  $F$  represents the fraction of absorbance remaining.



**Figure AII.11:** Time dependence of the reduction of 100 mg/L (left panel) and 500 mg/L (right panel) SRHA using a **50-fold mass excess** of sodium borohydride. Reductions were performed at initial pH=10 and open to air. Note that  $\Delta A > 0$  represents a loss of absorbance while  $F$  represents the fraction of absorbance remaining.



**Figure AII.12:** Time dependence of the reduction of 100 mg/L (left panel) and 500 mg/L (right panel) SRHA using a **100-fold mass excess** of sodium borohydride. Reductions were performed at initial pH=10 and open to air. Note that  $\Delta A > 0$  represents a loss of absorbance while  $F$  represents the fraction of absorbance remaining. Spectra marked with \*\*\* are impacted by the presence of gas bubbles in solution at the time of acquisition.

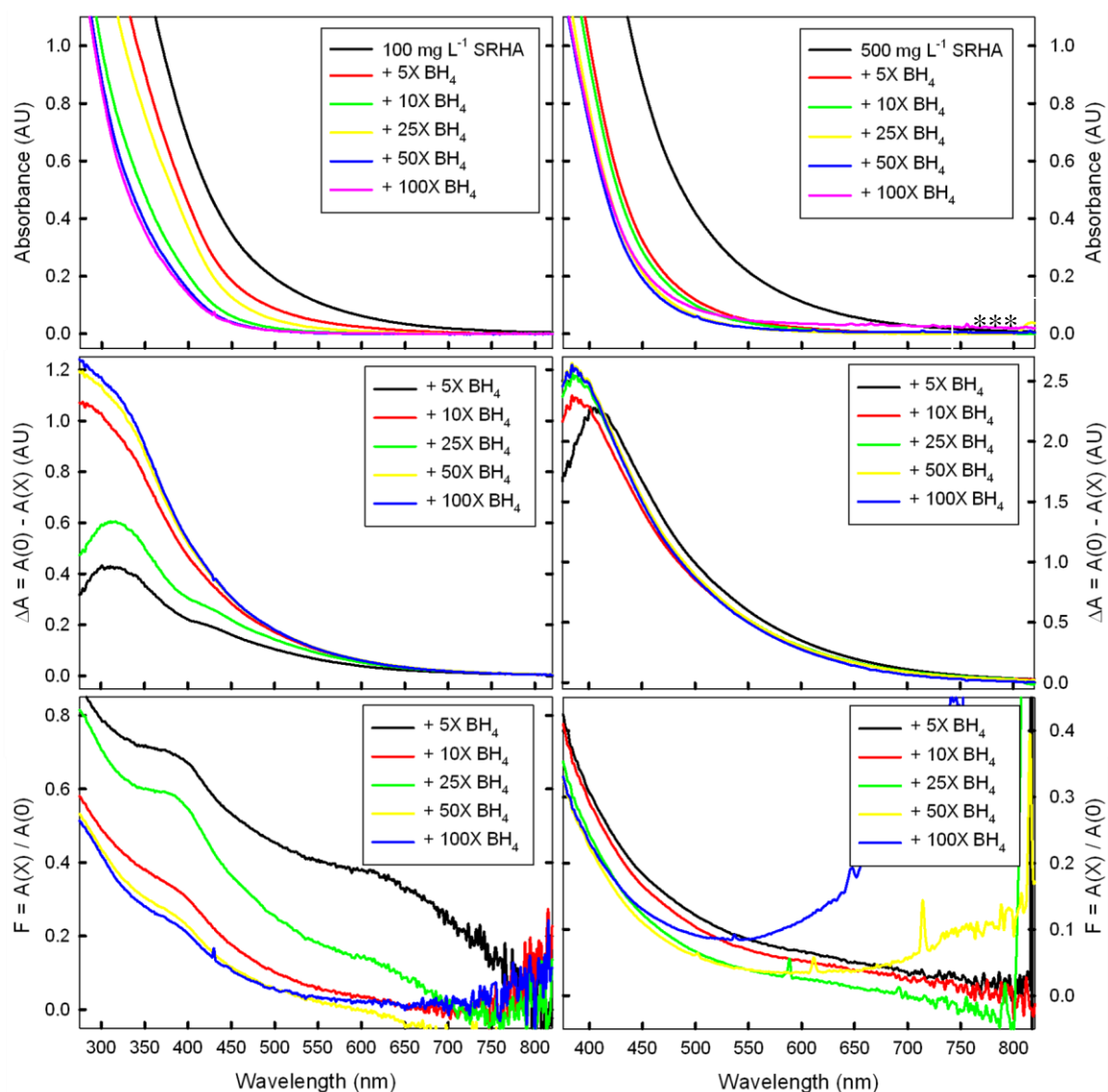


Figure AII.13: SUMMARY of optical properties of 100 mg/L (left panel) and 500 mg/L (right panel) SRHA at the time of maximum absorbance loss (All  $t = 24$  hours except  $t = 72$  hours: 5X for 100 and 500 mg/L SRHA and 100X for 100 mg/L SRHA) during  $\text{NaBH}_4$  reduction using 5X, 10X, 25X, 50X or 100X mass excess ratio of  $\text{NaBH}_4$ : SRHA. All solutions are at  $\text{pH} = 10$ . Spectra marked with \*\*\* are impacted by the presence of gas bubbles in solution at the time of acquisition.

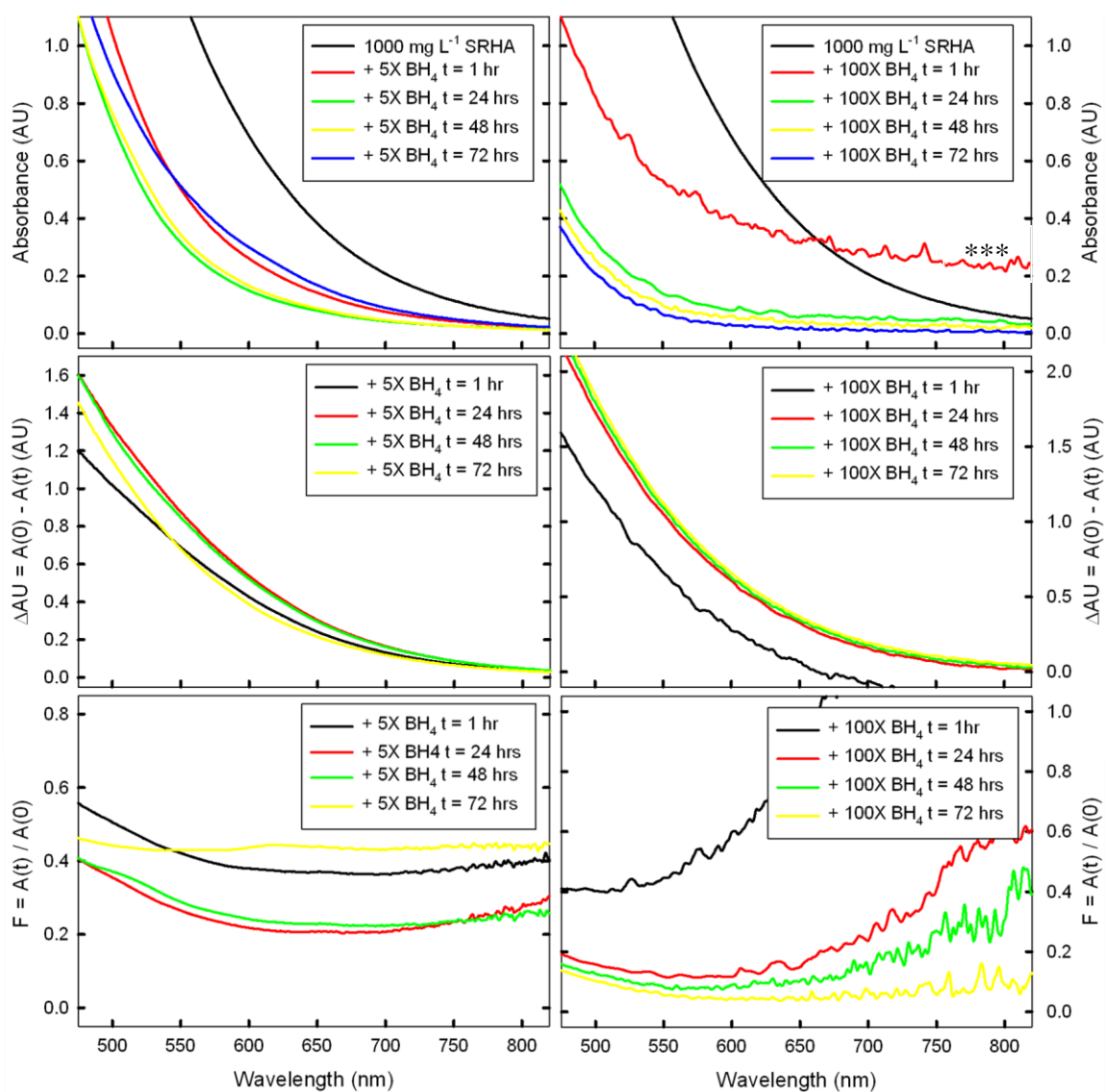
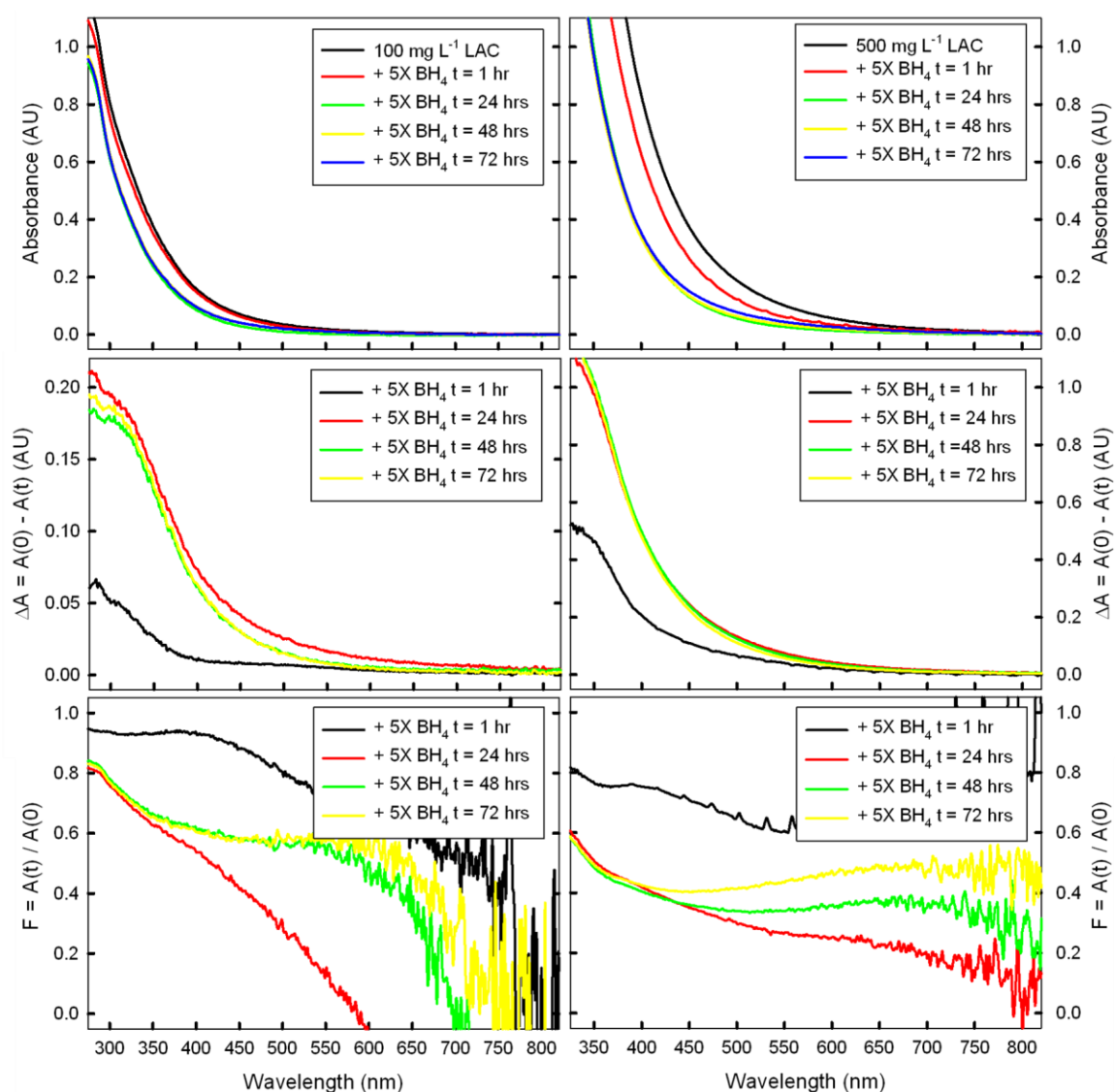
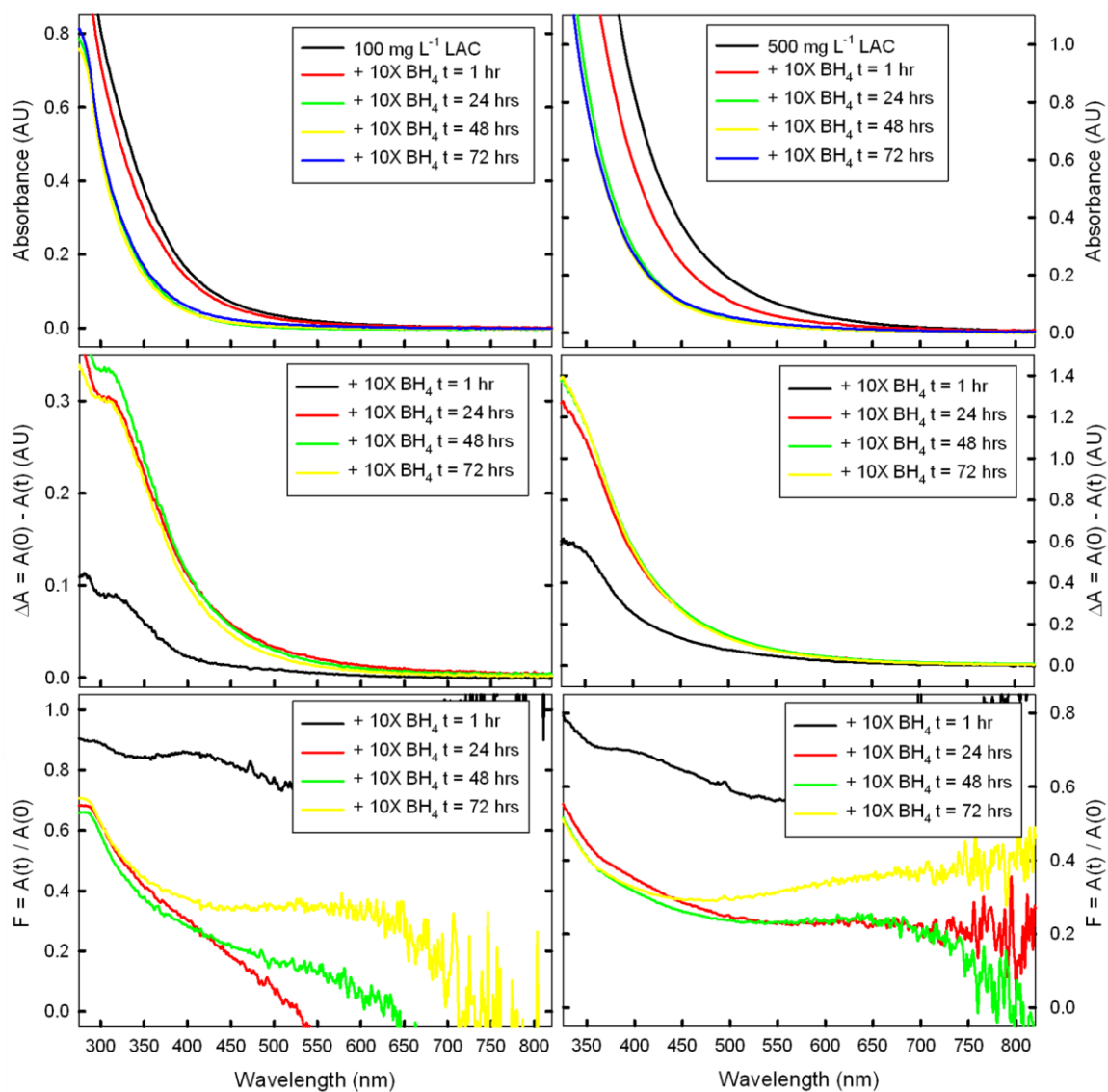


Figure AII.14: Time dependence of the reduction of 1000 mg L<sup>-1</sup> SRHA using a **5-fold** (left panel) and **100-fold** (right panel) mass excess of sodium borohydride. Reductions were performed at initial pH=10 and open to air. Note that  $\Delta A > 0$  represents loss of absorbance while  $F$  represents fraction of absorbance remaining. Spectra marked with \*\*\* are impacted by the presence of gas bubbles in solution at the time of acquisition.

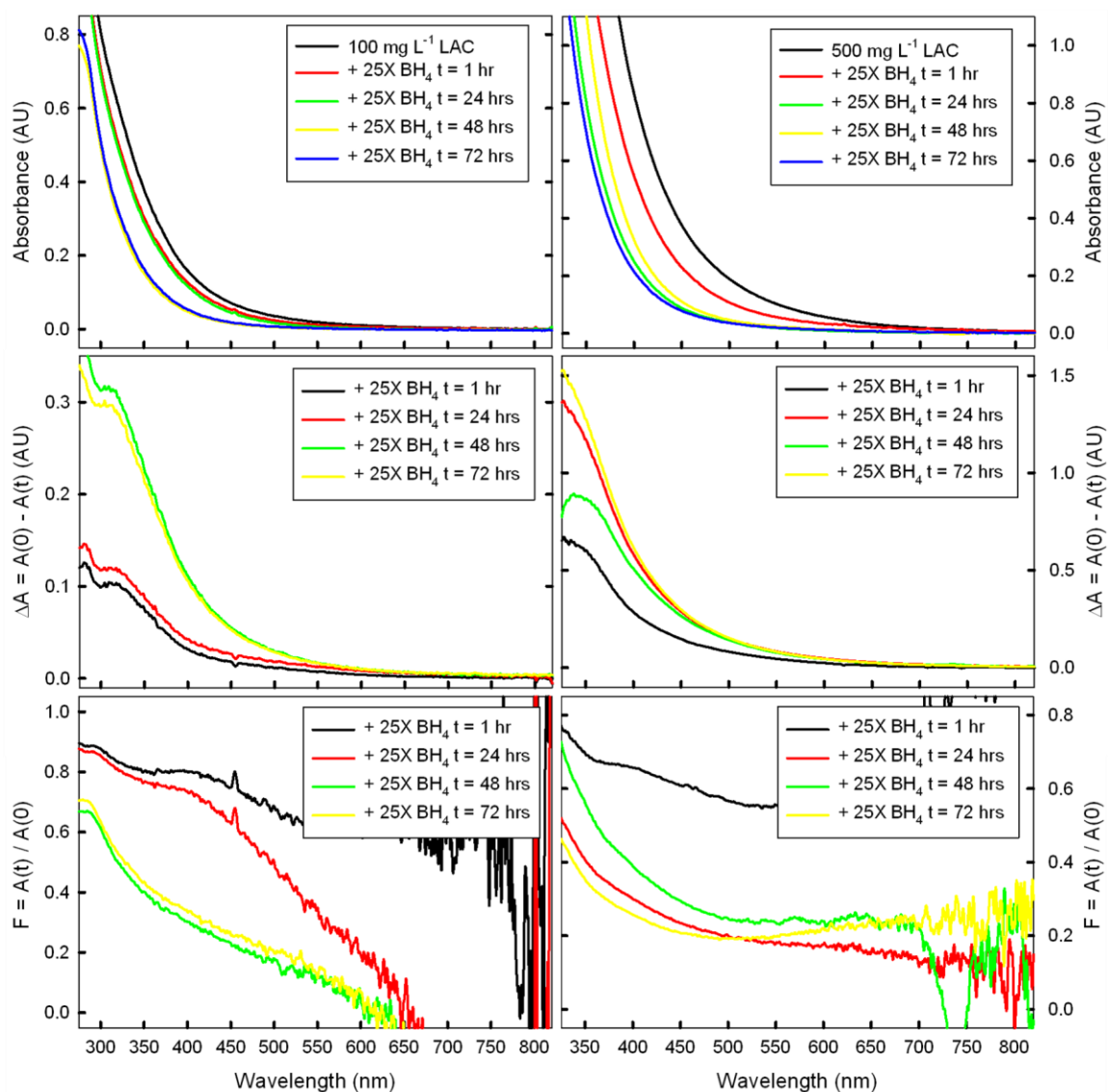


**Figure AII.15:** Time dependence of the reduction of 100 mg L<sup>-1</sup> (left panel) and 500 mg L<sup>-1</sup> (right panel) LAC using a **5 fold mass excess** of sodium borohydride. Reductions were performed at initial pH=10 and open to air. Note that  $\Delta A > 0$  represents loss of absorbance while  $F$  represents fraction of absorbance remaining.



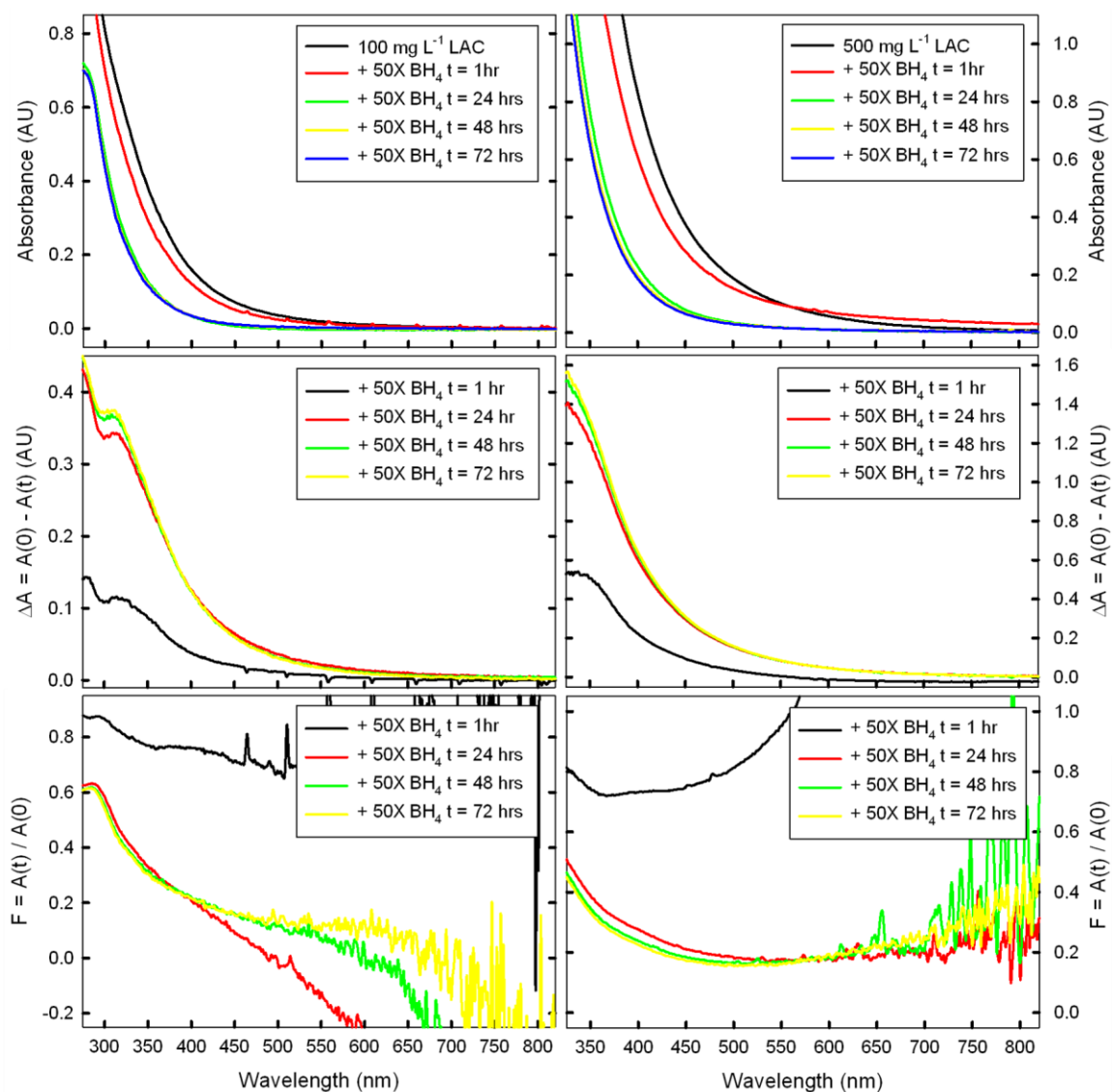
**Figure AII.16:** Time dependence of the reduction of 100 mg L<sup>-1</sup> (left panel) and 500 mg L<sup>-1</sup> (right panel) LAC using a **10-fold mass excess** of sodium borohydride. Reductions were performed at initial pH=10 and open to air. Note that  $\Delta A > 0$  represents loss of absorbance while F represents fraction of absorbance remaining.



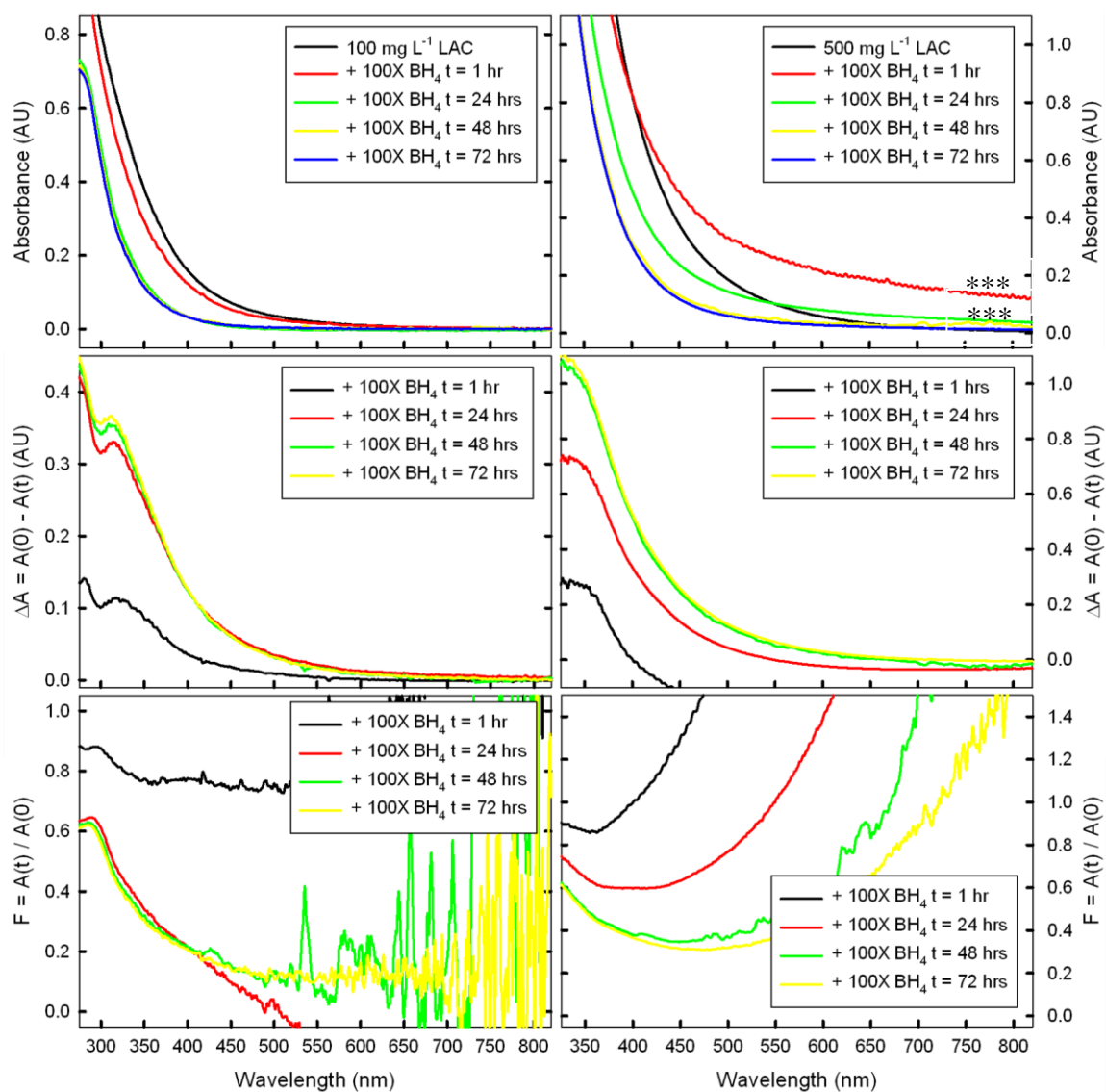


**Figure AII.17:** Time dependence of the reduction of 100 mg L<sup>-1</sup> (left panel) and 500 mg L<sup>-1</sup> (right panel) LAC using a **25-fold mass excess** of sodium borohydride. Reductions were performed at initial pH=10 and open to air. Note that  $\Delta A > 0$  represents loss of absorbance while F represents fraction of absorbance remaining.





**Figure AII.18:** Time dependence of the reduction of 100 mg L<sup>-1</sup> (left panel) and 500 mg L<sup>-1</sup> (right panel) LAC using a **50-fold mass excess** of sodium borohydride. Reductions were performed at initial pH=10 and open to air. Note that  $\Delta A > 0$  represents loss of absorbance while  $F$  represents fraction of absorbance remaining.



**Figure AII.19:** Time dependence of the reduction of 100 mg L<sup>-1</sup> (left panel) and 500 mg L<sup>-1</sup> (right panel) LAC using a **100-fold mass excess** of sodium borohydride. Reductions were performed at initial pH=10 and open to air. Note that  $\Delta A > 0$  represents loss of absorbance while F represents fraction of absorbance remaining. Spectra marked with \*\*\* are impacted by the presence of gas bubbles in solution at the time of acquisition.





## BIBLIOGRAPHY

Aeschbacher, M.; Sander, M.; Schwarzenbach, R.P. Novel electrochemical approach to assess the redox properties of humic substances. *Environ. Sci. Technol.* **2010**, *44*, 87-93.

Afghan, B.; Sherry, J.; Apsimon, J.; Collier, L.; Wilkinson, R.; Albro, P. The use of radioimmunoassay for the detection of polychlorinated dibenzo-para-dioxins in fish samples. *Chemosphere*, **1989**, *19*, 255-261.

Aguer, J-P.; Richard, C. Reactive species produced on irradiation at 365 nm of aqueous solutions of humic acids. *J. Photochem. Photobiol. A: Chem.* **1996**, *93*, 193-198.

Aguer, J-P.; Richard, C.; Andreux, F. Comparison of the photoinductive properties of commercial, synthetic and soil-extracted humic substances. *J. Photochem. Photobiol. A: Chem.* **1997**, *103*, 163-168.

Aguer, J-P.; Richard, C.; Andreux, F. Effect of light on humic substances: Production of reactive species. *Analisis*, **1999**, *27*, 387-390.

Aguer, J-P.; Tétégan, D.; Richard, C. Humic substances mediated phototransformation of 2,4,6-trimethylphenol: a catalytic reaction. *Photochem. Photobiol. Sci.* **2005**, *4*, 451-453.

Al Housari, F.; Vione, D.; Chiron, S.; Barbati, S. Reactive photoinduced species in estuarine waters. Characterization of hydroxyl radical singlet oxygen and dissolved organic matter triplet state in natural oxidation processes. *Photochem. Photobiol. Sci.* **2010**, *9*, 78-86.

Amada, I.; Yamaji, M.; Sase, M.; Shizuka, H. Laser flash photolysis studies on hydrogen atom abstraction from phenol by triplet naphthoquinones in acetonitrile. *J. Chem. Soc. Faraday. Trans.* **1995**, *91*, 2751-2759.

Ariese, F.; van Assema, S.; Goojer, C. Bruccoleri, A.G.; Langford, C.H. Comparison of Laurentian Fulvic Acid luminescence with that of the hydroquinone/quinone model system: Evidence from low temperature fluorescence studies and EPR spectroscopy. *Aquat. Sci.* **2004**, *66*, 86-94.

Barron, M.A.; Haber, L.; Maier, A.; Zhao, J.; Dourson, M. Toxicological Review of Phenol, In Support of Summary Information on the Integrated Risk Information System (IRIS). U.S. Environmental Protection Agency, 2002, CAS 108-95-2. (<http://www.epa.gov/iris/toxreviews/0088tr.pdf>).

Bisby, R.H.; Parker, A.W. Reactions of excited triplet duroquinone with  $\alpha$ -Tocopherol and ascorbate: A nanosecond laser flash photolysis and time-resolved resonance raman investigation. *J. Am. Chem. Soc.* **1995**, *117*, 5664-5670.

Blough, N.V.; Del Vecchio, R. *In Biogeochemistry of Marine Dissolved Organic Matter*, Hansel, D.A., Carlson, C.A., Eds.; Academic Press: San Diego, **2002**; pp 509-546.

Blough, N.V.; Zarifiriou, O.C.; Bonilla, J. Optical absorption spectra of waters from the Orinoco River outflow: Terrestrial input of colored organic matter to the Caribbean *J. Geophys. Res.* **1993**, 98, 2271-2278.

Blough, N.V.; Zepp, R.G. Reactive oxygen species in natural waters, p. 280-333. *In* C.S. Foote *et. al.* [eds.], *Active oxygen: Reactive oxygen in chemistry*, Chapman and Hall.

Blough, N.V.; Green, S.A. *In the Role of Nonliving Organic Matter in the Earth's Carbon Cycle*, Zepp, R.G., Sonntag, C., Eds. John Wiley and Sons: Chichester, **1995**; pp 23-45.

Blough, N.V. Photochemistry in the sea surface microlayer. *In The sea surface and global change*; Liss, P.S.; Duce, R.A., Eds; Cambridge University Press: Cambridge; **1997**; pp 383-424.

Boreen, A. L.; Arnold, W. A.; McNeill, K. Photodegradation of pharmaceuticals in the environment: A review. *Aquat. Sci.* **2003**, 65, 320-341

Boreen, A.L.; Arnold, W.A.; McNeill, K. Triplet-sensitized photodegradation of sulfa drugs containing six-membered heterocyclic groups: Identification of an SO<sub>2</sub> extrusion photoproduct. *Environ. Sci. Technol.* **2005**, 39, 3630-3638.

Boyle, E.S. Guerriero, N.; Thalliet, A.; Del Vecchio, R.; Blough, N.V. Optical properties of humic substances and CDOM: Relation to structure. *Environ. Sci. Technol.* **2009**, 43, 2262-2268.

Burns, S. E.; Hassett, J. P.; Rossi, M. V. Binding effects on humic-mediated photoreaction: intrahumic dechlorination of mirex in water. *Environ. Sci. Technol.* **1996**, 30, 2934-2941.

Canonica, S.; Jans, U.; Stemmler, K.; Hoigné, J. Transformation kinetics of phenols in water: photosensitization by dissolved natural organic matter and aromatic ketones. *Environ. Sci. Technol.* **1995**, 29, 1822-1831.

Canonica, S.; Hoigné, J. Enhanced oxidation of methoxyphenols at micromolar concentration photosensitized by dissolved natural organic material. *Chemosphere.* **1995**, 30, 2365-2374.

Canonica, S.; Hellrung, B.; Wirz, J. Oxidation of phenols by triplet aromatic ketones in aqueous solution. *J. Phys. Chem. A.* **2000**, 104, 1226-1232.

Canonica, S.; Frieburghaus, M. Electron-rich phenols for probing the photochemical reactivity of freshwaters. *Environ. Sci. Technol.* **2001**, 35, 690-695.

Canonica, S.; Hellrung, B.; Müller, P.; Wirz, J. Aqueous oxidation of phenylurea herbicides by triplet aromatic ketones. *Environ. Sci. Technol.* **2006**, *40*, 6636-6641.

Canonica, S. Oxidation of aquatic organic contaminants induced by excited triplet states. *Chimia*, **2007**, *61*, 641-644.

Canonica, S.; Laubscher, H-U. Inhibitory effect of dissolved organic matter on triplet-induced oxidation of aquatic contaminants. *Photochem. Photobiol. Sci.* **2008**, *7*, 547-551.

Cawley, K.M.; Hakala, J.A.; Chin, Y-P. Evaluating the triplet state photoreactivity of dissolved organic matter by chromatography and ultrafiltration using an alkylphenol probe molecule. *Limnol. Oceanogr.: Methods.* **2009**, *7*, 391-398.

Chin, Y.-P.; Miller, P. L.; Zeng, L.; Cawley, K.; Weavers, L. K. Photosensitized degradation of bisphenol A by dissolved organic matter. *Environ. Sci. Technol.* **2004**, *38*, 5888-5894.

Coble, P.G.; Marine Optical Biogeochemistry: The Chemistry of Ocean Color. *Chem. Rev.* **2007**, *107*, 402-418.

Dalrymple, R.M.; Carfagno, A.K.; Sharpless, C.M. Correlations between dissolved organic matter optical properties and quantum yields of singlet oxygen and hydrogen peroxide. *Environ. Sci. Technol.* **2010**, *44*, 5824-5829.

Das, P.K.; Encinas, M.V.; Scaiano, J.C. Laser flash photolysis study of the reactions of carbonyl triplets with phenols and photochemistry of p-hydroxypropiophenone. *J. Am. Chem. Soc.* **1981**, *103*, 4154-4162.

Das, P.K.; Bhattacharyya, S.N. Laser flash photolysis study of electron transfer reactions of phenolate ions with aromatic carbonyl triplets. *J. Phys. Chem.* **1981**, *85*, 1391-1395.

de Haan, H.; Werlemark, G.; Beboer, T. Effect of pH on molecular weight and size of fulvic acids in drainage water from peaty grassland in NW Netherlands. *Plant and Soil*, **1983**, *1*, 63-73.

de Haan, H. Use of ultraviolet spectroscopy, gel filtration, pyrolysis/mass spectrometry and numbers of benzoate-metabolizing bacteria in the study of humification and degradation of aquatic organic matter. In *Aquatic and Terrestrial Humic Material*; Christman, R. F., Gjessing, E. T., Eds.; Ann Arbor Science, **1983**.

de Mora, S.; Demers, S.; Vernet, M. The Effects of UV Radiation in the Marine Environment; Cambridge University Press: Cambridge, 2000.

DeZuane, J. Handbook of Drinking Water Quality, 1997 John Wiley and Sons, 2<sup>nd</sup> Edition, New York, NY.

Del Vecchio, R.; Blough, N.V. Photobleaching of chromophoric dissolved organic matter in natural waters: kinetics and modeling. *Mar. Chem.* **2002**, 78, 231-253.

Del Vecchio, R.; Blough, N.V. On the origin of the optical properties of humic substances. *Environ. Sci. Technol.* **2004**, 38, 3885-3891.

Draper, W.M.; Crosby, D.G.; Bowers, J.B. Measurement of photochemical oxidants in agricultural field water. *Abstracts of the Am. Chem. Soc.* **1976**, 172, 64-64.

Encinas, M.V.; Lissi, E.A.; Olea, A.F. Quenching of triplet benzophenone by vitamins C and E and by sulfur containing amino acids and peptides. *Photochem. Photobiol.* **1985**, 42, 347-352.

Faust, B.C.; Hoigné, J. Sensitized photooxidation of phenols by fulvic acid in natural waters. *Environ. Sci. Technol.* **1987**, 21, 957-964.

Garg, S.; Rose, A.L.; Waite, D.L. Production of reactive oxygen species on photolysis of dilute aqueous quinone solutions. *Photochem. Photobiol.* **2007**, 83, 904-913.

Gerecke, A. C.; Canonica, S.; Müller; Sharer, M.; Schwarzenbach, R. P. Quantification of dissolved natural organic matter (DOM) mediated phototransformation of phenylurea herbicides in lakes. *Environ. Sci. Technol.* **2001**, 35, 3915-3923.

Glover, C. and Rosario-Ortiz, F., Impact of halides on the photoproduction of reactive intermediates from organic matter. *Environ. Sci. Technol.* **2013**, 47, 13949-13956

Goldstone, J.V.; Del Vecchio, R.; Blough, N.V. A multicomponent model of chromophoric dissolved organic matter photobleaching. *Photochem. Photobiol.* 2004, 80, 52-60.

Grannas, A. M.; Cory, R. M.; Miller, P. L.; Chin, Y.-P.; McKnight, D. M. The role of dissolved organic matter in arctic surface waters in the photolysis of hexachlorobenzene and lindane. *J. Geophys. Res.* **2012**, 117, G01003.

Grebel, J. E.; Pignatello, J.J.; Mitch, W.A. Effect of halide ions and carbonates on organic contaminant degradation by hydroxyl radical-based advanced oxidation processes in saline waters. *Environmental Technology*, **2010**, 44, 6822-6828.

Green, S.A.; and Blough, N.V. Optical-absorption and fluorescence properties of chromophoric dissolved organic matter in natural waters. *Limnol. Oceanogr.* **1994**, 39, 1903-1916.

Guerard, J.J.; Miller, P.L.; Trouts, T.D.; Chin, Y-P. The role of fulvic acid composition in the photosensitized degradation of aquatic contaminants. *Aquat. Sci.* **2009**, 71, 160-169.



Guerard, J.J.; Chin, Y-P.; Mash, H.; Hadad, C.M. Photochemical fate of sulfadimethoxine in aquaculture waters. *Environ. Sci. Technol.* **2009**, *43*, 8587-8592.

Gutiérrez, I.; Bertolotti, S.G.; Biasutti, M.A.; Soltermann, A.T.; García, N.A. Quinones and hydroquinones as generators and quenchers of singlet molecular oxygen. *Can. J. Chem.* **1997**, *75*, 423-428.

Haag, W.R.; Hoigné, J.; Gassman, E.; Braun, A.M. Singlet oxygen in surface waters – Part II: Quantum yields of its production by some natural humic materials as a function of wavelength. *Chemosphere*, **1984**, *13*, 641-650.

Haag, W.R.; Hoigné, J. Photo-sensitized oxidation in natural water via OH radicals. *Chemosphere*. **1985**, *14*, 1659-1671.

Halladja, S.; Ter Halle, A.; Aguer, J-P.; Boulkamh, A.; Richard, C. Inhibition of humic substances mediated photooxygenation of furfuryl alcohol by 2,4,6-trimethylphenol. Evidence for reactivity of the phenol with humic triplet excited states. *Environ. Sci. Technol.* **2007**, *41*, 6066-6073.

Halladja, S.; ter Halle, A.; Pilichowski, J-F.; Boulkamh, A.; Richard, C. Fulvic acid-mediated phototransformation of mecoprop. A pH-dependent reaction. *Photochem. Photobiol. Sci.* **2009**, *8*, 1066-1071.

Hertkorn, N.; Benner, R.; Frommberger, M.; Schmitt-Kopplin, P.; Witt, M.; Kaiser, K.; Kettrup, A.; Hedges, J. I. Characterization of a major refractory component of marine dissolved organic matter. *Geochim. Cosmochim. Acta* **2006**, *70*, 2990-3010.

Jammoul, A.; Dumas, S.; D'Anna, B.; George, C. Photoinduced oxidation of sea salt halides by aromatic ketones: a source of halogenated radicals. *Atmospheric Chemistry and Physics*, **2009**, *9*, 4229-4237.

Johnson, M.R.; Rickborn, B. Sodium borohydride reduction of conjugated aldehydes and ketones. *J. Org. Chem.* **1970**, *35*, 1041-1045.

Johnson, C.G.; Caron, S.; Blough, N.V. Combined liquid chromatography/mass spectrometry of the radical adducts of a fluorescamine-derived nitroxide. *Anal. Chem.* **1996**, *68*, 867-872.

Jonsson, M.; Lind, J.; Reitberger, T.; Eriksen, T. E.; Memnyi, G. *J. Phys. Chem.* **1993**, *97*, 8229-8233.

Kawaguchi, H. Rates of sensitized photo-oxidation of 2,4,6-trimethylphenol by humic acid. *Chemosphere*. **1993**, *27*, 2177-2182.

Kieber, D.J.; Blough, N.V. Determination of carbon-centered radicals in aqueous solution by liquid chromatography with fluorescence detection. *Anal. Chem.* **1990**, *62*, 2275-2283.

Kujawinski, E. B.; Del Vecchio, R.; Blough, N. V.; Klein, G. C.; Marshall, A. G. Probing molecular-level transformations of dissolved organic matter: insights on photochemical degradation and protozoan modification of DOM from electrospray ionization Fourier transform ion cyclotron resonance mass spectrometry. *Mar. Chem.* **2004**, 92, 23-37.

Kujawinski, E.B.; Longnecker, K.; Blough, N.V.; Del Vecchio, R.; Finlay, L.; Kitner, J.B.; Giovannoni, S.J. Identification of possible source markers in marine dissolved organic matter using ultra-high resolution mass spectrometry. *Geochim. Cosmochim. Acta* **2009**, 73, 4384-4399.

Lakatos, B.; Tibai, T.; Meisel, J. EPR spectra of humic acids and their metal complexes. *Geoderma* 1977, 19, 319-338.

Lambrych, K.L.; Hassett, J.P. Wavelength-dependent photoreactivity of mirex in Lake Ontario. *Environ. Sci. Technol.* **2006**, 40, 858-863.

Latch, D. E.; Stender, B. L.; Arnold, W. A.; McNeill, K. Photochemical fate of pharmaceuticals in the environment: cimetidine and ranitidine. *Environ. Sci. Technol.* **2003**, 37, 3342-3350.

Leenheer, J.A.; Wershaw, R.L.; Reddy, M.M. Strong-acid structures in fulvic acid from the Suwanee River, Georgia. 1. Minor Structures. *Environ. Sci. Technol.* **1995**, 29, 393-398.

Lin, K.; Carlson, D. Photo-induced degradation of tracer phenols added to marine surface microlayers. *Mar. Chem.* **1991**, 33, 9-22.

Lind, J.; Shen, X.; Eriksen, T. E.; Mer6nyi G. The one-electron reduction potential of 4-substituted phenoxyl radicals in water. *J. Am. Chem. Soc.* **1990**, 112, 479-482.

Lundqvist, M.J.; Eriksson, L.A. Hydroxyl radical reactions with phenol as a model for generation of biologically reactive tyrosyl radicals. *J. Phys. Chem. B*, **2000**, 104, 848-855.

Ma, J.; DelVecchio, R.; Golanoski, K.S.; Boyle, E.S.; Blough, N.V. Optical properties of humic substances and CDOM: Effects of borohydride reduction. *Environ. Sci. Technol.* **2010**, 44, 5395-5402.

MacCarthy, P.; Deluca, S. J.; Voorhees, K. J.; Malcom, R. L.; Thurman, E. M. Pyrolysis-mass spectrometry/pattern recognition on a well-characterized suite of humic substances. *Geochim. Cosmochim. Acta* **1985**, 49, 2091-2096.

McKnight, D. M.; Andrews, E. D.; Spaulding, S. A.; Aiken, G. R. Aquatic fulvic acids in algal-rich arctic ponds. *Limnol. Oceanogr.* **1994**, 39, 1972-1979.

Mill, T.; Hendry, D.G.; Richardson, H. Free-radical oxidants in natural waters. *Science*. **1980**, 207, 886-887.

Mopper, K.; Kieber, D. J. Photochemistry and cycling of carbon, sulfur, nitrogen and phosphorus. In *Biogeochemistry of Marine Dissolved Organic Matter*; Hansell, D. A., Carlson, C. A., Eds.; Academic Press, **2002**.

Mopper, K.; Stubbins, A.; Ritchie, J. D.; Bialk, H. M.; Hatcher, P. G. Advanced instrumental approaches for characterization of marine dissolved organic matter: extraction techniques, mass spectrometry, and nuclear magnetic resonance spectroscopy. *Chem. Rev.* **2007**, 107, 419-442.

Murov, S. L.; Carmichael, I.; Hug, G. L. *Handbook of Photochemistry*, 2nd ed.; Marcel Dekker: New York, 1993.

Neta, P.; Huie, R.; Ross, A.B. Rate constants for reactions of peroxy radicals in fluid solutions. *J. Phys. Chem. Ref. Data*. **1990**, 19, 413-513.

Nelson, N.B.; Siegel, D.A.; Michaels, A.F. Seasonal dynamics of colored dissolved organic matter in the Sargasso Sea. *Deep-Sea Res.* **1998**, 17, 931-957.

Packer, J. L.; Werner, J. J.; Latch, D. E.; McNeill, K.; Arnold, W. A. Photochemical fate of pharmaceuticals in the environment: Naproxen, diclofenac, clofibric acid and ibuprofen. *Aquat. Sci.* **2003**, 65, 342-351.

Paul, A.; Hackbarth, S.; Vogt, R.D.; Roder, B.; Burnison, B.K.; Steinberg, C.-E.W. Photogeneration of singlet oxygen by humic substances: comparison of humic substances of aquatic and terrestrial origin. *Photochem. Photobiol. Sci.* **2004**, 3, 273.

Paul, A.; Stösser, R.; Zehl, A.; Zwirnmann, E.; Vogt, R. D.; Steinberg, C. E. W. Nature and abundance of organic radicals in natural organic matter: effect of pH and irradiation. *Environ. Sci. Technol.* **2006**, 40, 5897-5903.

Power, J.F.; Langford, C.H. Optical absorbance of dissolved organic matter in natural water studies using the thermal lens effect. *Anal. Chem.* **1988**, 60, 842-846.

Remucal, C. K.; Cory, R. M.; Sander, M.; McNeill, K. Low molecular weight components in an aquatic humic substance as characterized by membrane dialysis and orbitrap mass spectrometry. *Environ. Sci. Technol.* **2012**, 46, 9350-9359.

Richard, C.; Trubetskaya, O.; Trubetskoj, O.; Reznikova, O.; Afanas'eva, G.; Aguer, J-P.; Guyot, G. Key role of the low molecular size fraction of soil humic acids for fluorescence and photoinductive activity. *Environ. Sci. Technol.* **2004**, 38, 2052-2057.

Ross, R.D.; Crosby, D.G. Photolysis of Ethylenethiourea. *J. Agr. Food Chem.* **1973**, 21, 335-337

Ross, R.D.; Crosby, D.G. Characterization of photosensitizers in water from agricultural practice. *Abstracts of papers of the Am. Chem. Soc.* **1975**, 169, 87-87.

Sandvik, S.L.H.; Bilski, P. Pakulski, J.D.; Chignell, C.F.; Coffin, R.B. Photogeneration of singlet oxygen and free radicals in dissolved organic matter isolated from the Mississippi and Atchafalaya River plumes. *Mar. Chem.* **2000**, 69, 139.

Schulten, H.-R.; Gleixner, G. Analytical pyrolysis of humic substances and dissolved organic matter in aquatic systems: structure and origin. *Wat. Res.* **1999**, 33, 2489-2498.

Schweitzer, C.; Schmidt, R. Physical mechanisms of generation and deactivation of singlet oxygen. *Chem. Rev.* **2003**, 103, 1685-1757.

Scully, F.E.; Hoigné, J. Rate Constants for reactions of singlet oxygen with phenols and other compounds in water. *Chemosphere.* **1987**, 16, 681-694.

Sheldon, L.S.; Hites, R.A. Organic Compounds in the Delaware River. *Environ. Sci. Technol.*, **1978**, 12, 1188.

Stenson, A. C.; Marshall, A. G.; Cooper, W. T. Exact masses and chemical formulas of individual Suwannee River fulvic acids from ultrahigh resolution electrospray ionization Fourier transform ion cyclotron resonance mass spectrometry. *Anal. Chem.* **2003**, 75, 1275-1284.

Stevenson, F.J. Humus Chemistry: Genesis, Composition, Reactions, 2<sup>nd</sup> Ed. John Wiley and Sons, New York, NY **1994**.

Stubbins, A.; Law, C. S.; Uher, G.; Upstill-Goddard, R. C. Carbon monoxide apparent quantum yields and photoproduction in the Tyne estuary. *Biogeosci.* 2011, 8, 703-713. 13.

Thomas-Smith, T.E.; Blough, N.V. Photoproduction of hydrated electron from constituents of natural waters. *Environ. Sci. Technol.* **2001**, 35, 2721-2726.

Thorn, K. A.; Folan, D. W.; MacCarthy, P. Characterization of the International Humic Substances Society standard and reference fulvic and humic acids by solution state carbon-13 (13C) and hydrogen-1 (1H) nuclear magnetic resonance spectrometry; Water-Resources Investigations Report 89-4196; U.S. Geological Survey: Denver, **1989**.

Thorn, K.A.; Pettigrew, P.J.; Goldenberg, W.S.; Weber, E.J.; Covalent binding of aniline to humic substances .2. N-15 NMR studies of nucleophilic addition reactions. *Environ. Sci. Technol.* **1996**, 30, 2764.

Tinnacher, R.M.; Honeyman, B.D. A new method to radiolabel natural organic matter by chemical reduction with tritiated sodium borohydride. *Environ. Sci. Technol.* **2007**, *41*, 6776-6782.

Tinnacher, R.M.; Honeyman, B.D. Modeling the chemical conversion of organic compounds in sodium borohydride reduction reactions. *Org. Process Res. and Dev.* **2008**, *12*, 456-463.

Tratnyek, P.G.; Hoigné, J. Oxidation of substituted phenols in the environment: A QSAR analysis of rate constants for reaction with singlet oxygen. *Environ. Sci. Technol.* **1991**, *25*, 1596-1604.

Tratnyek, P.G.; Hoigné, J. Photo-oxidation of 2,4,6-trimethylphenol in aqueous laboratory solutions and natural waters: kinetics of reaction with singlet oxygen. *J. Photochem. Photobiol. A: Chem.* **1994**, *84*, 153-160.

Trubetskaya, O.; Trubetskoj, O.; Richard, C. Photodegrading properties of soil humic acids fractionated by SEC-PAGE set-up. Are they connected with absorbance? *J. Photochem. Photobiol. A: Chem.* **2007**, *189*, 247-252.

Twardowski, M.S.; Boss, E.; Sullivan, J.M.; Donaghay, P.L. Modeling the spectral shape of absorption by chromophoric dissolved organic matter. *Marine Chemistry*, **2004**, *89*, 69-88.

Vaughan, P.P.; Blough, N.V. Photochemical formation of hydroxyl radical by constituents of natural waters. *Environ. Sci. Technol.* **1998**, *32*, 2947-2953.

Vialaton, D.; Richard, C.; Aguer, J.-P.; Andreux, F. Transformation of monuron photosensitized by soil-extracted humic substances: energy or hydrogen atom transfer? *J. Photochem Photobiol., A* **1997**, *111*, 265-271.

Vodacek, A.; Blough, N.V.; DeGrandpre, M.D.; Peltzer, E.T.; Nelson, R.K. Seasonal variation of CDOM and DOC in the Middle Atlantic Bight: Terrestrial inputs and photooxidation. *Limnol. Oceanogr.* **1997**, *42*, 674-686.

Werner, J.J.; McNeill, K.; Arnold, W.A. Environmental photodegradation of mefenamic acid. *Chemosphere*. **2005**, *58*, 1339-1346.

Weber, E.J.; Spidle, D.L.; Thorn, K.A. Covalent binding of aniline to humic substances .1. Kinetic studies. *Environ. Sci. Technol.* **1996**, *30*, 2755.

Wenk, J.; von Gunten, U.; Canonica, S. Effect of dissolved organic matter on the transformation of contaminants induced by excited triplet states and hydroxyl radical. *Environ. Sci. Technol.* **2011**, *45*, 1334-1340.

White, E. M.; Kieber, D. J.; Sherrard, J.; Miller, W. L.; Mopper, K. Carbon dioxide and

carbon monoxide photoproduction quantum yields in the Delaware Estuary. *Mar. Chem.* **2010**, *118*, 11-21.

Wilkinson, F.; Helman, W.P.; Ross, A.B. Quantum yields for the photosensitized formation of the lowest electronically excited singlet state of molecular oxygen in solution. *J. Phys. Chem. Ref. Data.* **1993**, *22*, 113-262.

Zafiriou, O.C.; Joussot-Dubien, J.; Zepp, R.G.; Zika, R.G. Photochemistry of natural waters. *Environ. Sci. Technol.* **1984**, *18*, 358-371.

Zepp, R.G.; Wolfe, N.L.; Gordon, J.A.; Baughman, G.L. Dynamics of 2,4-esters in surface waters – hydrolysis, photolysis and vaporization. *Environ. Sci. Technol.* **1975**, *9*, 1144-1150.

Zepp, R.G.; Cline, D.M.; Rates of Direct Photolysis in Aquatic Environment, *Environ. Sci. Technol.* **1977**, *11*, 359-366.

Zepp, R.G.; Wolfe, N.L.; Baughman, G.L.; Hollis, R.C. Singlet oxygen in natural waters. *Nature*, **1977**, *267*, 421-423.

Zepp, R.G.; Baughman, G.L.; Schlautzhauer, P.F. Photosensitization of pesticide reactions by humic substances. *Abstracts of the Am. Chem. Soc.* **1980**, *180*, 6-6.

Zepp, R.G.; Baughman, G.L. Schlautzhauer, P.F. Comparison of photochemical behavior of various humic substances in water: I. Sunlight induced reactions of aquatic pollutants photosensitized by humic substances. *Chemosphere*, **1981**, *10*, 109-117.

Zepp, R.G.; Shlotzhauer, P.F.; Merritt-Sink, R. Photosensitized transformations involving electronic energy transfer in natural waters: role of humic substances. *Environ. Sci. Technol.* **1985**, *19*, 74.

Zepp, R.G.; Hoigné, J.; Bader, H. Nitrate-induced photooxidation of trace organic chemicals in water. *Environ. Sci. Technol.* **1987**, *21*, 443-450.

Zhan, M.; Yang, X.; Xian, Q.; Kong, L. Photosensitized degradation of bisphenol A involving reactive oxygen species in the presence of humic substances. *Chemosphere* **2006**, *63*, 378-386.